

**Mammalian NDR Kinases:  
Tumor Suppressors with Essential Functions in  
Embryonic Development**

**Inauguraldissertation**

zur

Erlangung der Würde eines Doktors der Philosophie

vorgelegt der

Philosophisch-Naturwissenschaftlichen Fakultät

der Universität Basel

von

**Debora Schmitz-Rohmer**

aus Nienburg / Deutschland

Basel 2011

Genehmigt von der Philosophisch-Naturwissenschaftlichen Fakultät der  
Universität Basel auf Auftrag von Dr. Brian A. Hemmings, Prof. Dr. Michael Hall and  
Prof. Dr. Ruth Chiquet.

Basel, den 19.10. 2010

**Prof. Dr. Martin Spiess**

(Dekan)

*To Luc and my Parents*

## Table of Content

Abbreviations .....	6
Summary .....	8
1. General Introduction .....	10
1.1 Structure and regulation of NDR kinases .....	10
1.2 Functions of NDR kinases.....	13
1.3 Studying <i>in vivo</i> protein function in mouse models.....	14
1.4 Milestones in intrauterine development.....	15
1.5 The first mouse model of <i>Ndr</i> deficiency reveals tumor suppressive functions of mammalian NDR kinases.....	23
2. Aim and Scope of the Thesis.....	27
3. Results.....	28
3.1 Mammalian NDR Kinases are Essential for Cardiac Looping and Contribute to Left/Right Symmetry of the Embryo .....	29
3.1.1 Abstract .....	30
3.1.2 Introduction.....	31
3.1.3 Results.....	33
3.1.4 Discussion .....	53
3.1.5 Materials and Methods .....	61
3.1.6 References .....	70
3.1.7 Acknowledgements .....	84
3.1.8 Supplementary Material.....	86
3.2 Complete Loss of NDR Kinases in the Intestinal Epithelium Induces Rectal Prolapse and Increases Susceptibility to Azoxymethane-induced Colon Carcinogenesis .....	92
3.2.1 Introduction.....	93
3.2.2 Results.....	95
3.2.3 Discussion .....	100
3.2.4 Materials and Methods .....	103
3.2.5 References .....	104
3.2.6 Supplementary Material.....	108
4. General Discussion.....	109
5. General References.....	118
6. Appendix: Co-authorships and Contributions to Publications .....	132
A.1 Differential NDR/LATS Interactions with the Human MOB Family Reveal a Negative Role for hMOB2 in the Regulation of Human NDR Kinases.....	133

A.2. Ablation of the Kinase NDR1 Predisposes Mice to the Development of T cell Lymphoma .....	134
A.3. NDR Kinase is Activated by RASSF1A/MST1 in Response to Fas Receptor Stimulation and Promotes Apoptosis .....	135
A.4. The MST1 and hMOB1 Tumor Suppressors Control Human Centrosome Duplication by Regulating NDR Kinase Phosphorylation .....	136
A.5. The Human Tumour Suppressor LATS1 is Activated by Human MOB1 at the Membrane .....	137
A.6. NDR Kinases Regulate Essential Cell Processes From Yeast to Humans .....	138
7. Curriculum Vitae .....	139
8. Acknowledgements.....	141

## Abbreviations

AOM	azoxymethane
AS	activation segment
bp	base pair
<i>C.elegans</i>	<i>Caenorabditis elegans</i>
cKO	conditional knock-out
<i>D. melanogaster</i>	<i>Drosophila melanogaster</i>
DAB	3,3'-diaminobenzidine
dpc	days post coitum
E	embryonic day
EDTA	Ethylenediaminetetraacetic acid
EtOH	Ethanol
fx	floxed
HCl	Hydrogen Chloride
HM	hydrophobic motif
ICM	inner cell mass
KO	knock-out
LATS	large antigen tumor suppressor
LOF	loss-of-function
LS-(0-III)	looping stage (0-III)
MetOH	Methanol
min	minute(s)

MOB	Mps one binder
MST	mammalian Ste-20 like kinase
<i>N. crassa</i>	<i>Neurospora crassa</i> , red bred mold
NaCl	Sodium Chloride
NDR	nuclear dbf- related
PBS	phosphate-buffered saline
PBT	PBS with 0.1% Tween
PCR	polymerase chain reaction
PMSF	phenylmethylsulfonyl fluoride, serine protease inhibitor
RT	room temperature
<i>S.cerevisiae</i>	<i>Saccharomyces cerevisiae</i> , budding yeast
<i>S.pombe</i>	<i>Schizosaccharomyces pombe</i> , fission yeast
<i>sax-1</i>	<i>C. elegans</i> gene: <i>sensory axon guidance 1</i>
SDS PAGE	sodium dodecyl sulfate polyacrylamide gel electrophoresis
TBS	Tris-buffered saline
TBST	Tris-buffered saline with 0.1% Tween
TE	Tris-EDTA
<i>trc</i>	<i>D. melanogaster</i> gene: <i>tricornered</i>
wt	wild type

## Summary

NDR kinases are highly conserved from yeast to man. Loss-of-function models of *Ndr* homologs in yeast and fly demonstrate essential functions of the respective kinases. Mammalian *Ndr1* and *Ndr2* are widely expressed and share a high degree of sequence identity. Human NDR kinases function in centriole duplication, mitotic chromosome alignment, apoptosis and proliferation. Mice that lack functional NDR1 protein are phenotypically normal, but protein levels of NDR2 are up-regulated in *Ndr1*-null tissues suggesting a compensatory link between both isoforms. Aged *Ndr1* knock-out (KO) mice develop T-cell lymphoma, indicating a tumor suppressive function of mammalian NDR kinases. Several reports describe deregulated *Ndr* transcript levels in human cancers but the functional relevance of the expression changes has not been addressed.

The present study reveals that mice carrying a targeted deletion of *Ndr2* are phenotypically normal but show an up-regulation of NDR1 protein levels. Combined loss of *Ndr1* and *Ndr2* results in embryonic lethality, demonstrating that NDR kinases play essential roles in mammalian development. *Ndr*-null embryos are small and developmentally delayed at embryonic day (E) 8 and die around E10. Transcript levels of the CDK inhibitors p21 and p27 are up-regulated in *Ndr*-null embryos at E8.5, suggesting that NDR kinases positively regulate proliferation *in vivo*. Mutant somites are small and irregularly shaped. Asymmetric expression of the somite-clock genes *Lunatic Fringe* and *Hes7* in mutant embryos indicates that NDR kinases contribute to ensure bilateral symmetry in the embryo. In the absence of NDR kinases, heart development arrests at the linear heart tube stage and does not proceed to cardiac looping. Proper establishment of the left / right axis is a



prerequisite for rightward cardiac looping. Cardiac malformation is most likely the primary cause for embryonic lethality of *Ndr*-null embryos. Asymmetric gene expression and impaired cardiac looping might reflect a general symmetry defect in NDR-deficient embryos.

Embryonic lethality precludes the analysis of *in vivo* functions of NDR kinases in the adult mouse. To address the role of NDR in the context of tumorigenesis, I have generated an intestinal epithelium specific *Ndr1/2* double KO (*Ndr1*<sup>-/-</sup> *Ndr2*<sup>Δ/ΔVilCre</sup>) mouse line. *Ndr1*<sup>-/-</sup> *Ndr2*<sup>Δ/ΔVilCre</sup> mice develop rectal prolapse, a symptom of chronic inflammation of the colon. Importantly, patients suffering from chronic colitis are at increased risk of developing colorectal cancer (CRC). Although *Ndr1*<sup>-/-</sup> *Ndr2*<sup>Δ/ΔVilCre</sup> mice do not spontaneously develop colon cancer, initial studies indicate that *Ndr1*<sup>-/-</sup> *Ndr2*<sup>Δ/ΔVilCre</sup> mice are more susceptible to Azoxymethane (AOM)-induced colon carcinogenesis. Therefore, *Ndr1*<sup>-/-</sup> *Ndr2*<sup>Δ/ΔVilCre</sup> mice could provide a new model system to study the molecular mechanisms that underlie the increased risk of CRC formation in patients with chronic colonic inflammation.

In summary, this study demonstrates that mammalian NDR kinases are essential for embryonic development. They positively regulate growth, somitogenesis and heart development. Whether the defect in bilateral symmetry and the cardiac phenotype are causally connected remains to be addressed. Complete loss of NDR kinases in the intestinal epithelium causes rectal prolapse and increased susceptibility to AOM-induced CRC formation. Lastly, the conditional *Ndr* double KO mouse line represents a valuable tool to address additional *in vivo* functions of mammalian NDR kinases in normal physiology and disease.

# 1 General Introduction

Almost two decades ago, the Serine/Threonine kinase NDR was isolated in a screen designed to identify human homologues of an overlapping pair of *C.elegans* ESTs (expressed sequence tags). The clones had been described as worm homologs of human Protein Kinase B and the cell-cycle regulating kinase *dbf2* in *S.cerevisiae*, respectively. The screen identified a highly conserved *dbf2*-related yet distinct protein kinase open-reading frame in both *Drosophila* and human cDNA libraries which was termed NDR (nuclear *dbf*-related) (1).

Protein kinases are enzymes that catalyze the transfer of a phosphate group from adenosine triphosphate (ATP) to serine, threonine or tyrosine residues of specific protein substrates (2). Protein phosphorylation serves important regulatory functions in the cell. If the substrate is an enzyme, phosphorylation can trigger conformational changes that activate or deactivate its catalytic activity (3). Alternatively, protein phosphorylation can regulate the cellular localization of a given protein or target it for degradation. The human genome encodes 518 protein kinases (3) which have been categorized into different families based on the structure of their catalytic domains (4). Many protein kinases function in series in so-called signaling cascades which relay and amplify signals from the plasma membrane to intracellular effectors. Independently of their catalytic activity, certain kinases also serve as scaffold or adapter proteins (5-10).

## 1.1 Structure and regulation of NDR kinases

Based on the structure of their catalytic domain, NDR kinases belong to the AGC (PKA, PKG, PKC) kinase subgroup (3, 4, 11). They possess an activation segment (AS) which is located in catalytic subdomain VII and a hydrophobic motif (HM) in the

C-terminus. A unique feature of NDR kinases is their split catalytic domain which is separated into two parts (subdomains I-VII and VIII-XII) by a stretch of basic amino acids that is thought to auto-inhibit NDR kinase activity (12). Moreover, NDR kinases contain an N-terminal binding site for MOB proteins which serve as positive and negative regulators of NDR kinase activity (11, 13-19).

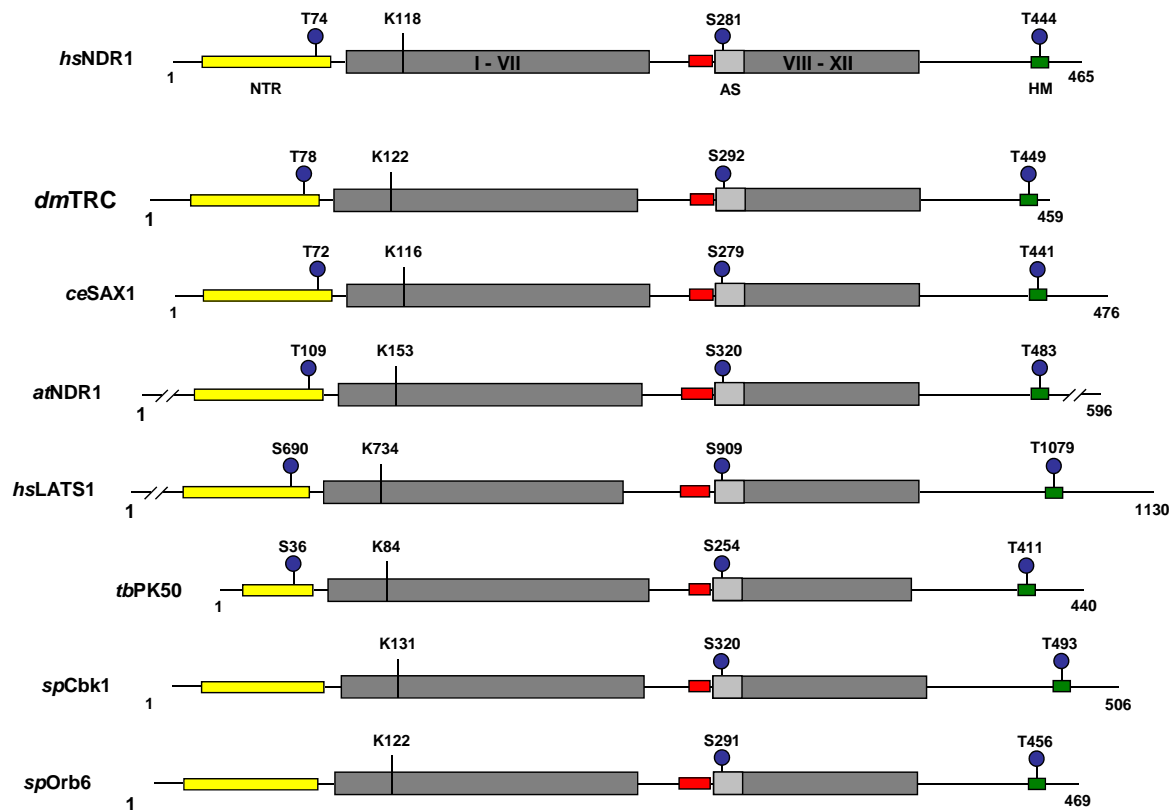


**Figure 1. Primary structure of selected nuclear Dbf2-related (NDR) family members.** Eight members of the NDR kinase family are depicted from unicellular organisms (*Saccharomyces cerevisiae* (S.c.), *Schizosaccharomyces pombe* (S.p.) and *Trypanosoma brucei* (T.b.)), animals (*Caenorhabditis elegans* (C.e.), *Drosophila melanogaster* (D.m.) and *Homo sapiens* (H.s.)) and plants. The *Arabidopsis thaliana* (A.t.) sequence, originally termed At2g2047, is referred to as NDR1. Subdomain VIII, which harbours the activation segment (AS), is shaded in bright grey. The remaining catalytic subdomains are dark grey. The C-terminally located hydrophobic motif (HM) is shown in green. Solid blue spheres indicate key regulatory phosphorylation sites, as shown experimentally (*H. sapiens* NDR1, *H. sapiens* large tumour suppressor-1 (LATS1), *D. melanogaster* tricornered (Trc), *S. cerevisiae* Cbk1, *S. pombe* Orb6) or predicted from homology (*C. elegans* sensory axon guidance-1 (SAX-1), *A. thaliana* NDR1, *T. brucei* PK50). The position of the catalytic lysine that is located in subdomain II is indicated. The insert in the kinase domain that separates the subdomains VII and VIII contains a putative auto-inhibitory sequence (AIS) and is shown in red. The N-terminal regulatory domain (NTR) is highlighted in yellow. **This figure was generated by me. A slightly modified version has been published in (13).**

Although the majority of functional studies has been performed in yeast and fly, the regulation of NDR kinase activity has mostly been delineated in mammalian cell culture systems (12, 20-25). A schematic summary of NDR activation is shown in Figure 2. Catalytic activity of mammalian NDR kinases requires phosphorylation of the activation segment (AS) and the hydrophobic motif (HM) (21-25). Both AS and HM phosphorylation sites are conserved in all NDR kinase family members identified today (13), suggesting that the mechanism of activation by phosphorylation is conserved throughout the entire family. While NDR kinases auto-phosphorylate at the AS (25), HM phosphorylation is catalyzed by the Ste-20-like kinase family members MST1, MST2 and MST3 (10, 23, 26, 27). The MOB1 protein functions as a co-activator of NDR kinases by stimulating both auto-phosphorylation at the AS (12) and HM phosphorylation by the up-stream kinases (21, 26, 27). Its homolog MOB2 acts as a negative regulator of NDR kinases and competes with MOB1 for NDR binding (16).

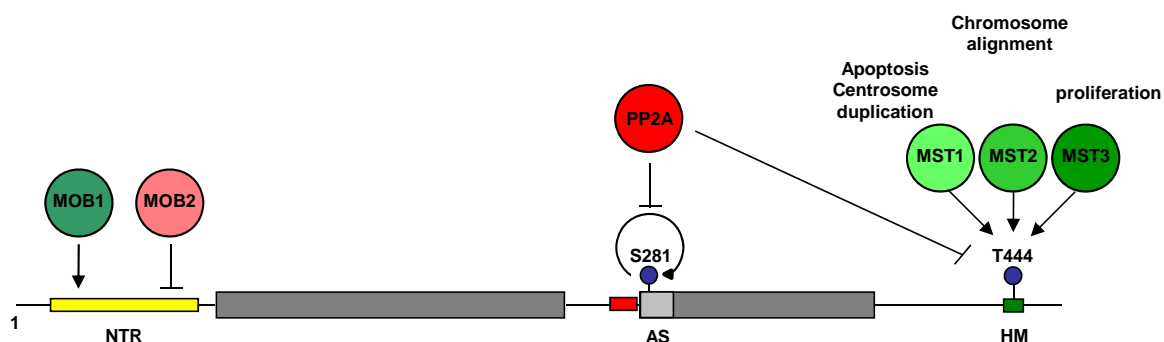


**Figure 2. Regulation of NDR kinases at the molecular level in humans.** Primary structure of human NDR1. Color code of N-terminal regulatory domain, split catalytic domain and regulatory phosphorylation sites as in Figure 1. The MOB proteins MOB1 and MOB2 bind to the N-terminal regulatory domain (NTR). MOB1 binding stimulates both autophosphorylation at the activation segment (AS) and phosphorylation of the hydrophobic motif (HM) by up-stream kinases MST1, MST2 and MST3 (21, 26, 27), MOB2 competes with MOB1 for NDR binding and represses NDR kinase activity (16). Phosphatase PP2A dephosphorylates both Ser281 and T444. MST1 functions as the up-stream kinase in apoptosis and centrosome duplication (26, 27), MST2 in mitotic chromosome alignment and MST3 in proliferation (38). **Adapted from (13)**

## **1.2 Functions of NDR kinases**

NDR kinases are highly conserved from yeast to man (Figure 1). Knock-out models of *Ndr* homologs in yeast and fly indicate essential functions of the respective kinases (reviewed in (13)). Cbk1, the NDR homolog in *S. cerevisiae*, is indispensable for polarized growth and cell separation (28). NDR kinases in *S. pombe* and *N. crassa* play similar roles in controlling polarized cell growth (reviewed in (29)). Organismal loss of the NDR homolog Trc in *D. melanogaster* is lethal, and mosaic loss of function results in a sensory bristle defect with abnormally split and branched bristles (30). Trc controls dendritic tiling and branching of *Drosophila* sensory neuron dendrites (31, 32). Similarly, the *C.elegans* NDR homolog Sax-1 regulates mechanosensory tiling (33) and contributes to establish and maintain neuronal cell shape (34, 35). Despite the insights gained into the biological functions of NDR kinases in yeast, fly and worm, their substrates remain unknown.

Due to an expansion of the kinome, the mammalian genome encodes two NDR kinase isoforms, NDR1 and NDR2 which share 86% identical residues (24). NDR1 and NDR2 are expressed in broad but distinct patterns in adult mouse tissues (24, 36). While NDR1 protein levels are high in thymus, spleen and lymph nodes, NDR2 is strongly expressed in colon and brain (36). Every murine tissue analyzed so far expresses at least one of the two NDR isoforms (24, 36), suggesting that NDR kinases play important roles in mammalian biology. Mammalian NDR localizes to centrosomes and regulates centrosome duplication (37). Moreover, it mediates Fas-receptor induced apoptosis and decreased NDR levels confer partial resistance to apoptosis induction (27, 36). MST1 functions as the main HM kinase of NDR in centrosome duplication and apoptosis (26, 27). Interestingly, the SARAH domain of

MST1 is only required for NDR activation in apoptosis (27) but dispensable for NDR regulation in centrosome duplication (26). This finding suggests distinct up-stream regulatory pathways of NDR activity in centrosome duplication and apoptosis induction. Additionally, NDR1 kinase activity is required for the precise alignment of chromosomes in mitosis (38). In this context, NDR is activated by MST2. Recently, NDR was shown to regulate G1/S transition downstream of MST3 by directly controlling p21 and c-myc protein stability (10). Importantly, this study identifies p21 as the first endogenous substrate of NDR kinases (10). All of the functions described for mammalian NDR today have been identified in tissue cultured cells. Therefore, their physiological relevance remains to be confirmed *in vivo*.

### ***1.3 Studying in vivo protein function in mouse models***

Despite the obvious physiognomic differences between mice and men, their physiology and the underlying molecular pathways are highly conserved between the two species. Therefore, the mouse has become a widely appreciated model system for studying *in vivo* functions of mammalian proteins. Many aspects of mammalian development have been studied in the mouse and the general concepts appear to be conserved between mouse and human. Spontaneous and targeted genetic loss-of-function (LOF) models in the mouse have helped to discover key molecular pathways that are highly relevant to normal human physiology and disease. Two prominent examples are the morphogen Sonic Hedgehog (Shh) and the cardiac transcription factor Nkx2.5. Disruption of the *Shh* gene in the mouse causes holoprosencephaly (HPE) (39), the most common developmental defect of the forebrain and midface in humans. Concurrently, disruption of the Sonic Hedgehog pathway is the major common effector of mutations that cause human HPE (40). Moreover, mouse models

have significantly contributed to delineate the central role of Hedgehog-signaling in several human malignancies (reviewed in (41)). The cardiac transcription factor *Nkx2.5* was originally identified as a murine homolog of the *Drosophila* homeobox gene *NK4* (42). Its expression pattern and the study of *Nkx2.5* KO mouse models have revealed essential roles of *Nkx2.5* in mammalian heart development (reviewed in (43)). Today, human *Nkx2.5* is known as the most commonly mutated gene in congenital heart disease (44-49). These and other examples underscore the relevance of developmental studies in the mouse to delineate the genetic basis underlying normal human development and disease.

#### ***1.4 Milestones in intrauterine development***

Throughout the course of development, the mammalian embryo has to meet several developmental milestones. Failure to do so results in embryonic lethality. In addition to the morphological phenotype, the time-point of embryonic lethality has proven to be a good indicator of the underlying biological defect (50). Therefore, LOF mouse models that result in defective embryonic development are valuable tools to study the *in vivo* function of a given protein, as demonstrated by the present study. The following section describes the milestones of intrauterine development that have helped to delineate gene product functions based on LOF phenotypes (51, 52).

##### **Blastocyst formation and implantation**

Approximately one day after fertilization, the zygote undergoes its first cleavage, giving rise to two blastomeres. From this stage onwards, embryonic development depends on regulatory proteins that orchestrate replication, recombination and transcription. Embryos that lack cyclin-dependent kinases 1 (CDK1) are incapable of undergoing cell division and arrest at the two-cell stage (53). Loss of components

that participate in DNA double strand generation, repair and chromosome remodeling leads to developmental arrest at the 4- to 16-cell stage (54-56). During the first days following fertilization, the developing embryo moves freely through the oviduct and into the uterus. Moreover, embryos generated by *in vitro* fertilization can easily be cultured to the blastocyst stage (E3.5) (52), suggesting that the embryo initially develops independently of maternal cues. However, development beyond the blastocyst stage requires a physical connection to the mother. The trophoblast cell lineage is established from the outer cell layer of the blastocyst, marking the first differentiation event in the embryo. Recent studies suggest that the mammalian Hippo pathway plays an important role in translating cell position within the blastocyst into trophoblast (outside) or inner cell mass (ICM, inside) cell identity (57).

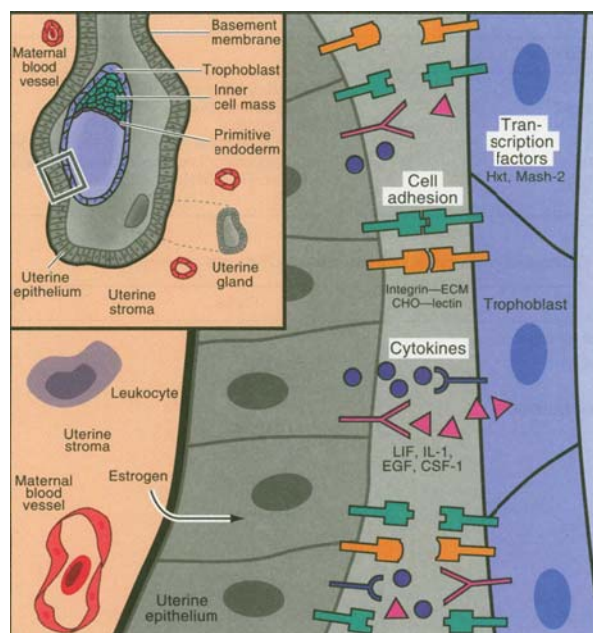


**Figure 3. Implanting blastocyst.** At day 4.5 of mouse development, the blastocyst attaches to the uterine epithelium and the uterus clamps around the blastocyst. Extensive molecular communication via cytokines (IL-1, Interleukin 1; LIF, leukemia-inhibitory factor; CSF-1, colony-stimulating factor1), hormones (estrogen) and growth factors (EGF, epidermal growth factor) between the embryo and the mother is essential for successful implantation. **Taken from (52)**



Trophoblast cells subsequently adhere to the uterine wall and mediate implantation of the embryo around E4.5 (Figure 3). The importance of trophoblast contribution to normal development is reflected in the large number of mouse mutants that die at the peri-implantation stage due to trophoblast defects (reviewed in (58, 59)). Contrarily to the first period of embryonic development, implantation critically depends on extensive communication between embryo and mother. In the so-called decidual response, the uterus prepares a favorable environment for the embryo (52). On the other hand, secretion of IL-1 and other cytokines by the blastocyst is equally essential for implantation (60). While trophoblast cells are essential in establishing the primary contact with the uterine epithelium, cells from the primitive embryonic endoderm contribute to form a functional interface between mother and embryo. The primitive endoderm gives rise to extra-embryonic parietal endoderm which migrates onto the basal surface of the trophoblast layer and deposits a thick basement membrane, so-called Reichert's membrane. Trophoblast layer, Reichert's membrane and parietal endoderm form the yolk sac placenta, which supplies the embryo with nutrients from maternal blood sinus at the interface of uterine epithelium and trophoblast layer. The yolk sac placenta is the principal transport organ between mother and embryo until the chorioallantoic placenta starts to function around E10.

### **Development of the cardiovascular system**

Contrary to various other embryonic systems and organs, the cardiovascular system is essential for embryonic survival (51). It comprises three main entities, namely the heart, vessels and blood. The majority of these structures is of mesodermal origin.

Mesoderm forms during gastrulation, where cells from the epiblast migrate through the primitive streak, giving rise to mesoderm and definitive endoderm (Figure 4).

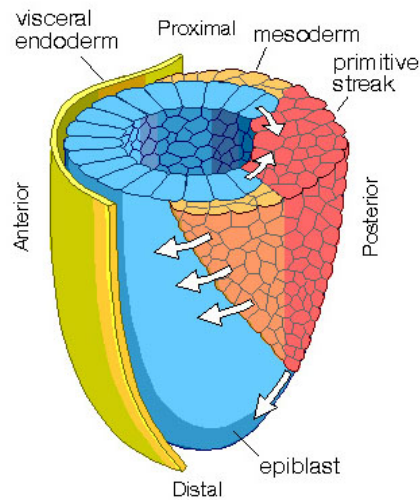


**Figure 4. The mouse embryo at the onset of gastrulation.** At the onset of gastrulation at E6.5, cells from the epiblast (blue) migrate through the primitive streak to generate mesoderm (orange) and definitive endoderm (not shown). *Image taken from the website of the Department of Biology (BIOL3530) with Dr. Brian E. Staveley, Memorial University of Newfoundland, Canada*

Primitive streak formation around E6.5 marks the onset of gastrulation which generates the three definitive germ layers ectoderm, mesoderm and endoderm (61). Cell migration is a major morphogenetic hallmark of gastrulation. Consequently, genetic ablation of components that are essential for cellular migration, such as the extra-cellular matrix component fibronectin and its cellular receptor integrin  $\alpha_5$ , results in mesodermal defects and embryonic lethality by mid-gestation (62, 63). Soon after the onset of gastrulation, around E7.5, blood islands start to form in the mesodermal layer of the yolk sac. The time-line of murine blood and blood vessel development is shown in Figure 5.

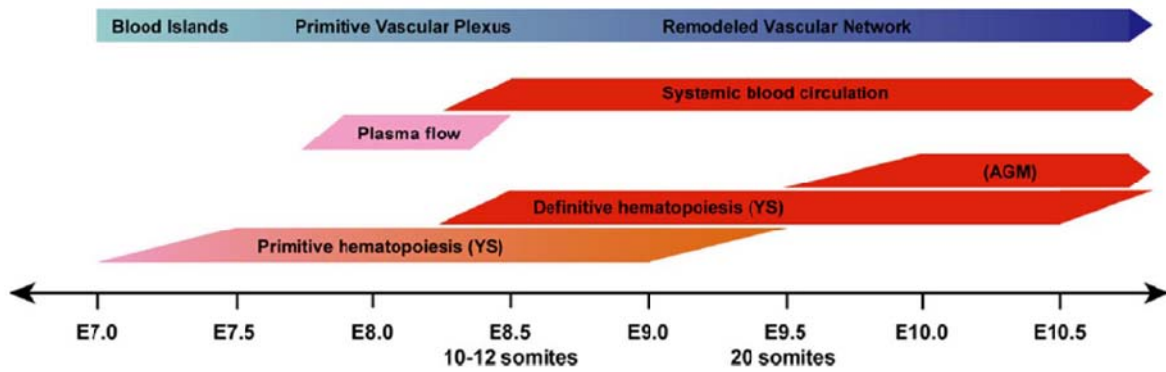


**Figure 5. Time-line of murine blood and blood vessel development during embryogenesis.** YS: yolk sac; AGM: aorta gonad mesonephros. *Taken from (114).*

Blood islands contain both primitive endothelial and hematopoietic cells. Whether they arise from a common progenitor remains subject of debate (64). Endoderm derived molecular signals, namely FGF2 (Fibroblast growth factor), Indian Hedgehog (IHH) and VEGF (Vascular Endothelial Growth Factor) indisputably play an important role in the specification of endothelial and hematopoietic precursors (reviewed in (64)). Their importance is underlined by the prominent vascular defects of *Vegfa* and *Vefgr2* KO embryos (65, 66). Coalescing blood islands in the yolk sac give rise to vascular channels, the precursors of blood vessels. Between E8.5 and E9.5 the primitive vascular plexus of the yolk sac undergoes extensive remodeling, a highly complex process that requires over 60 known genes (67). Concomitantly, definitive hematopoiesis starts in the aorta gonad mesonephros (AGM) of the embryo proper which is soon replaced by the liver as a major site of definitive embryonic hematopoiesis (68). Compromised liver-hematopoiesis seems to be the reason for embryonic lethality of *Rb*, *keratin 8* and *c-myb* KO mice (69-72).

The heart develops in parallel to embryonic vasculature and hematopoietic cells. Murine heart development between E6.5 and E10.5 is summarized in Figure 6.

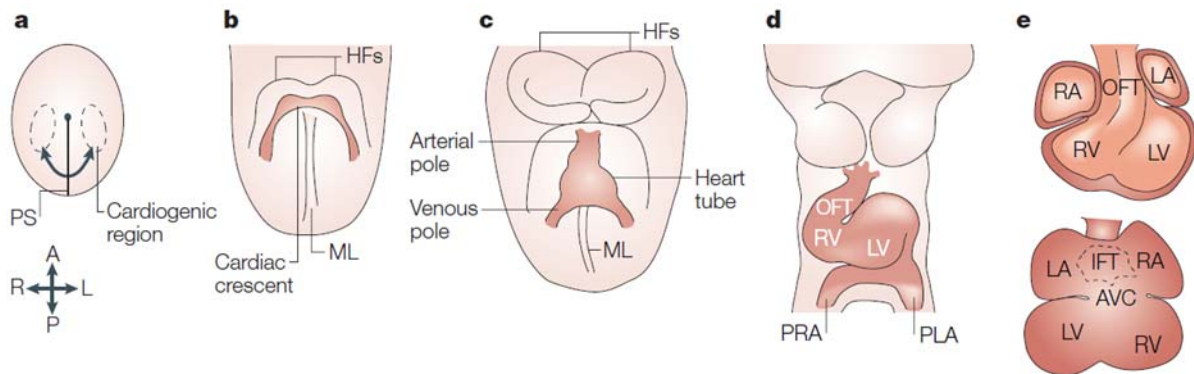


**Figure 6. Morphogenesis of the mouse heart.** **a** Myocardial progenitor cells originate in the primitive streak (PS), from where they migrate to the anterior of the embryo at about embryonic day E6.5. **b** These cells come to lie under the head folds (HF) and form the cardiac crescent, where differentiated myocardial cells are now observed (E7.5). **c** The early cardiac tube forms through fusion of the cardiac crescent at the midline (ML) (E8). **d** It subsequently undergoes looping (E8.5). **e** By E10.5 the heart has acquired well-defined chambers, but is still a tube (upper panel, ventral view; lower panel, dorsal view). Anterior (A)–posterior (P) and right (R)–left (L) axes are indicated. AVC, atrioventricular canal; IFT, inflow tract; OFT, outflow tract; PLA primitive left atrium; PRA, primitive right atrium. **Taken from (75)**

The cardiogenic regions left and right of the anterior primitive streak give rise to the cardiac crescent which becomes apparent at E7.5. The crescent subsequently forms two bulges which fuse and become the primitive linear heart tube (73). Heart beat is evident at the 3-somite stage and generates plasma flow at early E8 which precedes the onset of systemic blood circulation (67). Hemodynamic forces generated by cardiac contraction are essential for the remodeling of yolk sac vasculature and promote embryonic hematopoiesis (67, 74). Almost immediately after the heart tube has formed, it begins to loop (73). Cardiac looping and subsequent chamber formation transform the linear heart tube into the four chambered heart. As exemplary described above for the cardiac master regulator *Nkx2.5*, numerous other cardiac transcription factors and their contribution to cardiac development have been studied in knock-out mouse models (reviewed in (75)). A common theme that has emerged from these studies is that severe defects in cardiac looping and chamber formation result in embryonic lethality around E10 (76-82). This indicates that proper

cardiac function is essential for embryonic survival beyond the first half of gestation. Less severe cardiac defects that result in poor cardiac function lead to delayed embryonic lethality (83-87). In general, mice with structural cardiovascular defects tend to die earlier than those with hematopoietic problems (51). This observation further supports the hypothesis that hemodynamic force generated by blood flow is at least as important as nutrient and oxygen transport during early cardiovascular development (88).

### **Formation of the chorioallantoic placenta**

As mentioned above, the visceral yolk sac constitutes the first principal interface for nutrient and waste exchange between mother and embryo (52). At around E10 it is replaced by the chorioallantoic placenta which is composed of fetal and maternal components. Failure to establish a functional placenta becomes limiting to embryonic growth and development between E10 and E11 (51). A schematic representation of placental development is shown in Figure 7. The trophoblast layer of the placenta arises from trophectoderm cells, the outer layer of the blastocyst. Following blastocyst implantation, the ectoplacental cone (EPC), a trophoblast structure, is tightly apposed to the maternal decidua. At E8.5, the allantois grows out from the posterior end of the embryo and makes contact with the chorion that has concomitantly been formed by extra-embryonic ectoderm underlying the EPC. The allantois gives rise to embryonic vessels which eventually form the umbilical chord. Chorionic trophoblasts differentiate into the various specialized trophoblast lineages that constitute the labyrinth layer of the placenta. Embryonic vessels invade the labyrinth layer which is also pervaded by maternal blood sinus. The labyrinth layer of

the placenta thus forms the direct interface for nutrient and waste exchange between fetal and maternal blood. Trophoblasts are important components of the placenta and defects in trophoblast development, stem cell maintenance and differentiation can result in embryonic lethality (59). Moreover, defects in chorioallantoic attachment as well as branching morphogenesis and vascularization of the labyrinth also compromise embryonic development (59, 89). These observations demonstrate that extra-embryonic membranes and tissues – trophoblast cells, yolk sac placenta and chorioallantoic placenta – make essential contributions to mammalian embryonic development.

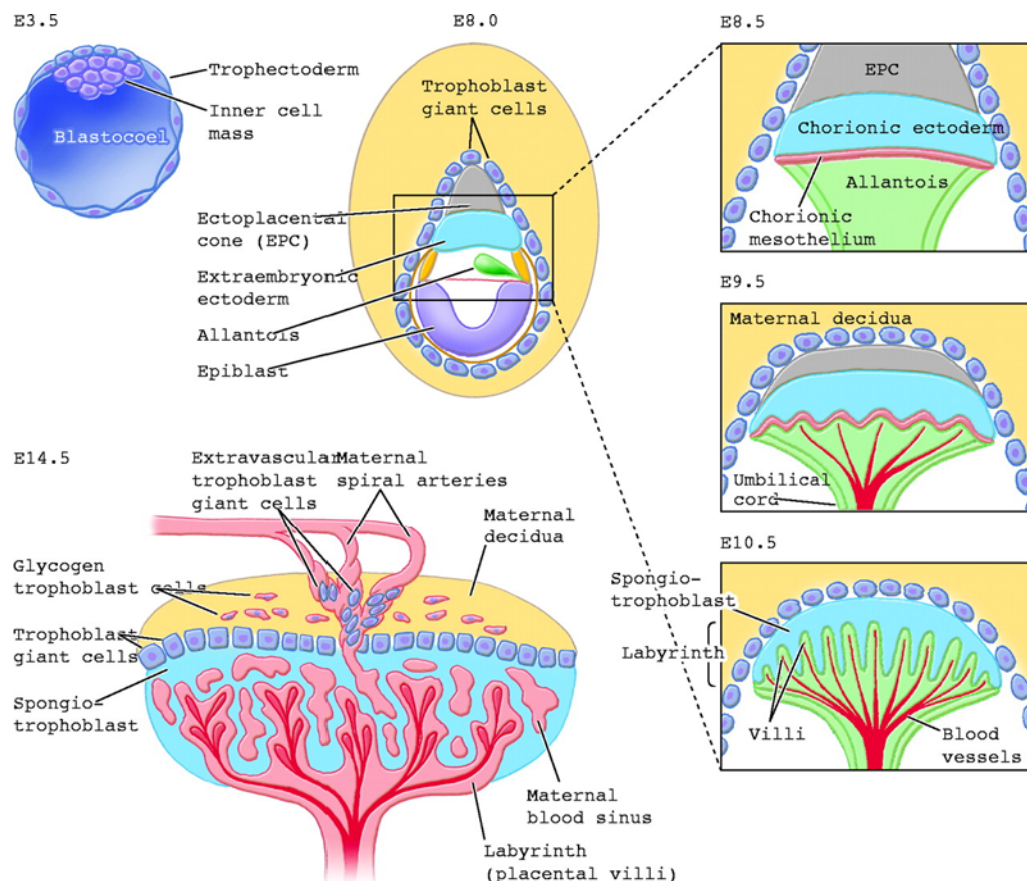


**Figure 7. Placental development of the mouse.** The origins of the extra embryonic lineages begin at embryonic day (E) 3.5 with the formation of the blastocyst. At E8.0, chorioallantoic attachment occurs, followed by branching morphogenesis of the labyrinth to form dense villi, within which nutrients are exchanged (E8.5–10.5). The mature placenta (E14.5) consists of three layers: the labyrinth, the spongiotrophoblast, and the maternal decidua. **Taken from (89)**

Mammalian embryonic development is highly complex. During its course, a single cell gives rise to an entire organism with many different cell types and tissues. Numerous studies with mouse mutants have shown that despite its complexity, embryonic development can be broken down to several well defined milestones which the embryo has to meet (51, 52). The zygote has to undergo cell divisions to form the blastocyst which subsequently implants into the maternal uterine wall at E4.5. Development of the vascular and the hematopoietic system initiates in the yolk sac around E7.5, the primitive heart tube forms shortly afterwards and begins to beat at early E8. Development of the heart, vasculature and blood is highly interdependent. Contrary to other embryonic organs that develop slightly later, the cardiovascular system and the chorioallantoic placenta are the only systems that are essential for embryonic survival (51). Complete failure to establish cardiovascular circulation results in embryonic lethality by E10.5. The relevance of the enumerated developmental milestones is underlined by large numbers of mouse mutants whose phenotypes are characteristic of the milestone that they have failed to meet (53-56, 58, 62, 63, 65, 66, 69-72, 76-87, 89).

### ***1.5 The first mouse model of Ndr deficiency reveals tumor suppressive functions of mammalian NDR kinases***

The first loss-of-function mouse model for mammalian NDR kinases has been reported recently (36). Mice that lack *Ndr1* are viable, fertile and initially indistinguishable from wild type littermates. However, aged heterozygous and homozygous *Ndr1* KO mice are highly susceptible to develop T-cell lymphoma. As described above, mammalian NDR is activated in response to apoptotic stimuli and loss of NDR results in increased resistance to apoptosis induction (27, 36).

Importantly, apoptotic cell numbers are decreased in tumors with low NDR protein levels (36). Resistance to apoptosis is a common theme in tumor development and could endow NDR with tumor suppressor function as postulated by *Cornils et al.* (36). Several reports describe deregulated *Ndr* transcript and protein levels in different human cancer types but their impact on tumor development remains unknown (summarized in (90)). The extended mammalian NDR kinase family comprises four members, NDR1/2 and LATS/2 (large antigen tumor suppressor). NDR and LATS kinases are highly conserved at the C-terminus which contains the catalytic domain but differ at the N-terminus where LATS kinases possess a long N-terminal sequence that is absent in NDR (Figure 1 and (13)). The *lats/warts* kinase was originally identified in *Drosophila* as a potent tumor suppressor (91). NDR and LATS kinases are positively regulated by the co-activator MOB1 (12, 21, 26, 27, 92, 93). Moreover, they share common up-stream kinases, namely MST1 and MST2 in mammals and the single MST kinase in fly which was termed *hippo* and subsequently lent its name to the pathway (reviewed in (13)). A schematic overview of the Hippo pathway in mammals is shown in Figure 8. Although both NDR and LATS are activated by MST1/2, only LATS has been shown to phosphorylate the transcriptional co-activator YAP in tissue cultured cells (94). YAP promotes growth via activating transcription factors of the TEAD family (95). YAP phosphorylation results in cytoplasmic sequestration and thus suppresses its transcriptional activity (96). In summary, the mammalian Hippo pathway negatively regulates growth via YAP phosphorylation (reviewed in (97-99)). Numerous studies in fly and mammalian tissue cultured cells have demonstrated that loss-of-function of Hippo pathway components – such as *hippo/MST*, *mats/MOB1*, *lats/LATS1* and *sav/WW45* – results in nuclear YAP



localization and unrestricted growth (reviewed in (99, 100)). Concurrently, several recent reports demonstrate that YAP over-expression leads to tissue-overgrowth and cancer (101-104). At present, evidence for YAP phosphorylation by NDR kinases is limited to *in vitro* kinase assay data with recombinant protein while co-expression of NDR and YAP in Cos-7 cells did not result in YAP phosphorylation (94). However, a recent report describes YAP phosphorylation in the liver by a kinase distinct from LATS (105). Moreover, YAP phosphorylation in mouse embryos and MEFs is not affected by combined loss of *Mst1* and *Mst2* (106, 107), also suggesting that an additional kinase other than LATS can phosphorylate YAP. In summary, based on current evidence it cannot be excluded that NDR also phosphorylates YAP *in vivo*.

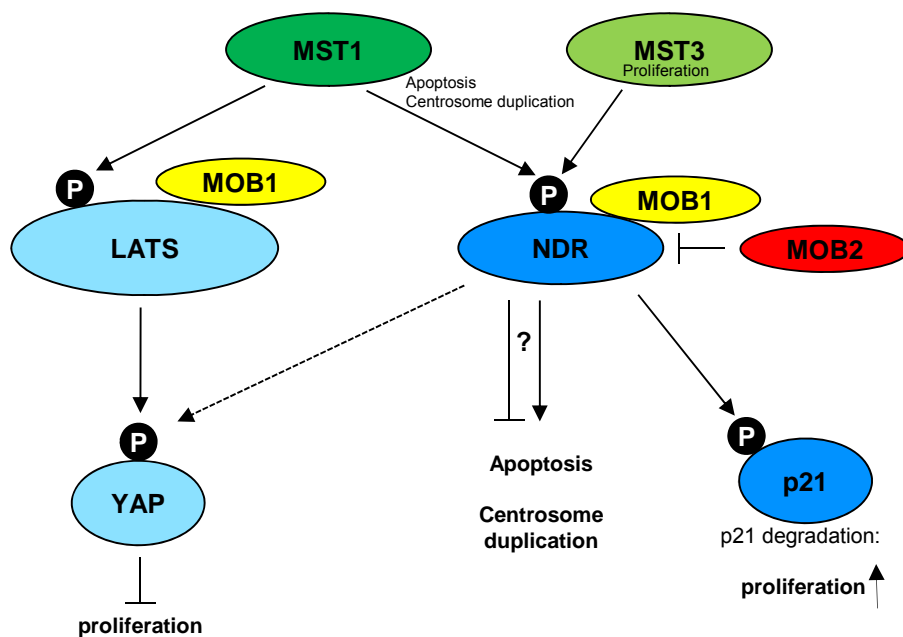


**Figure 8. The mammalian Hippo pathway.** The mammalian Hippo homolog MST1 phosphorylates and activates both LATS and NDR kinases. The co-activator MOB1 stimulates both LATS and NDR kinase activity. MOB2 binds and negatively regulates exclusively NDR. The only known down-stream targets of the mammalian Hippo pathway are YAP (yes-associated protein) for LATS and p21 for NDR. Recombinant NDR phosphorylates YAP *in vitro* (dashed line), but has not been shown to do so in cells.

Conversely, NDR kinases could also possess oncogenic properties as suggested by the observation that *Ndr* transcript levels are up-regulated in certain human cancers (summarized in (90)). Over-expression of human NDR in tissue-cultured cells leads

to centrosome over-duplication (37). A recent report shows that extra centrosomes alone promote chromosome missegregation during bipolar cell division (108). Chromosomal missegregation results in chromosomal instability, a hallmark of many tumors that correlates with the presence of extra centrosomes (109-112). Moreover, a recent study identifies mammalian NDR kinases as positive regulators of cell cycle progression (10), indicating that over-activation of NDR kinases could potentially drive excess proliferation. In summary, several lines of evidence suggest that NDR kinases might be linked to cancer development. However, additional over-expression and loss-of-function studies are needed to further elucidate the putative dual nature of mammalian NDR kinases as tumor suppressors and oncogenes *in vivo*.

As mentioned above, mice with a targeted *Ndr1* deletion do not show an obvious morphological phenotype until they come of age. However, NDR2 protein levels are up-regulated in *Ndr1* KO tissues with high intrinsic NDR1 levels, namely thymus, spleen and lymph nodes. Therefore, the lack of an early developmental phenotype might be due to isoform compensation by NDR2. Interestingly, a similar situation has been reported for the up-stream kinases MST1 and MST2 (106, 107). Mice that lack *Mst1* alone display a T-cell restricted phenotype but are otherwise normal (113). *Mst2*-null mice do not show an overt phenotype (106, 107). However, combined loss of *Mst1* and *Mst2* results in embryonic lethality between E9.5 and E11.5 (106, 107), indicating that MST1 and MST2 can mutually compensate for each other. Tissue-specific loss of *Mst1* and *Mst2* in the adult liver results in hepatocellular carcinoma (105, 107). Analogously, combined ablation of *Ndr1* and *Ndr2* in the mouse is warranted to confirm and expand initial insights into the *in vivo* functions of mammalian NDR kinases and their role(s) in tumorigenesis.

## 2. Aim and Scope of the Thesis

The aim of the present study was to identify *in vivo* functions of mammalian NDR kinases. Studies in tissue cultured cell lines have demonstrated roles for mammalian NDR kinases in centrosome duplication, the alignment of mitotic chromosomes, proliferation and apoptosis. However, little is known about the *in vivo* roles of NDR kinases in mammals. When I joined the laboratory, the *Ndr1* knock-out (KO) mouse had been generated. It does not display an overt morphological phenotype, but NDR2 protein levels are up-regulated in several tissues of *Ndr1*-null mice, suggesting that NDR2 might compensate for loss of NDR1. Moreover, aged *Ndr1*-null mice develop T-cell lymphoma, indicating a tumor suppressive function of NDR kinases. Several reports describe deregulated *Ndr* transcript levels in human cancers but the functional relevance of the expression changes has not been addressed.

To study the physiological roles of mammalian NDR kinases in general and their impact on tumorigenesis in particular, I have generated a conditional *Ndr1/2* double KO mouse line. Complete loss of *Ndr1/2* results in embryonic lethality and reveals essential roles for mammalian NDR kinases in proliferation, somitogenesis and cardiac development. As embryonic lethality precludes the analysis of *in vivo* roles of NDR kinases in the adult mouse, I have generated a mouse model where *Ndr2* is specifically deleted in the intestinal epithelium of *Ndr1*-null mice. This model is used to study the role of NDR kinases in colon cancer. Initial data suggest that complete loss of NDR kinases in the intestinal epithelium predisposes mice to AOM-induced colon carcinogenesis.

### 3. Results

I have arranged the results section into two parts which are organized as separate manuscripts. Both parts contain a separate bibliography and numbering system for the figures, i.e. the first figure in each part is numbered as “1”. References from the general introduction and the general discussion are summarized in a common reference section situated after the general discussion.

The first manuscript – “Mammalian NDR kinases are essential for cardiac looping and contribute to left / right symmetry in the embryo” will be submitted to the journal “Development” as soon as the final experiments are completed (*Hand1*, *Hand2* and *Nodal* mRNA *in situ* hybridization and proliferation curve and beating kinetics of NDR pro- and deficient cardiomyocytes).

The second part summarizes the work that has been done with the intestinal epithelium-specific *Ndr* double knock-out mouse line to address the role of NDR kinases in the context of colon carcinogenesis. This project is ongoing and will be continued in collaboration with Lei Zhang.

### 3.1 Mammalian NDR kinases are Essential for Cardiac Looping and Contribute to L/R Symmetry of the Embryo

Debora Schmitz-Rohmer<sup>1</sup>, Simone Probst<sup>2</sup>, Alexander Hergovich<sup>1,4</sup>, Mario Stegert<sup>1</sup>, Zhong-Zhou Yang<sup>3</sup>, Michael Stadler<sup>1</sup>, Rolf Zeller<sup>2</sup> and Brian A. Hemmings<sup>1</sup>

<sup>1</sup> Friedrich Miescher Institut for Biomedical Research, Maulbeerstrasse 66, CH-4058 Basel, Switzerland

<sup>2</sup> Department Biomedizin, Mattenstrasse 28, CH-4058 Basel, Switzerland

<sup>3</sup> Model Animal Research Center of NanJing University, 12 Xue-Fu Road, Pukou District, NanJing, P.R. China 210061

<sup>4</sup> current address: UCL Cancer Institut, University College London, London WC1E 6BT, United Kingdom

#### Contributions of Co-authors and FMI facilities to the work described in this manuscript

**Simone Probst** taught me how to dissect mouse embryos at E8.5 and E9.5. We jointly dissected the embryos for the microarray analysis and for the mRNA *in situ* hybridization experiments. Certain mRNA *in situ* hybridization experiments were performed by her (*Lnfg*, *Hes7*), others were performed jointly. Results were discussed with her, leading to the design of subsequent experiments. Her critique helped to improve the manuscript.

**Alexander Hergovich** taught me the practical basics of molecular cloning, gave advice on targeting vector design and performed one critical cloning step in the targeting vector generation.

**Mario Stegert** generated the *Ndr1* knock-out mouse line which I used to generate the *Ndr1/2* double knock-out mouse line.

**Zhong-Zhou Yang** prompted me to consider the heart phenotype of *Ndr*-null mutants as a primary defect directly linked to the loss-of-function of NDR kinases.

**Michael Stadler** implemented the mathematical model to approximate the effect of increased cell cycle duration on embryo size in the R program (Figure SXY, Supplementary Materials)

**Rolf Zeller** facilitated the collaboration with Simone Probst and contributed scientific advice to the embryo work.

The conditional *Ndr2* knock-out mouse line was generated with the help of the Transgenic Facility. The labeling, hybridization and quality control of the microarray experiment was performed by the Genomics Facility.

All other work was performed by me unless specifically indicated in the text.

### 3.1.1 Abstract

The mammalian NDR kinases NDR1 and NDR2 are widely expressed and share a high degree of sequence identity (1-3). Human NDR kinases function in centriole duplication, proliferation, apoptosis and proper alignment of mitotic chromosomes (4-7). Mice lacking either *Ndr* isoform alone are phenotypically normal. Only aged *Ndr1* knock-out (KO) mice frequently develop T-cell lymphoma (1). The remaining NDR isoform is up-regulated in distinct tissues of single KO mice, suggesting a compensatory link between both isoforms. To test this hypothesis *in vivo*, we generated the *Ndr1/2* double KO line. Mice with a single allele of either *Ndr1* or *Ndr2* develop normally but we never obtained viable *Ndr*-null offspring. *Ndr*-null embryos are smaller and developmentally delayed at embryonic day (E) 8 and die around E10. Transcript levels of the CDK inhibitors p21 and p27 are increased in mutant embryos, suggesting that NDR kinases positively regulate proliferation *in vivo*. Mutant embryos also display aberrant somite morphology. The somite-clock genes *Lunatic Fringe* and *Hes7* are asymmetrically expressed in the presomitic mesoderm, indicating a role for NDR kinases in the control of L/R symmetry. However, aberrant somitogenesis is unlikely to cause embryonic death. Embryonic heart development of *Ndr*-null mutants arrests at the linear heart tube stage and does not proceed to cardiac looping. Importantly, proper establishment of the L/R axis is essential for rightward cardiac looping (8, 9). Mutant myocardium is thickened and the heart lumen partially obstructed. Cardiac malformation is most likely the primary cause for embryonic lethality of *Ndr*-null mutants. In summary, we demonstrate that mammalian NDR kinases are essential for embryonic development. They positively regulate growth, somitogenesis and heart development. Whether the defect in L/R symmetry control and the cardiac phenotype are causally connected remains to be addressed.

### 3.1.2 Introduction

NDR kinases are highly conserved from yeast to man (3, 10, 11). Loss-of-function models for *Ndr* homologs in yeast and fly demonstrate essential functions of the respective kinases (reviewed in (11)). *Cbk1*, the *Ndr* homolog in *S. cerevisiae*, is indispensable for polarized growth and cell separation (12). NDR kinases in *S.pombe* and *N.crassa* play similar roles in controlling polarized cell growth (reviewed in (10)). Organismal loss of the *Ndr* homolog *trc* in *D. melanogaster* is lethal, and mosaic loss of function results in a sensory bristle defect with abnormally split and branched bristles (13). Importantly, *trc* and *sax-1*, the *Ndr* homolog in *C.elegans*, control dendritic tiling and branching of sensory neuron dendrites in fly and worm (14-16). The mammalian genome encodes two *Ndr* kinase isoforms – *Ndr1* and *Ndr2* (3) – which are expressed in a broad but distinct pattern in adult mouse tissues (1, 3). Mammalian NDR kinases positively regulate centrosome duplication (6) and proper alignment of mitotic chromosomes (4). Moreover, they function in apoptosis induction down-stream of RASSF1A (7). Decreased NDR levels confer partial resistance to apoptotic stimuli (1, 7). Lastly, NDR kinases control G1/S transition by directly regulating p21 and c-myc protein stability (5).

The catalytic activity of mammalian NDR kinases is regulated by phosphorylation of a serine residue in the activation segment (AS) and a threonine residue in the hydrophobic motif (HM) (3, 17-20). While NDR kinases autophosphorylate at the activation loop (20), hydrophobic motif phosphorylation is catalyzed by the Ste-20-like kinase family members MST1, MST2 and MST3 (5, 7, 19, 21).

The first mammalian loss-of-function model for NDR kinases has been reported recently (1). Mice that lack *Ndr1* are initially indistinguishable from wildtype littermates. However, aged heterozygous and homozygous *Ndr1* KO mice develop T-cell lymphoma (1). Importantly, NDR2 protein levels are up-regulated in *Ndr1* KO tissues. Therefore, isoform compensation by NDR2 might prevent an early developmental phenotype. Interestingly, a similar situation has been reported for the up-stream kinases MST1 and MST2 (22, 23). Mice that lack *Mst1* display a T-cell restricted phenotype (24) but are otherwise normal. *Mst2*-null mice do not show an overt phenotype (22, 23). However, combined loss of *Mst1* and *Mst2* results in embryonic lethality by mid-gestation (22, 23), indicating that MST1 and MST2 can mutually compensate for each other. To address whether the restricted phenotype of *Ndr1*-null mice reflects isoform compensation and to further elucidate the *in vivo* roles of mammalian NDR kinases, we have generated a conditional targeted deletion of the *Ndr2* gene and the *Ndr1/Ndr2* double knock-out mouse line.

We identify mammalian NDR kinases as essential positive regulators of growth, somitogenesis and heart development *in vivo*. *Ndr2*-null mice are phenotypically normal, but combined loss of *Ndr1* and *Ndr2* results in embryonic lethality by mid-gestation. This demonstrates that NDR1 and NDR2 can mutually compensate for each other. *Ndr*-null embryos are smaller, display aberrant somite morphology and fail to complete cardiac looping. Impaired cardiac function is the primary cause for embryonic death.



### 3.1.3 Results

#### ***Conditionally targeting the murine Ndr2 locus***

The mammalian homologs NDR1 and NDR2 are highly conserved and widely expressed (1, 19). Knock-out models for *Ndr* homologs in yeast and fly indicate essential functions of the respective kinases (13, 25-27). However, mice carrying a homozygous targeted deletion of *Ndr1* are born in the expected mendelian ratio, viable and fertile (1). One potential explanation for this restricted phenotype is the compensatory up-regulation of NDR2 which the authors have observed in distinct tissues (1). To test this hypothesis and to further elucidate the *in vivo* functions of mammalian NDR, we have generated a conditional targeted deletion of the *Ndr2* gene in the mouse.

We isolated and sequenced 9080 base pairs (bp) of genomic DNA surrounding exon 2 of *Ndr2* in Ola129 ES cells. In two regions, the obtained sequence differed significantly from the published sequence of the C57BL/6 strain: one deletion of 254 bp located downstream of exon 1 and one insertion of approximately 200 bp located upstream of exon 3. Additionally, we found numerous base pair exchanges spread out over the entire sequence analyzed, underlining the importance of sequence heterogeneity between the Ola129 and the C57BL/6 mouse strain. As detailed in Materials and Methods, we engineered a targeting vector to introduce *loxP* sites up- and downstream of exon 2. As shown in Figure 1A, Cre-mediated removal of exon 2 should lead to loss of functional NDR2 protein. Offspring with a conditionally targeted *Ndr2* locus was crossed with Meox2-Cre or FLP-deleter mice to generate the complete *Ndr2* knock-out (KO) or the clean conditional KO, respectively. Genotyping and Western blot

analysis confirmed successful targeting (Figure 1B, C). A clear decrease of NDR2 protein levels was already apparent in the heterozygous situation (Figure 1C). This gene-dosage effect was also observed in the *Ndr1* single KO (1). Mice lacking NDR2 protein were viable, born in the expected mendelian ratio (Figure 1D) and fertile, indicating that NDR2 is dispensable for normal development in the *Ndr1* wild type background.

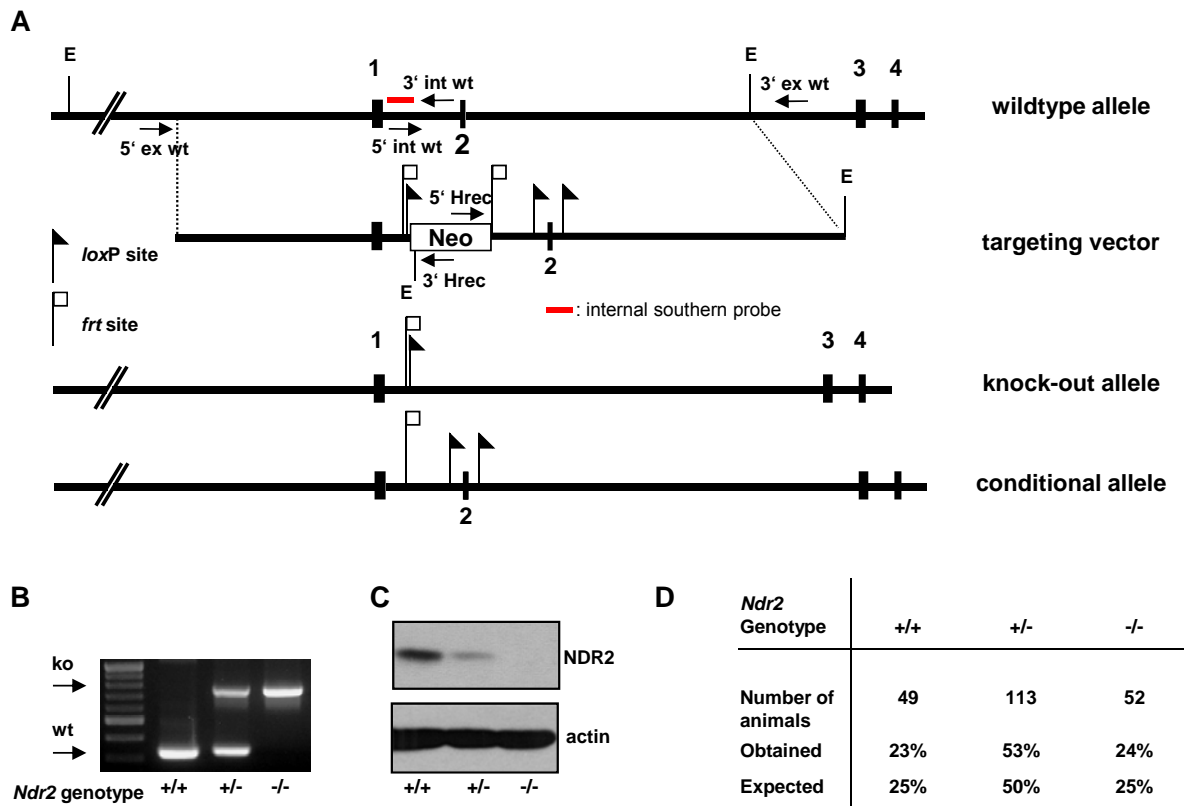


**Figure 1 Targeting scheme and validation of the conditional *Ndr2* knock-out in the mouse.** **A** Genomic structure of the *Ndr2* locus in the mouse and targeting vector for conditional *Ndr2* knock-out. Primer binding sites for ES cell screening are indicated (Ex com 5'/3' – common external 5'/3' primer; wt 5'/3' – wild type internal primers; H rec 5'/3' – homologous recombination primers in Neo cassette). E: EcoRI restriction sites used for Southern blot validation of single integration. See Materials and Methods section for detailed description of the targeting strategy. **B** Genotyping PCR of wild type, heterozygous and homozygous *Ndr2* knock-out ear notch samples. **C** Western blot analysis confirms loss of NDR2 protein in *Ndr2* knock-out. **D** *Ndr2* heterozygous and homozygous offspring from *Ndr2* heterozygous intercrosses are born in the expected Mendelian ratio. Genotypes were determined at weaning

***NDR1* protein and phosphorylation levels are up-regulated in distinct *Ndr2* knock-out tissues**

NDR2 levels are up-regulated upon ablation of NDR1, suggesting a compensatory link between the two isoforms (1). More precisely, up-regulation of NDR2 occurs particularly in tissues with high *Ndr1* expression in the wild type situation, notably thymus, spleen and lymph nodes (1). In general, *Ndr1* and *Ndr2* expression patterns partially overlap. So far, all mouse tissues examined expressed at least one of the two *Ndr* isoforms. While NDR1 protein levels are highest in organs of the immune system – thymus, spleen and lymph nodes – NDR2 protein levels peak in the colon and the brain (1-3).

To address whether loss of NDR2 protein conversely results in the up-regulation of NDR1 protein, we analyzed tissues of *Ndr2* wild type, heterozygous and knock-out littermate adult mice (Figure 2A).

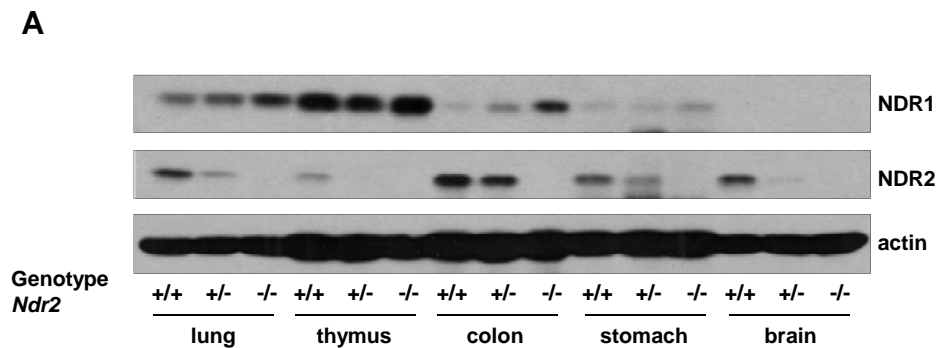


**Figure 2A NDR1 protein levels are up-regulated in distinct *Ndr2* knock-out tissues.** Westernblot analysis of NDR1 and NDR2 levels in wild type, heterozygous and homozygous *Ndr2* knock-out tissues of indicated organs. NDR2 levels are clearly gene-dose dependent. They are decreased in *Ndr2* heterozygous tissues and absent in all *Ndr2* knock-out tissues as expected. Conversely, NDR1 levels are up-regulated in lung and colon of *Ndr2* heterozygous and knock-out mice. Although NDR2 levels are intrinsically high in the brain, NDR1 levels are not up-regulated in *Ndr2* knock-out brain. Actin serves as loading control.

Our results mirrored the findings from the *Ndr1* KO (1), namely that loss of *Ndr2* resulted in an up-regulation of NDR1 in tissues with high intrinsic NDR2 levels – such as colon and lung. Moreover, we also found that mRNA levels of *Ndr1* remained constant in *Ndr2* KO colon (Figure S1, Supplementary Material), indicating that NDR1 protein

levels are increased by a post-transcriptional mechanism. The brain, however, differed from this pattern. In the wild type brain NDR2 levels were high, but we did not detect any NDR1. Even when we completely abolished *Ndr2* expression, total NDR1 protein did not come up to detectable levels. The adult brain was thus the only tissue analyzed which did not counter-act loss of endogenous NDR by the up-regulation of the remaining isoform.

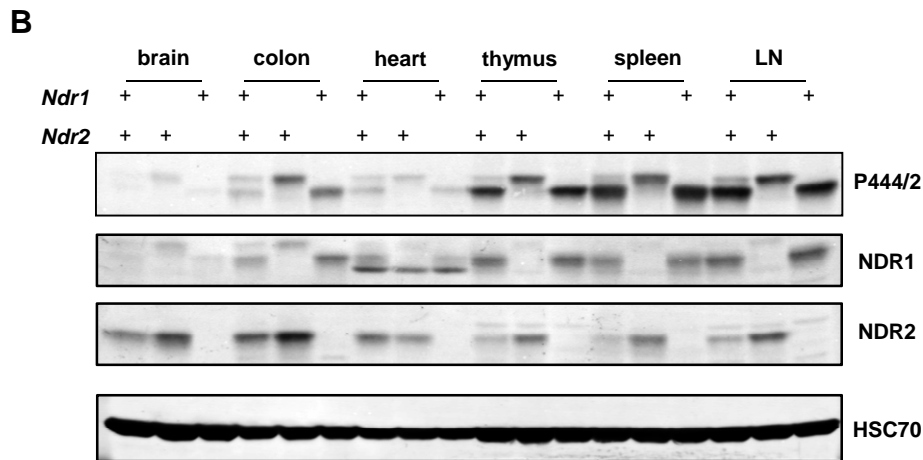


**Figure 2B.** The up-regulation of the remaining NDR isoform in *Ndr* single knock-out tissues is accompanied by hydrophobic motif phosphorylation. In colon, thymus, spleen and LN of *Ndr1* knock-out mice both total and phospho-NDR2 levels are strongly increased, suggesting that the kinase is catalytically active. Similarly, total and phospho-NDR1 levels rise in the colon of *Ndr2* knock-out mice. Hydrophobic motif phosphorylation in wildtype, *Ndr1* and *Ndr2* single knock-out tissues was detected by the phospho-444/2 antibody. Upper band in 444/2 panel: NDR2; lower band: NDR1 phosphorylated at the hydrophobic motif. HSC-70 serves as loading control. LN: lymph nodes. Amount of protein loaded per lane: 1 mg.

Human NDR was recently shown to play a role in centrosome duplication (6), apoptosis (7) and c-myc stabilization in the context of cell cycle progression (5). In all three processes, hydrophobic motif phosphorylation is essential as rescue-experiments with T444A mutants do not restore the wild type situation. Therefore, we asked whether the up-regulation of NDR protein was paralleled with an increase in hydrophobic motif (HM) phosphorylation, also indicative of catalytically active NDR. We found prominent increases in HM phosphorylation of NDR2 in thymus, spleen and lymph nodes of *Ndr1* deficient mice, where it is almost absent in the wild type and strongly up-regulated in

*Ndr1* knock-out tissue (Figure 2B). Similarly, phospho-HM levels of NDR1 rose – albeit to a lesser extent – in the colon when *Ndr2* was lost. On the contrary, we barely detected phospho-HM of either NDR1 or NDR2 in the brain although total NDR2 levels were high in wild type mice. The complete absence of NDR in *Ndr2* KO brain is exceptional and warrants in depth analysis of *Ndr2*<sup>-/-</sup> brains, especially in light of the finding that *Pax6* was down-regulated 1.5 fold in *Ndr1/2* double KO mouse embryos at E8.5 (data not shown, available upon request). *Pax6* KO mice display an axonal wiring defect (28). In summary, we show that the increase in protein levels of the remaining NDR isoform was paralleled by an increase in HM phosphorylation, suggesting that it is catalytically active. Taking into account that HM phosphorylation was shown to be essential for the three biological functions of the kinase described so far, our findings support the hypothesis that mammalian NDR1 and NDR2 can compensate for each other.

### ***The compound Ndr1/Ndr2 double knock-out is embryonic lethal***

To address whether NDR kinases play an essential *in vivo* role in mammalian biology, we generated the compound *Ndr1/Ndr2* double knock-out by crossing the respective *Ndr* single KOs. When we intercrossed *ndr1*<sup>+/-</sup>*ndr2*<sup>+/-</sup> mice, we did not obtain any double knock-out offspring (Table 1). All other genotypes were represented in approximately the expected mendelian ratio. Moreover, they were fertile and did not present any overt phenotype. This indicates that complete absence of NDR results in embryonic lethality while a single remaining *Ndr* allele is sufficient for normal development and reproduction.

**Table 1 The *Ndr1/2* double knock-out is embryonic lethal but a single *Ndr*-allele is sufficient for normal development.** Genotype distribution of offspring from *Ndr1/2* double-heterozygous intercrossings at weaning. No *Ndr1/2* double KO embryos were detected. All other genotypes were obtained at approximately the expected Mendelian ratio. Total numbers and expected and obtained ratios are indicated.

<i>Ndr1-Ndr2</i> GT	wt-wt	wt-ko	ko-ko	ko-wt	wt-het	het-ko	ko-het	het-wt	het-het
offspring numbers	37	23	0	28	44	54	42	53	134
theoretical (%)	6.25	6.25	6.25	6.25	12.5	12.5	12.5	12.5	25
actual (%)	8.92	5.54	0.00	6.75	10.60	13.01	10.12	12.77	32.29

n = 415

To elucidate how lack of NDR results in embryonic lethality, we intercrossed *Ndr* single allele mice. We collected embryos at different stages of development to determine the time window of embryonic lethality and did not detect *Ndr*-null embryos after embryonic day (E) 10.5. At E10.5, we recovered *Ndr1/2* double KO embryos which were severely growth retarded and had already started to undergo the resorption process (data not shown), indicating that NDR is essential for normal embryonic development prior to this time-point. Therefore, we analyzed embryos at earlier time-points, namely E8.5 and E9.5. At these stages, double KO embryos were detected at the expected Mendelian ratio (Table 2).

**Table 2 Complete loss of *Ndr1/2* is embryonic lethal around E10.** Genotype distribution of offspring from *Ndr*-single allele matings at indicated time-points. Between E8.5 and E9.5 *Ndr*-null embryos were recovered in the expected Mendelian ratios. All mutant embryos that were recovered at E10.5 were dead and had started to undergo the resorption process, indicating that mammalian NDR kinases are essential for survival beyond E9.5.

stage	<i>Ndr1-Ndr2</i> genotype					
	het-het	het-ko	ko-het	ko-ko	unknown	total
E8.5 - E9.5	53	54	56	56	7	226
E10.5	4	6	5	5 <sup>a</sup>	1	21
postnatal	69	65	59	0	0	193

<sup>a</sup>: all embryos recovered at E10.5 were dead and had started to disintegrate

Gross analysis revealed that at E8.5 mutant embryos were slightly smaller and developmentally delayed as judged by somite numbers (3A, B). While normal littermates had developed an average of ten somites, mutant embryos had only between six and seven (Figure 3C). Significantly, mutant somites appeared smaller and less well defined. The notochord, a rod-like structure underlying the neural tube (29), patterns the surrounding tissues, including somites, by secreting the morphogen Sonic Hedgehog (30-34). While Shh is essential for notochord maintenance (30), notochord formation critically depends on the T-box transcription factor T/Brachyury (35-39). To address whether altered somite morphology in *Ndr*-null embryos was a result of compromised notochord function, we analyzed the expression patterns of *Brachyury* and *Sonic hedgehog* (*Shh*) (Figure S2, Supplementary Material). Expression of both genes was normal in *Ndr*-null embryos at E8.5, indicating that NDR is dispensable for the formation of a continuous notochord and *Shh* expression.

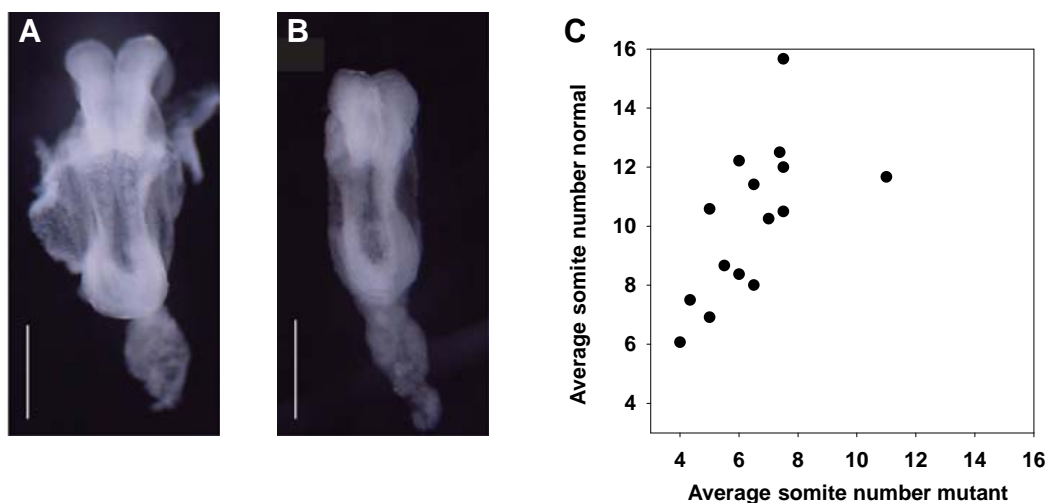


**Figure 3. *Ndr1/2*-null embryos are smaller and developmentally delayed from E8.5.** Brightfield image of **A** normal and **B** *Ndr*-null (mutant) littermate at E8.5, both embryos are at the 6-somite stage. Mutant somites are small and irregular. **C** Average somite numbers of normal and mutant littermates at E8.5. Mutant embryos are developmentally delayed by approximately 4 somites Average somite number normal embryos: 10.2, mutant embryos: 6.4. n = 15 litters. Scale bar in A, B: 0.5 mm

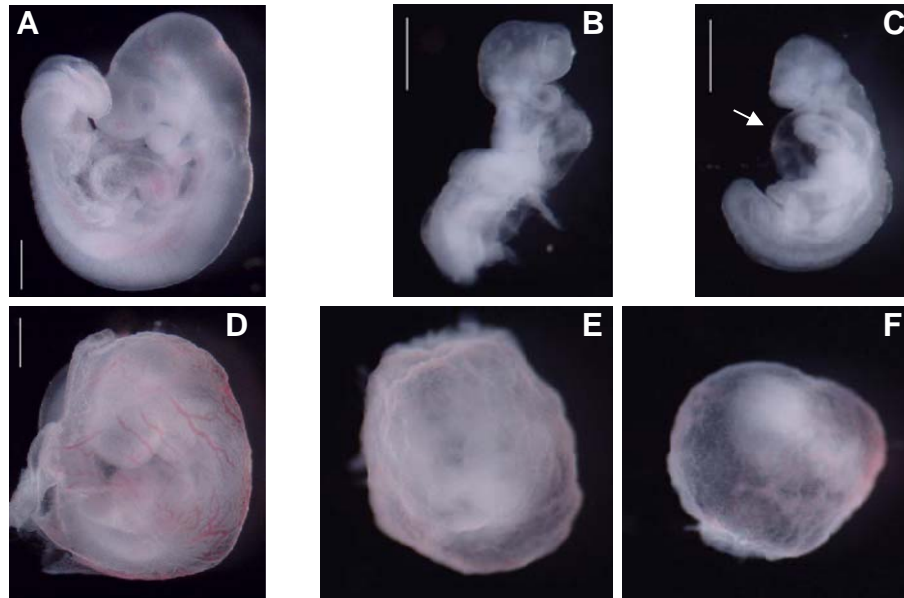


**Figure 4. *Ndr*-null embryos fail to remodel yolk sac vasculature and develop pericardial edema by E9.5** A normal littermate (A) and its yolk sac (D) and two mutants (B,C) and their yolk sacs (E,F) are shown. Mutant embryos (B, C) are significantly smaller, not all mutants have completed embryonic turning (B), yolk sac vasculature has not been remodeled (E,F). Distinct remodeled vessels are apparent in the normal yolk sac (D). Significantly, several mutants have developed pericardial edema (C, arrow), indicative of cardiac insufficiency. Heartbeat was detected in mutant embryos until E9.5. Scale bars = 0.5 mm.

At E9.5, the size difference between mutant and normal littermates had approximately doubled (Figure 4) and about half of the mutant embryos were still unturned. In normal embryos, the turning process is initiated at the six to eight somite stage (40). Moreover, about half of the mutants had developed pericardial edema (Figure 4C), indicative of pathologic fluid accumulation in the heart region due to cardiac malfunction. However, we did observe cardiac contractions in several mutants at E9.5. Mutant yolks sacs also differed strikingly from their normal counterparts. While the vascular plexus of normal yolk sacs had undergone extensive remodeling and macroscopic vessel structures filled with red blood cells were readily detectable, large remodeled vessels were absent in mutant yolk sacs (Figure 4E,F). We did observe a faint mesh of red lines in certain areas of mutant yolk sacs, indicating that primitive hematopoiesis had taken place to some extent. Moreover, mutant yolk sacs had a distinct “ruffled” appearance. The



allantois of mutant embryos, however, appeared always well developed and had attached to the chorion. The allantois is primarily of mesodermal origin (41), indicating that loss of NDR did not negatively affect mesoderm formation in general. In summary, we show that NDR kinases are essential for embryonic development and survival beyond E10.5. From early somite stages onwards, the size of *Ndr*-null embryos was reduced compared to normal littermates. Secondly, mutant somites were smaller and irregularly shaped. Thirdly, mutant heart function appeared compromised and vessel remodeling in the yolk sac had not taken place by E9.5. Our findings thus confirm that the up-regulation observed in the respective *Ndr* single knock-outs represents functional compensation by the remaining isoform.

***The cyclin dependent kinase inhibitors p21 and p27 are up-regulated in Ndr-null embryos***

To pursue our search for a molecular explanation of the observed embryonic lethality, we performed microarray analysis of *Ndr*-null versus normal embryos. Although the phenotype was more severe in E9.5 mutant embryos, we focused our analyses on E8.5 embryos to address the primary defect caused by loss of NDR. Both *Ndr1* and *Ndr2* are broadly expressed at E8.5 as assessed by RNA *in situ* hybridization (Figure S3, Supplementary Material). At this stage, embryonic development proceeds extremely fast reflecting rapid gene expression changes. Therefore, we set our experimental window to include only embryos with seven to nine somites. The complete lists of up- and down-regulated genes is available upon request and will be deposited in the Gene Expression Omnibus (GEO) of the NCBI (National Center for Biotechnology

Information) at the time of publication. Microarray analysis revealed that *cdkn1a* and *cdkn1b* transcripts, encoding the cyclin-dependent kinase (CDK) inhibitors p21 and p27, respectively, were each up-regulated about 1.5 fold in NDR-deficient embryos (Table 3A).

**Table 3. CDK inhibitors and somitogenesis-related genes are deregulated in *Ndr*-null embryos at E8.5.** mRNA of *Ndr*-null and *Ndr* double heterozygous male embryos was subjected to microarray analysis as described in Materials and Methods. **A** Transcripts of *Cdkn1A* and *Cdkn1B* – encoding the CDK inhibitors p21 and p27 – are up-regulated in *Ndr*-null embryos. **B** Somitogenesis-related genes are down-regulated in *Ndr*-null embryos. For each gene, p-value and linear fold change are indicated. N = 3 embryos

<b>A</b>	linear FC	Gene symbol	Description	p-Value
	+1.50	<i>Cdkn1a</i>	cyclin-dependent kinase inhibitor 1A (P21)	0.0011
	+1.48	<i>Cdkn1b</i>	cyclin-dependent kinase inhibitor 1B (p27)	0.0193
	+1.45	<i>Klf6</i>	Kruppel-like factor 6	0.0013

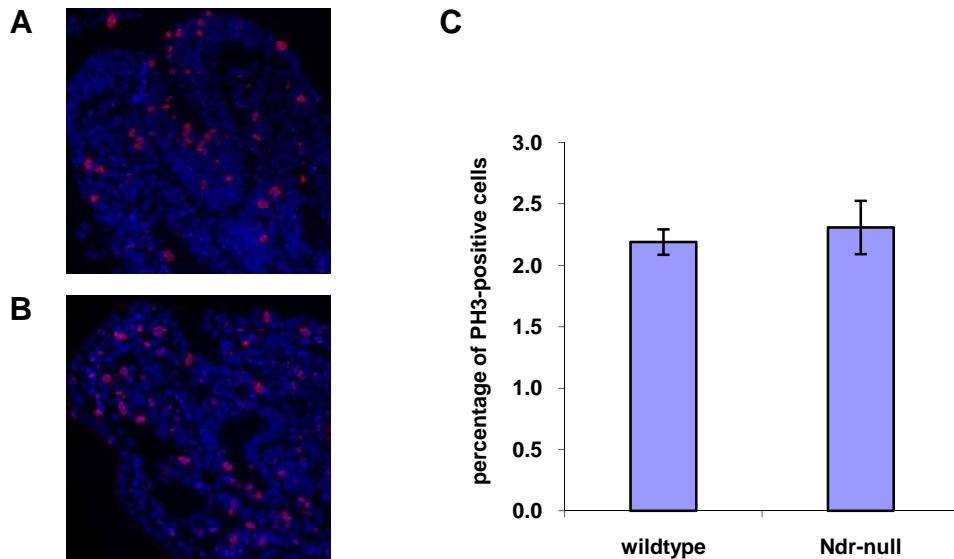
  

<b>B</b>	linear FC	Gene symbol	Description	p-Value
	-1.61	<i>Meox1</i>	mesenchyme homeobox 1	0.0005
	-1.33	<i>Tbx6</i>	T-box 6	0.0011
	-1.33	<i>Aldh1a2 = Raldh2</i>	aldehyde dehydrogenase family 1, subfamily A2	0.0224
	-1.30	<i>Dll1</i>	delta-like 1 ( <i>Drosophila</i> )	0.0018
	-1.30	<i>Sfrp1</i>	secreted frizzled-related protein 1	0.0076
	-1.29	<i>Dll3</i>	delta-like 3 ( <i>Drosophila</i> )	0.0422
	-1.28	<i>Msgn1</i>	mesogenin 1	0.0105
	-1.27	<i>Meox2</i>	mesenchyme homeobox 2	0.0193
	-1.21	<i>Lfng</i>	lunatic fringe	0.0207

Moreover, *klf6* transcript levels were also up-regulated 1.45 fold. The *Klf6* gene encodes the transcription factor Krüppel-like 6 which directly activates transcription of *Cdkn1A* both *in vitro* and *in vivo* (42, 43). The up-regulation of cell cycle inhibitors could negatively affect proliferation and thus provide a straightforward explanation for the reduced size of *Ndr*-null embryos. Although the list of differentially-regulated genes did not contain an apoptotic signature, we performed TUNEL analysis on embryo sections to exclude that the observed size reduction of *Ndr*-null embryos was due to an

increased rate of apoptosis. As expected, we detected only very few apoptotic cells in both normal and mutant embryos (S4, Supplementary Material). In summary, we present initial evidence that the size reduction of *Ndr*-null embryos might be due to the concurrent up-regulation of the two CDK inhibitors p21 and p27.

To address whether the up-regulation of *p21* and *p27* resulted in a decreased proliferation rate, we tested three different cellular markers for proliferation, namely Ki67, BrdU incorporation and histone 3 phosphorylation (poshpo-H3). We dismissed Ki67 because almost every cell both in wild type and mutant embryo sections stained positive. BrdU labeling of cells in the embryo was more restricted but introduces additional variables into the analysis. In particular, BrdU is injected into the mother and reaches the embryo via its yolk sac. As described above (Figure 4E,F), *Ndr*-null yolk sacs were clearly affected and might thus influence the final incorporation rate into dividing cells in the embryo. Therefore, we determined the proliferation index of wild type and mutant embryos based on the fraction of phospho-H3-positive cells. Serine 10 of histone 3 is strongly phosphorylated in mitotic cells (44). Representative embryo sections stained with an anti-phospho-H3 antibody are shown in Figure 5. Unexpectedly, we found the proliferation index – defined as the percentage of phospho H3 positive cells over total cells – to be almost identical in both groups (Figure 5C). In conclusion, the immunohistochemical approximation of the mitotic cell fraction did not confirm a decreased proliferation rate in *Ndr*-null embryos at E8.5. However, this does not exclude the possibility that complete loss of NDR did result in a proliferation defect which might have been too small to be picked up by this method. Only FACS analysis of total embryos could provide a definitive evaluation of these hypotheses.



**Figure 5. The mitotic index of wildtype and *Ndr*-null embryos is comparable at E8.5.** Mitotic cells in **A** wildtype and **B** *Ndr*-null embryos were labeled on paraffin sections with an anti-phospho Histone 3 antibody, nuclei were counterstained by DAPI. The mitotic index was defined as the percentage of phospho-H3 positive cells per embryo. **C** Quantitative approximation of the mitotic index of wildtype and *Ndr*-null embryos. Four embryos per genotype and five sections per embryo were quantified, amounting to a total of > 40 000 cells counted per genotype. Error bars indicate the standard error of the mean (SEM).

### ***Abnormal somite morphology in NDR deficient embryos***

As described earlier, *Ndr*-null mutants also displayed smaller and irregularly shaped somites. Significantly, our microarray data also contained a set of down-regulated genes that are predominantly expressed in somites or implicated in somitogenesis (Table 3B). The most prominently down-regulated gene, ***Meox1***, is a transcription factor commonly used as a somite marker (45). The second member of the Meox family, ***Meox2***, is also down-regulated in *Ndr*-null embryos. Concerted action of MEOX1 and MEOX2 is required upstream of genetic pathways essential for the formation, patterning and differentiation of somites (46). The transcription factor ***Tbx6*** is expressed in the presomitic mesoderm (PSM) (47) and was reduced in *Ndr*-null embryos as well. Reduced levels of *Tbx6* result in defective somite patterning (48, 49). *Tbx6* and WNT signaling synergistically controls the expression of ***Mesogenin1***, a transcription factor

that is essential for maturation of the PSM and that was also down-regulated in *Ndr*-null embryos (50). Expression of ***Sfrp1*** (secreted frizzled-related protein 1) was also decreased in mutant embryos. Members of the Sfrp family bind directly to WNT proteins and thus antagonize WNT signaling (51, 52). *Sfrp1* was shown to regulate anterior-posterior axis elongation and somite segmentation in conjunction with *Sfrp2* in the mouse embryo (53). Lastly, three components of the Notch pathway were down-regulated in NDR deficient embryos, namely ***Lunatic fringe (Lnfg)*** and the Notch ligands ***Dll1*** and ***Dll3***. LNFG negatively regulates Notch signaling and *Lnfg*-null mice present somitogenesis defects (54). Dll1 and Dll3 play each essential roles in somite formation (55, 56) and cooperate to establish inter-somitic boundaries (57). In summary, all genes described above are tightly linked to somitogenesis and their down-regulation reflects the somite defect detected in NDR deficient embryos. Loss of NDR negatively affected three components of the Notch pathway, indicating that NDR might interact with it.

To validate and expand our microarray data on the somite phenotype, we performed RNA *in situ* hybridization and histological analyses. *In situ* hybridization confirmed that *Tbx6* levels were significantly down-regulated in *Ndr*-null embryos (Supplementary Materials, Figure S5). In wild-type embryos, *Meox1* was uniformly and strongly expressed in all somites and clearly demarcated somite borders from the surrounding tissue. Distances along the anterior – posterior (A-P) axis between neighboring somite pairs were evenly spaced (Figure 6A, left embryo). This was not the case in the *Ndr*-null embryo, where *meox1* levels were generally decreased, somite borders were fuzzy and distances between somites on the AP axis tended to vary

between the left and the right somite (Figure 6A, right embryo). Moreover, the location of the most recently formed somite was unclear. These findings confirmed a decrease in *Meox1* levels and further highlighted the altered somite morphology in *Ndr*-null embryos. Next, we analyzed the polarity of mutant and normal somites. Within the newly formed somite, expression of *Uncx4*, a member of the paired-related class of homeodomain transcription factors, is restricted to the caudal half (58). This caudal restriction was maintained in *Ndr*-null embryos at the six and eight somite stage (Figure 5B, C and data not shown, respectively), indicating that cranio-caudal polarity was established. However, as already observed with the *Meox1* expression domains, *Uncx4* levels were heterogeneous and not contained within clear borders. Distances between A-P neighbor somite pairs were symmetrical in the wild type, but again unevenly spaced in the mutants.

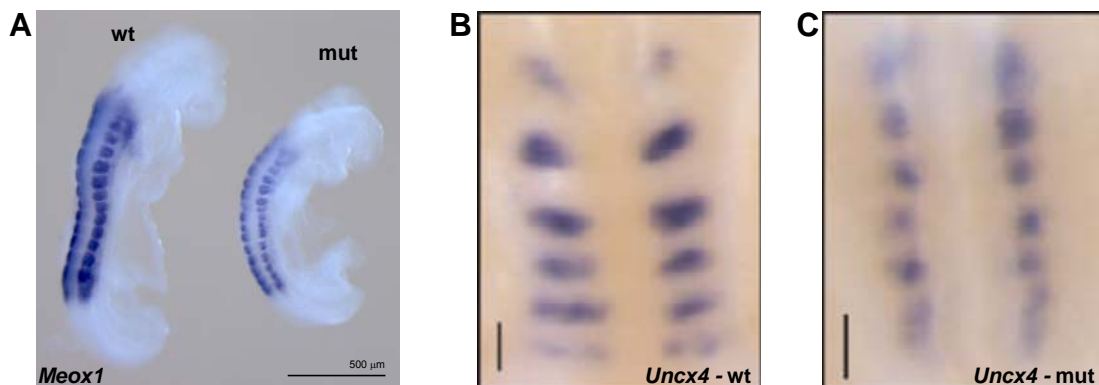


**Figure 6 Altered somite morphology in *Ndr*-null embryos at E8.5.** A *Meox1* mRNA *in situ* hybridization demarcates small and irregularly shaped somites in mutant embryos (right) compared to normal littermate (left) B,C *Uncx4* *in situ* hybridization of wildtype (B) and mutant (C) embryos reveals that rostro-caudal identity is correctly established in mutant embryos.

We subsequently performed H&E stainings on paraffin sections to further analyze somite morphology at the cellular level. Transversal and parasagittal sections of wild type and *Ndr*-null somites at the six somite stage revealed that size and cell number of mutant somites were significantly reduced (Figure 7A-D). In summary, we show that the

absence of NDR lead to a down-regulation of somite markers and genes implicated in somitogenesis by E8.5. Three of these genes belong to the Notch pathway. Mutant somites retained their internal A-P polarity but were irregularly shaped and spaced over the embryonic A-P axis. Moreover, they were smaller due to a decrease in cell number. We conclude that NDR is essential for proper somite formation and spacing along the A-P axis and might exert this effect via interacting with the Notch pathway.

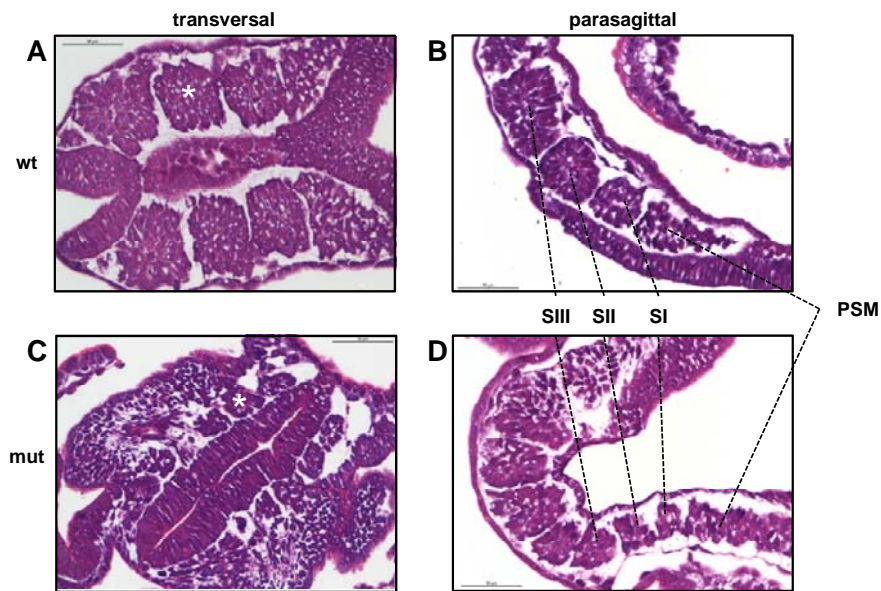


**Figure 7. Somites of *Ndr*-null embryos are smaller and contain less cells than wildtype somites.** Hematoxylin/Eosin staining of transversal (A,C) and parasagittal (B,D) sections of wildtype (A,B) and mutant (C,D) embryos at the 6-somite stage show that mutant somites (C, white asteriks) are significantly smaller and contain less cells than their wildtype counterparts (A, white asteriks). PSM: presomitic mesoderm; SI, SII, SIII: first, second and third somite. Scale bars = 50  $\mu$ m

### ***Asymmetric expression patterns of Notch pathway components in the presomitic mesoderm of *NDR* deficient embryos***

Somitogenesis is a highly symmetrical process. Pairs of somites periodically pinch off from the anterior tip of the PSM until a species-specific number of somite pairs has been generated. The so-called segmentation clock interacts with the wave front, an

anterior - posterior gradient of specific factors, to coordinate the reiterative process of somite formation (reviewed in (59)). The wave front was found to be an opposing gradient of retinoic acid (RA) and FGF8 (60). RALDH2 is the main enzyme responsible for RA synthesis in the embryo (61-63). At E8.5, *Raldh2* is expressed in the somites, the trunk mesoderm and the anterior PSM (62, 64), while *Fgf8* is expressed in the posterior PSM and certain regions of the developing brain (65). To address whether loss of NDR disturbs this gradient, we determined the expression patterns of *Raldh2* and *Fgf8* (Figure 8). We found that *Raldh2* was expressed in comparable levels in wild type and mutant embryos. *Fgf8* expression in the PSM, however, was significantly weaker in the *Ndr*-null embryo while *Fgf8* levels in anterior expression areas – such as the prospective forebrain and the midbrain-hindbrain barrier – were comparable in wild type and mutant embryos. This shows that NDR is required for high *Fgf8* expression levels in the PSM but dispensable for *Raldh2* expression.

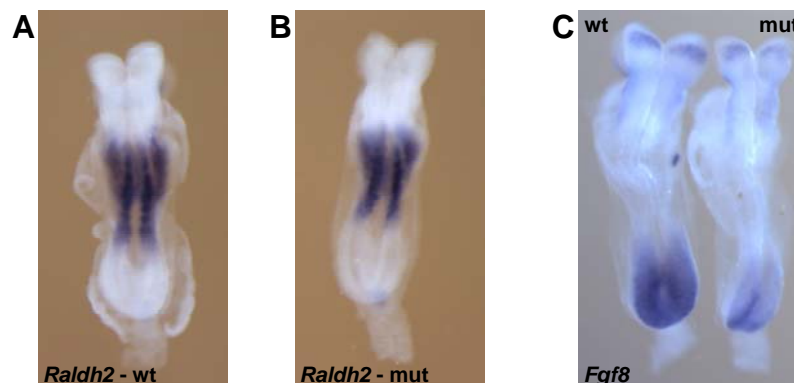


**Figure 8.** *Fgf8* levels in the presomitic mesoderm are decreased in *Ndr*-null embryos at E8.5. *Raldh2* mRNA *in situ* hybridization in wildtype (A) and mutant (B) embryos indicates similar expression patterns. C *Fgf8* levels are decreased in the presomitic mesoderm of mutant embryos (wildtype: left, mutant: right) but similar in anterior expression domains.



As delineated by Dequeant et al. (66), the segmentation clock is implemented through cyclic expression of distinct genes belonging to the FGF, Wnt and Notch pathways. Cyclic FGF and Notch pathway members oscillate in phase, opposite to cyclic *Wnt* genes. Therefore, we analyzed the expression patterns of representative cycling members of the respective pathways by *in situ* hybridization. *Axin2*, a central cycling component of the Wnt pathway, was normally expressed in *Ndr*-null embryos (data not shown).

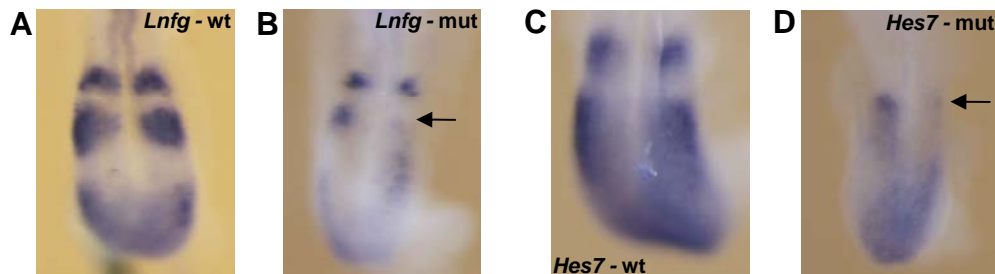


**Figure 9. The Notch pathway components *Lnf-g* and *Hes7* are asymmetrically expressed in *Ndr*-null embryos at E8.5. A,B** *Lnf-g* expression is lost in the posterior expression domain (arrow) on the right side in mutant embryos (A: wildtype, B: mutant). In general, *Lnf-g* expression is reduced, confirming the microarray data. **C,D** *Hes7* expression is lost in the anterior expression domain on the right side (arrow) in mutant embryos (C: wildtype, D: mutant).

However, *Lunatic fringe* (*Lnf-g*), a negative regulator of the Notch pathway, was asymmetrically expressed in approximately half of the *Ndr*-null embryos, while it was always symmetrically expressed in wild-type embryos (Figure 9 A,B). Moreover, the size of the prominent posterior expression stripe was significantly reduced in all mutants. A second oscillating member of the Notch pathway, *Hairy and enhancer of Split 7* (*Hes7*), was also asymmetrically expressed, albeit to a less striking degree, in mutant embryos only (Figure 9 C,D). Furthermore, *Hes7* levels were decreased in *NDR*-deficient embryos. Of note, asymmetric loss of expression of both *Lnf-g* and *Hes7* was always observed on the right side of the mutant PSM, although additional embryos have to be

analyzed to establish whether this finding is statistically significant. In summary, our findings show that loss of NDR negatively regulates *Fgf8* levels in the PSM while *Raldh2* expression is unaffected. Moreover, they indicate that NDR positively regulates both expression levels and symmetry of Notch pathway genes in the PSM, further supporting the hypothesis that NDR might interact with the Notch pathway.

### ***NDR is essential for cardiac looping***

Aberrant somitogenesis is unlikely to account for embryonic lethality. *Meox1/2* double KO mice show severely disrupted somite morphology and do not develop an axial skeleton, however, they survive until birth (46). The first organ that is essential for survival of the developing embryo is the heart (67). The primitive linear heart tube is established around E8.0 (68, 69). Consistent heart beat is detectable at the 3-somite stage followed by the onset of blood flow between the 4- to 6-somite stage (70, 71). The transition from the linear heart tube to the four-chambered adult heart proceeds via a process termed “cardiac looping” and represents the first symmetry-breaking event in the embryo. The initial steps of cardiac looping occur between E8.0 and E8.5 (8) and are categorized as looping stage (LS) 0 to III (72). When we analyzed the hearts of *Ndr*-null embryos at E8.5, we found that they were in LS-II (Figure 10C), while hearts of normal littermates had proceeded to LS-III with prominent rightward looping (Figure 10 A). Additionally, mutant hearts had adopted a bulbous character and appeared less transparent than wild type controls (Figure 10 C,D), suggesting a thickened myocardium and reduced heart lumen. To determine whether this phenotype resulted from a developmental delay or a developmental arrest, we analyzed embryos at E9.5. As

shown in Figure 10 G,H, hearts of mutant embryos at E9.5 where still in LS-II, indicating that heart development had arrested at this stage. Consequently, we never observed rightward looping of *Ndr*-null hearts. Importantly, the remainder of the mutant embryo had continued to develop – although slower than normal littermates (see also Figures 3 and 4) – indicating that only cardiac development had come to a complete arrest. The occurrence of pericardial edema in several mutant embryos at E9.5 (Figure 4C) is also indicative of defective heart development.

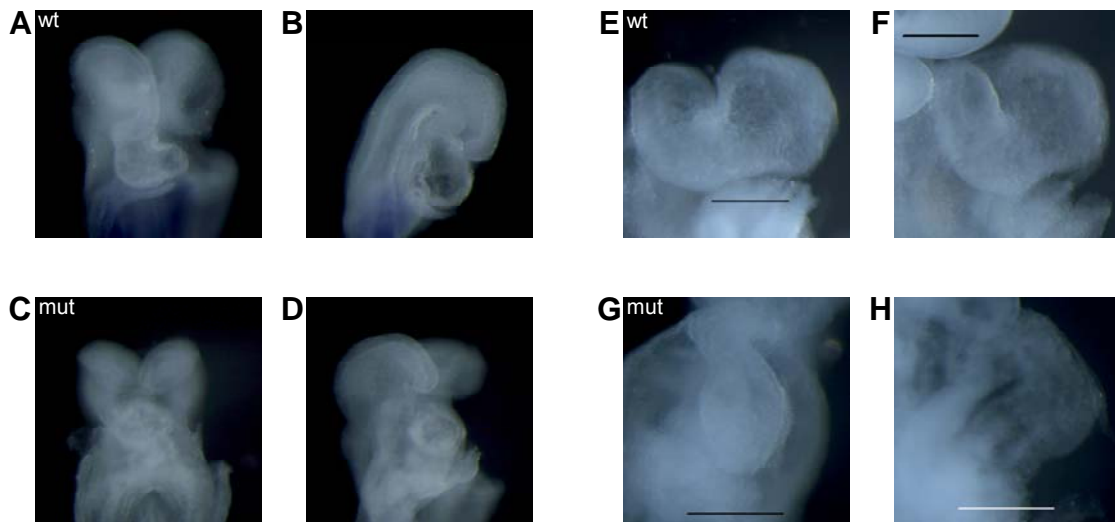


**Figure 10. Cardiac looping arrest and bulbous heart tubes in *Ndr*-null embryos at E8.5.** By E8.5, the heart tube of wildtype embryos has undergone rightward cardiac looping (A) and appears transparent in the lateral view (B). Heart tubes of *Ndr*-null embryos have not initiated looping (C) and display a bulbous and opaque heart tube (C,D). At E9.5, wildtype hearts have continued the looping process (E,F) while mutant hearts have remained arrested at the onset of cardiac looping (G,H). Images A-D were taken at 115x magnification. Scale bars in E-H: 100 nm. A,B: ventral and lateral view of wildtype embryo at E8.5; C,D: ventral and lateral view of mutant embryo at E8.5; E,F: ventral and lateral view of wildtype embryo at E9.5; G,H: ventral and lateral view of mutant embryo at E9.5

To analyze altered heart morphology in *Ndr*-null embryos on the cellular level, we performed H&E stainings on paraffin sections of mutant and wild type embryos at the 6-somite stage (Figure 11). We found the myocardium to be thickened (Figure 11F-G) and the heart lumen to be filled with abnormal cell masses, resulting in the opacity of mutant hearts described above. Both partial constriction and obstruction reduce the flow of

plasma and blood even in the presence of normal cardiac contraction. Plasma and blood flow are critical to sustain and promote embryonic development on different levels. In particular, remodeling of the yolk sac vasculature was shown to depend on hemodynamic forces exerted by plasma and blood flow (71). The reduction of flow could thus explain the yolk sac vasculature remodeling defect observed in *NDR* deficient embryos (Figure 4E,F). On these grounds, we conclude that cardiac malformation is the primary cause for embryonic lethality of *Ndr*-null embryos.

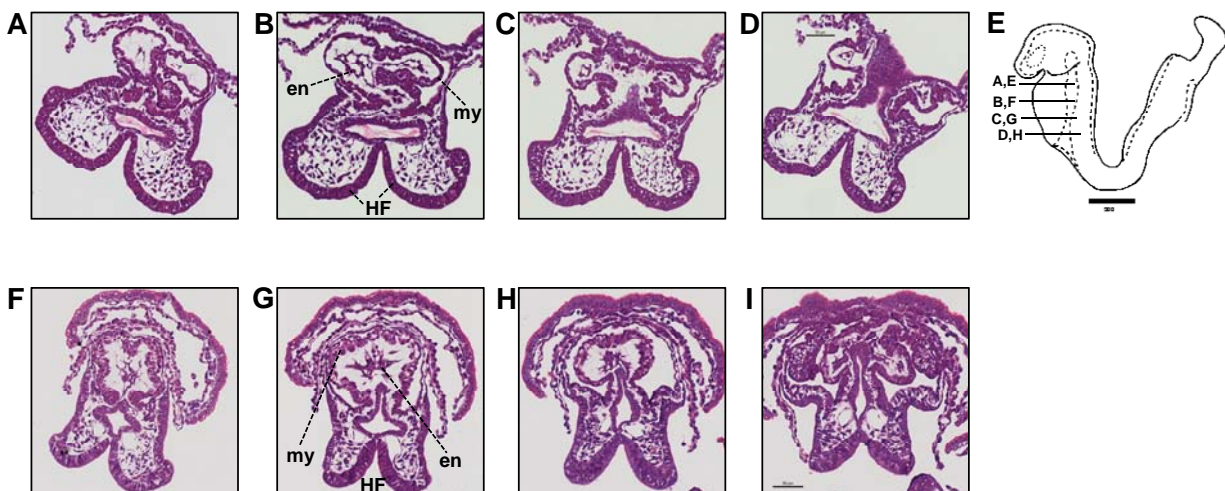


**Figure 11. Thickened myocardium and abnormal endocardium in *Ndr*-null hearts at E8.5.** Transversal sections of a wildtype (A-D) and a mutant (F-I) heart at the 6-somite stage. Thickened myocardium and abnormally expanded endocardium are most likely the cause for cardiac insufficiency and embryonic lethality of *Ndr*-null embryos. E: schematic representation of the localization of the sections within the embryo. Myocardium (my), endocardium (en) and headfolds (HF) are indicated in B and G. Distance between the sections ~ 30  $\mu$ m

Interestingly, we did detect heart beat in both E8.5 and E9.5 mutant embryos and obtained comparable numbers of beating foci when we differentiated *NDR* pro- and deficient ES cells into cardiomyocytes (Supplementary Materials, Figure S6), indicating that *NDR* is dispensable for cardiac contraction. In this regard, the cardiac phenotype of *Ndr*-null embryos was almost identical to the one observed in knock-out embryos of the important cardiogenic regulator *Nkx2.5* (73). *NKX2.5* holds a pivotal position in the cardiac regulatory hierarchy and controls the expression of numerous other cardiac

transcription factors (74, 75). Of note, *Nkx2.5* transactivates the *Xin* promoter and knock-down of *Xin* in the chick results in cardiac looping defects and thickened myocardium (76). The striking resemblance of the *Ndr* and *Nkx2.5* knock-out heart phenotypes suggests that NDR might function in the same pathway as the cardiac master regulator *Nkx2.5*.

### 3.1.4 Discussion

NDR kinases are highly conserved within the eukaryote domain and play essential roles in yeast and fly (reviewed in (11)). Although loss of NDR kinases in lower eukaryotes results in embryonic lethality (13, 25-27), *Ndr1* KO mice develop normally (1). Similarly, we find that *Ndr2* KO mice are viable, fertile born in the expected mendelian ratio and do not display an overt phenotype (Figure 1). However, protein levels of the remaining NDR isoform are up-regulated in both *Ndr1* and *Ndr2* single KO mice, suggesting that they may compensate for each other ((1), Figure 2A). Moreover, we show that the up-regulation in *Ndr1* and *Ndr2* single KO tissues is paralleled by an increase in hydrophobic motif phosphorylation (Figure 2B). Given that hydrophobic motif phosphorylation is essential for NDR to exert its role in centrosome duplication and apoptosis (6, 7), this finding further supports the hypothesis that NDR1 and NDR2 compensate for each other in the respective single KOs. Combined loss of NDR1 and NDR2 results in embryonic lethality around E10 (Table 2), demonstrating that mammalian NDR kinases indeed compensate for each other and are essential for embryonic development. Interestingly, the up-stream kinases of NDR, MST1 and MST2 also exhibit mutual compensation as only the *Mst1/2* double KO is embryonic lethal (22).

This may indicate that isoform compensation is a general theme in the NDR pathway in mammals. In summary, we show that mammalian NDR kinases can compensate for each other and are essential for embryonic development.

*Ndr1/2* double KO embryos display multiple phenotypes. They are developmentally delayed and smaller from E8.5 (Figure 3) and their somites are small and abnormally shaped (Figure 6 and 7). Importantly, *Ndr*-null embryos arrest cardiac development at the onset of cardiac looping (Figure 10). To investigate the defects caused by loss of NDR on the molecular level, we have performed microarray analysis of mutant and control embryos at E8.5. Although mammalian NDR plays a role in apoptosis (1, 7), we do not observe expression changes in genes implicated in apoptosis. TUNEL analysis further confirms low and similar apoptotic cell numbers in mutant and wild type embryos (Figure S4) indicating that the reduced size of mutant embryos at E8.5 is not due to increased apoptosis. However, *cdkn1A* and *cdkn1B* transcript levels are up-regulated in mutant embryos (Table 3A). *Cdkn1A* and *Cdkn1B* encode the cyclin dependent kinase (CDK) inhibitors p21 and p27 which negatively regulate cell cycle progression by inhibiting the activity of CDKs (77-80). Therefore, increased p21 and p27 levels might result in reduced proliferation which could account for the smaller size of *Ndr*-null embryos. Indeed, a recent report shows that simultaneous knock-down of *Ndr1* and *Ndr2* in HeLa cells leads to increased p21 and p27 levels and G1-cell cycle arrest (5). A block in G1 would be expected to translate into a decrease of the mitotic fraction in the embryo. Surprisingly, the mitotic index of *NDR*-deficient and wild type embryos based on the ratio of phospho-H3 positive cells is comparable at E8.5 (Figure 5). However, in a rapidly growing embryo, even minor

increases in cell cycle duration could account for significant size differences. We have established a simple model to mathematically approximate the effect of increases in cell cycle duration from E7.5 to E8.5 in mouse development. Thereby we find that a 20% increase in mean cell cycle duration during this period would suffice to generate the 1.5 fold size difference that we observe between normal and *Ndr*-null littermates at E8.5 (Supplementary Material, Figure S7). Even smaller increases would translate into significant developmental differences if they occurred for longer time periods. Alternatively, loss of NDR could potentially affect cell size. Although we do not detect gross cell size difference by visual examination of the embryo sections, further analyses are required to exclude that loss of NDR negatively affects cell growth. Conditional primary *Ndr* double KO mouse embryonic fibroblasts will provide a complementary and homogeneous system to further characterize the function of NDR kinases in cell cycle progression in a non-transformed setting. Additional analyses, such as whole embryo FACS, are warranted to determine on which level loss of NDR negatively affects embryo growth prior to the onset of cardiac function. In summary, complete loss of NDR leads to increased *p21* and *p27* levels in the embryo. Increased *p21* and *p27* levels could result in a partial block in cell cycle progression and reduced proliferation, indicating a potential mechanism that could account for the growth defect observed in NDR kinase-deficient embryos at E8.5.

In addition to a general size reduction, NDR-deficient embryos also display small and irregularly shaped somites (Figure 6 and 7). Indeed, somite markers and genes linked to somitogenesis are down-regulated in NDR-deficient embryos at E8.5 (Table 3B), reflecting the morphological somite phenotype. Somites derive from the presomitic

mesoderm (PSM). Therefore, decreased expression levels of genes that are important for PSM maturation – such as *Tbx6* and *Mesogenin* (48-50) – or somite formation and patterning (*Meox1/2*, *Sfrp1*, *Lnfg*, *Hes7* and *Dll1/3* (46, 53-56, 81)) are expected to result in aberrant somitogenesis. *Meox1* and *Uncx4* *in situ* hybridization as well as histological analysis further illustrate small and irregularly shaped somites in *Ndr*-null embryos at E8.5 (Figure 6, 7 and 9). Interestingly, several of the affected genes belong to the Notch pathway, namely the ligands *Dll1* and *Dll3*, the negative regulator *Lunatic Fringe* and the target gene *Hes7*. Loss-of-function mouse models of all four genes display strong segmentation defects with disrupted somite patterning (54-56). The reported somite defects in these mutants are stronger than in *Ndr*-null embryos but were always analyzed after E9.5. Somite defects in NDR-deficient mutants might be also more pronounced at later stages, but general deterioration of NDR-deficient embryos precludes meaningful somite analysis after E8.5. Interestingly, at E8.5, *Lnfg* and *Hes7* transcripts are not only reduced but also asymmetrically expressed in several *Ndr*-null embryos (Figure 9), indicating that NDR kinases also contribute to symmetry decisions in the embryo. Intriguingly, *Dll1*-mediated Notch signaling is essential for left-sided *Nodal* expression in mice and *Dll1*-null mice display randomized laterality (82). Taken together, these observations point towards a potential role of NDR in (a)symmetry implementation, possibly in the context of Notch signaling. So far, NDR kinases have not been linked to Notch signaling. Interestingly, the Notch ICD bears two putative phosphorylation sites for NDR (R. Tamaskovic, unpublished observation). Therefore, it would be interesting to address a potential connection of NDR kinases and Notch signaling in the future. Its role in centriole duplication (6) could also provide a link



between NDR and symmetry. Modified centrioles, so-called basal bodies, are core components of primary cilia (83). Therefore, loss of NDR might result in defective primary cilia. Primary cilia in the node generate leftward flow of extra-embryonic fluid which induces left-restricted expression of *Nodal* and thus breaks the initially bilateral symmetry of the embryo (84-90). Importantly, impaired primary cilia function results in laterality defects in mice (91-96) and humans (summarized in (97)). Analysis of *Nodal* expression and other left-restricted factors (such as *Lefty2* and *Pitx2*) in *Ndr*-null embryos at early somite stages will show whether NDR participates in the initial breaking of bilateral symmetry in the embryo. In summary, NDR is required for proper somitogenesis and symmetrical expression of Notch pathway components in the presomitic mesoderm. Further studies addressing the potential link of NDR kinases and the Notch pathway and the role of NDR in cilia biogenesis and function in the context of L/R axis establishment are warranted.

A properly established L/R axis is essential for cardiac rightward looping. *NDR*-deficient hearts arrest at the onset of cardiac looping and present a thickened myocardium and abnormal cell masses in the heart tube lumen at E8.5 (Figure 10 and 11). Mutant embryos subsequently develop pericardial edema and fail to remodel their yolk sac vasculature, indicative of cardiac insufficiency and most likely the primary cause for embryonic death of around E10. Although loss of NDR increases resistance to apoptotic stimuli (1, 7), it seems unlikely that the thickened myocardium in *Ndr*-null mice is due to defective apoptosis because developmental apoptosis occurs primarily in the non-myocardial compartments and at later stages of heart development (98, 99).

Nevertheless, only quantitative TUNEL analysis of NDR-deficient heart tubes could formally exclude this hypothesis.

We do not observe expression changes of cardiac regulatory genes in our microarray analysis of whole embryos at E8.5 (microarray data available upon request; will be deposited in Gene Expression Omnibus (GEO) at NCBI at the time of publication). However, by E8.5 the developing embryo contains a variety of different cell types which compromises the detection of gene expression changes restricted to small cell populations such as the developing heart. Although overall transcript levels of the cardiac transcription factor *Nkx2.5* are not altered in *Ndr*-null embryos the cardiac phenotypes of *Ndr*-null and *Nkx2.5*-null embryos are strikingly similar (73). Loss of both NDR and *Nkx2.5* leads to the arrest of heart development at the onset of cardiac looping (Figure 10, (73)). Moreover, as observed in *Ndr*-null embryos (Figure 4), *Nkx2.5*-deficient yolk sacs fail to undergo remodeling of yolk sac vasculature and have a distinct “ruffled” appearance (100). In the absence of *Nkx2.5* or NDR, cardiac contractions are still observed both in the heart and in *in vitro* differentiated cardiomyocytes (Supplementary Material, Figure S6 and (73)). This indicates that loss of both *Nkx2.5* and NDR affects cardiac looping rather than cardiomyocyte differentiation. Taken together, the phenotypical similarities suggest that NDR and *Nkx2.5* act in the same pathway in the context of cardiac development. Phosphorylation of *Nkx2.5* has been reported (101), but whether this modification is functionally relevant *in vivo* and whether NDR can function as an up-stream kinase of *Nkx2.5* remains to be addressed. Although much progress has been made in deciphering the transcriptional networks that govern the patterning of the vertebrate heart (reviewed in (102-104)), the

cellular and biophysical bases of cardiac looping are less well defined (72, 105). One line of evidence proposes differential proliferation in the cardiac mesoderm (106) and the dorsal mesocardium (107) as a morphogenic driving force for cardiac looping whereby increased proliferation on the right side results in right-ward looping. This differential proliferation could be lost in the heart tube of NDR-deficient embryos. Equal proliferation rates on both sides could result in an elongation of the heart tube which might subsequently be compressed due to space constraints in the pericardial cavity leading to the thickened and bulbous character of *Ndr*-null hearts. Other lines of evidence suggest changes in myocardial cell shape, re-arrangements of intracellular actin bundles and extra-cellular matrix (ECM) remodeling as key effectors of cardiac looping (76, 107-115). Importantly, all of the proposed mechanisms implement cardiac looping based on previously established L/R identity. The knock-down phenotype of the actin bundling protein Xin (Chinese for “heart”) in chick embryos exemplifies the importance of the actin cytoskeleton in cardiac looping (76, 112, 116). *Xin*-depleted hearts display arrested or abnormal leftward cardiac looping (76). Importantly, their myocardium is thickened and forms invaginations into the heart cavity (76) as observed in *Ndr*-null hearts (Figure 11). The murine *Xin* promoter is activated by *Nkx2.5* (76), indicating that the cardiac looping arrest in *Nkx2.5*-null hearts (73) could at least in part be due to concurrent loss of Xin protein. Interestingly, over-expressed human NDR2 also co-localizes and interacts with actin and might be involved in controlling cell morphology (117). Moreover, the *Ndr* homolog *Cbk1* in yeast closely interacts with the cytoskeleton and is essential for polarized growth (12, 118, 119). Taken together, these parallels indicate that mammalian NDR might function in the re-arrangement of the

cytoskeleton during cardiac looping. In summary, our current data clearly demonstrate that NDR is essential for cardiac looping. However, whether NDR is essential to initially establish the L/R axis or whether it functions in the morphogenetic processes that interpret L/R identity to direct rightward cardiac looping remains an open question. While the cardiac phenotypes of *Nkx2.5* and *Ndr-null* embryos are very similar, only *Ndr-null* embryos are smaller than their normal littermates and developmentally delayed from early E8 (Figure 3). *Nkx2.5*-null embryos only deviate from the normal developmental rate at the 15-Somite stage, (73). This demonstrates that loss of NDR causes developmental defects prior to the onset of cardiac function, possibly via the up-regulation of *p21* and *p27* which might result in slowed embryo growth. Therefore, tissue-specific ablation of *Ndr* in the heart is warranted to specifically study the role of NDR in heart development. Embryonic lethality of the whole body *Ndr1/2* double KO precludes the identification of additional roles of NDR. Therefore, conditional ablation of *Ndr* in specific tissues and cellular systems has been initiated and will represent valuable tools to define additional *in vivo* functions of NDR kinases.

In summary, we demonstrate that mammalian NDR kinases are essential for embryonic development. Both NDR kinase isoforms compensate for each other with high efficiency, explaining the absence of a developmental phenotype in *Ndr1* and *Ndr2* single KO mice. We identify NDR kinases as positive regulators of growth, somitogenesis and heart development. Our data suggest that NDR kinases could promote growth by negatively regulating expression levels of the CDK inhibitors *p21* and *p27* in the embryo. Moreover, NDR kinases are essential for the symmetrical expression of the somite-clock genes *Lnfg* and *Hes7* in the presomitic mesoderm. The

most vital function of NDR kinases during embryonic organogenesis appears to be in cardiac looping. Proper establishment of the embryonic L/R axis is indispensable for cardiac rightward looping. Therefore, the symmetry defects in somite-clock gene expression and the cardiac looping arrest might reflect a general symmetry defect in *Ndr*-null embryos, suggesting that NDR kinases contribute to L/R symmetry decisions in the embryo.

### 3.1.5 Materials and Methods

#### ***Conditional targeting of the murine Ndr2 locus***

Genomic DNA from 129Ola (E14) ES cells served as a PCR template to generate the homology arms for the targeting vector. We used the following three primer pairs to amplify a region spanning 9080 bp of the *ndr2* locus:

F1fwd-gagcaagcttccagaaacctgatgagacctg,	F1rev-gcagatggaaatgaggactgtg;
F2fwd-gctgggataggtggataaatgg,	F2rev-gcacagggcctaacaataaacac;
F3fwd-ggtttcttgggagtcaggaactgtc,	F3rev-ctcacagactagctcaggtgac

The region encompasses exon 1 and exon 2. We introduced *loxP* sites up- and downstream of exon 2 using an over-lap PCR strategy as there are no suitable endogenous restriction sites in the vicinity of exon 2. Excision of exon 2 should result in the loss of functional NDR2 kinase because putative alternative splicing joining exon 1 and 3 or exon 1 and 4 results in a +1 frameshift which changes the catalytic lysine and thus abolishes kinase activity. We flanked the tk-neo sequence from pMC1 neo polyA

with *frt* sites to allow for later removal of the selection marker and inserted the cassette into the endogenous *XbaI* site downstream of exon 1. An additional *loxP* site was introduced upstream of the tk promoter to remove the neo gene and exon 2 at the same time when generating the complete full body *Ndr2* knock-out. The targeting vector was linearized with *SpeI* and electroporated into 129Ola cells which were subsequently grown in the presence of G418. Resistant clones were screened for the desired homologous recombination event using PCR reactions at the 5' and the 3' integration site (Primer binding sites are indicated in Figure 1A, PCR results are shown in Supplementary Materials, Figure S8). Each primer set contained one primer that bound outside of the targeting vector region in the endogenous locus sequence. Positive clones were screened for single targeting vector integration by southern blot analysis of *EcoRI* digested DNA with an internal probe hybridizing immediately up-stream of the neo cassette (Supplementary Materials, Figure S9). Finally, we sequenced all exons, intron-exon borders, *loxP* sites and *frt* sites to validate their integrity. Two independent validated clones were expanded and aggregated with d2.5 morulas followed by implantation into foster mothers. The resulting chimeric offspring was crossed with either the *Meox2*-Cre deleter (B6.129S4-*Meox2*<sup>tm1(cre)Sor</sup>/J) to obtain complete *ndr2* knock-out animals or the *Rosa*-FLP deleter strain (129S4/SvJaeSor-*Gt(ROSA)26Sor*<sup>tm1(FLP1)Dym</sup>/J) to remove the neo marker to establish the conditionally targeted *ndr2* mouse line. Both the *Meox2*-Cre and the *Rosa*-FLP deleter strain were obtained from the Jackson Laboratory, Main, USA.

### **Genotyping and gendertyping**

Genotyping reactions to distinguish between wild type (wt), full KO (fKO), floxed (fx) and conditional KO (cKO) *ndr2* alleles share a common forward primer  $5'gctgggataggtggataaatgg^3'$  and the following reverse primers:  $5'gcttaagtcttaagctcaacctc^3'$  for wt and fx, yielding PCR products of 424 bp (wt) and 513 bp (fx);  $5'gcctgcattgcagtccttagc^3'$  for the fKO allele yielding a PCR product of 843 bp and  $5'gacagtcattcatcagtgagg^3'$  for the cKO allele with a product of 665 bp. PCR reactions were performed on a Thermal Peltier Cycler (Biorad), the cycling protocol is described in Supplementary Materials (Figure S10A). Genotyping of *Ndr1* alleles was performed according to the protocol published by Cornils et al. (1). Embryo genders for the microarray experiment and ES cell genders for cardiomyocyte differentiation were determined using the smcx-1 primer ( $5'tgacagggaaaccgctgccaaattcttgg^3'$ ) and the smc4-1 primer ( $5'ctgaagcttttgctttgagcaggctac^3'$ ) yielding a single band around 300 bp for females and a double band for males. The cycling protocol is described in Supplementary Materials (Figure S10B).

### **Western blotting**

For tissue protein extracts, flash frozen tissues were homogenized in 6  $\mu$ l ice cold lysis buffer per mg tissue using a tissue homogenizer. Lysis buffer contained 50mM Tris-HCl (pH 7.5), 120 mM NaCl, 40 mM  $\beta$ -glycerophosphate and was supplemented with the following phosphatase and protease inhibitors: 1 mM NaF, 1 mM sodium pyrophosphate, 2  $\mu$ M Microcystin, 1 mM PMSF and 1 mM Benzamidine. Homogenized extracts were incubated on ice for 30 minutes prior to two consecutive centrifugation steps at 14000 g

to obtain clear lysates. For detection of NDR, samples were resolved on a 10% SDS PAGE gel, a 12% gel was used to detect MOB proteins. Total MOB1, MOB2, NDR1 and NDR2 protein as well as NDR phosphorylated at the hydrophobic motif were detected by polyclonal rabbit antibodies as described (MOB1: Hergovich et al., 2009; MOB2: Kohler et al., 2010; total NDR1 and NDR2: Cornils et al., 2010; phospho-444/2: Tamaskovic et al., 2003). The HSC-70 protein detected by a rat-monoclonal antibody (Clone 1B5, Stressgen) served as loading control. Fluorescence-labeled secondary antibodies (goat  $\alpha$ -rabbit IRDey®800CW, LI-COR Biosciences; goat  $\alpha$ -rat Alexa Fluor 680, Invitrogen) in conjunction with the Odyssey scanner (LI-COR Biosciences) were used to visualize protein bands.

### ***In situ probe synthesis***

The following probes were used: *Axin2* – Aulehla et al. (120); *Fgf8* – Crossley et al. (65); *Hes7* – Bessho et al. (81); *Lunatic Fringe* – Evrard et al. (121); 1993 #851}; *Meox1* – Mankoo et al. (122); *Raldh2* – Niederreither et al. (62); *Sonic hedgehog* – Echelard et al. (31); *T/brachyury* – Herrmann (123); *Tbx6* – Chapman et al. (47); *Uncx4* – Dequeant et al. (66). 20  $\mu$ g of each vector were linearized with the appropriate restriction enzyme. DNA was extracted by Phenol/Chloroform/Isoamylalcohol (25:24:1), precipitated with sodium acetate and taken up in 20  $\mu$ l of TE. Probe synthesis was performed by the sp6, T3 or T7 RNA polymerase at 37°C for 120 min in the presence of Placental Ribonuclease Inhibitor. Newly synthesized probes were purified by two consecutive precipitations with LPA (Linear Polyacrylamide), dissolved in TE and stored at -20°C.



### ***Whole-mount in situ hybridization***

Whole-mount in situ hybridization was performed according to Haramis et al. (124). In brief, pregnant females were sacrificed on E8.5. Uteri were removed, embryos dissected in ice cold PBS and fixed in 4% PFA over night. They were dehydrated through a graded series of MetOH and PBT (25% - 50% - 75% - 100%) and stored in 100% MetOH at -20°C until further use. At the beginning of the experiment, embryos were re-hydrated through the same graded MetOH / PBT series. All subsequent steps were performed in 2 ml Eppendorf tubes. Unless otherwise specified, each washing step was done for 5 min at room temperature. Embryos were treated with Proteinase K for 15 min which was subsequently inactivated by 2 mg / ml Glycine in PBT, followed by two washes in PBT. They were re-fixed with 4%PFA/0.2%Glutaraldehyde for 20 min and incubated in prehybridisation solution at 70°C for 1h. The prehybridisation solution (prehyb) contained: 50% formamide, 5x SSC pH 4.5, 2% blocking powder (Boehringer), 0.1%Tween, 0.5%CHAPS (Sigma), 50 µg/ml yeast RNA, 5 mM EDTA and 50 µg/ml Heparin (Sigma). 20xSSC stock solution contained 3 M NaCl, 0.3 M Sodiumcitrate:H<sub>2</sub>O<sub>2</sub>Probes and was adjusted to pH 4.5 with 1M HCl. Probes were heated to 85°C for 5 min, then added to embryos at a final concentration of 1 µg/ml and incubated at 70°C over night. Subsequently, embryos were washed with prehyb alone, followed by a graded series of 2x SSC / prehyb solutions (1/4, 1/2, 3/4). All washes were carried out at 70°C. Next, embryos were washed twice for 30 min with 2x SSC / 0.1% CHAPS at 70°C, then twice for 10 min with 100 mM maleic acid, 150 mM NaCl at pH7.5 at room temperature, followed by two additional washes with 100 mM maleic acid, 150 mM NaCl at pH7.5 at 70°C. Embryos were then washed three times with fresh TBST. Prior to antibody addition, embryos were blocked in 10% sheep serum in TBST for 60

min, then incubated in a 1:5000 dilution of anti-DIG-AP antibody (Boehringer Mannheim) in 1% sheep serum in TBST at 4°C over night. Next, embryos were washed 3 times with TBST, then five times with TBST changes every 90 min, followed by a final wash step at 4°C over night. Probe detection was performed in NTMT which contained 100 mM NaCl, 100 mM Tris pH 9.5, 50 mM MgCl<sub>2</sub> and 1% Tween-20. Embryos were washed three times in NTMT for 10 min, then incubated with 1 ml of BM purple (Roche) and protected from light. Progress of staining reaction was monitored regularly and eventually stopped with several washes in PBT, then PBS. Embryos were photographed under a Leica MZ16FA microscope (Leica), for long term storage 0.05% Azide were added to the PBS.

***Phospho-histone 3 detection and hematoxylin / eosin stainings on embryo paraffin sections***

Pregnant females were sacrificed on E8.5. Uteri were removed, embryos dissected in ice cold PBS and fixed in 4% PFA over night. Next, embryos were dehydrated through a graded EtOH / H<sub>2</sub>O series (30% - 50% - 70%). All following steps were performed in glass vials. Embryos were washed three times for 10 min with 100% EtOH, then three times for 10 min with Ultraoclear (Medite) at room temperature. Next, embryos were incubated in a 1:1 solution of HistoClear and paraffin at 60°C for 30 min. After three changes of paraffin for 20 min each, embryos were embedded on a Medite embedding station. Embedded embryos were sectioned at 2.5 µm and mounted on poly-lysine coated slides. Sections were stained for phosphorylated histone 3 on the Discovery XT system (Ventana) with antibody m14955 (Abcam) at a 1:1000 dilution. *Alexa Fluor® 568* goat *anti-mouse* IgG (Invitrogen) was used for detection at a 1:100 dilution. The FLUO

FMI staining protocol (Ventana) with slide pre-treatment by buffer CC1 (Ventana) for 30 minutes was used. Sections were mounted in Dapi-containing VectaShield mounting medium (Vector Laboratories). H&E stainings were performed with the Programmable Slide Stainer TST (Medita).

### ***Image analysis and quantification***

Phospho-H3 stained sections were analyzed by the Zeiss Z1 Widefield microscope. Images for quantification were acquired by the AxioCam MRm (Zeiss) in conjunction with the Axiovision software (Zeiss). Phospho-H3 cells and total cells were counted using the Imaris program (Bitplane Scientific Software). H&E stained sections were analyzed on the Nikon Eclipse E600 microscope, images were acquired with the Nikon DX1200 camera in conjunction with the Image Access software (Imagic).

### ***Microarray analysis of embryos***

Matings of single allele *ndr1* and single allele *ndr2* mice were setup. Pregnant females were sacrificed on day 8 after fertilization (E8.5). The uterus was dissected out and placed in PBS on ice. Embryos were dissected out with their yolk sacs. Only embryos with seven to nine somites were kept and placed into separate Eppendorf tubes filled with 200 ul of RNA later (and stored on ice until the entire litter had been processed). Next, total RNA was isolated on the same day using the Qiagen RNeasy Micro Kit. Embryos were homogenized using 1ml syringes with 26 Gauge needles. The remaining isolation procedure was carried out according to the protocol provided by the manufacturer. Genomic DNA for consecutive genotyping and gendertyping of the embryos was isolated from the flow-through of the RNeasy Micro column. To that end,

the DNeasy Blood and Tissue kit from Qiagen was used. Elution of genomic DNA was performed in a single step with 100 ul of bidest water to maximize DNA concentration. RNA concentration and purity were measured on the nanodrop apparatus (nd-1000 Spectrometer, Thermo Scientific). The *ndr1* and *ndr2* genotype were determined as detailed above. Only male embryos were used in the experiment. Embryos heterozygous for both *Ndr1* and *Ndr2* served as control for mutant embryos. All three embryos within each group – mutants and controls, respectively – originated from different litters to avoid litter-specific bias. RNA samples were stored at -80°C until all samples had been collected.

RNA was processed with the WT cDNA Synthesis & Amplification kit and labeling was performed with the WT Terminal Labeling kit from Affymetrix (Affymetrix, Santa Clara, CA) according to the manufacturer's instructions. GeneChip Mouse Gene 1.0 ST arrays were hybridized following the "GeneChip Whole Transcript (WT) Sense Target Labeling Assay Manual" (Affymetrix, Santa Clara, CA) with a hybridization time of 16h. The Affymetrix Fluidics protocol FS450\_0007 was used for washing. Scanning was performed with Affymetrix GCC Scan Control v. 3.0.1 on a GeneChip® Scanner 3000 with autoloader (Affymetrix). Probesets were summarized and probeset-level values normalized with justRMA() function from R (version 2.10.0) / Bioconductor (version 2.5) package affy using the CDF environment MoGene-1\_0-st-v1.r3.cdf (as provided by Bioconductor) and annotation from Netaffx ([www.netaffx.com](http://www.netaffx.com)). Differentially expressed genes were identified using the empirical Bayes method (F test) implemented in the LIMMA package and adjusted with the false discovery rate method (Wettenhall JM Smyth GK. limmaGUI: a graphical user interface for linear modeling of microarray data.

Bioinformatics (Oxford, England, 2004). Hierarchical clustering and visualization were done in R. Probe sets with a log 2 average contrast signal of at least 5, a P value of <0.05, and an absolute log 2 fold-change of >0.263 (1.2-fold in linear space) were selected leading to the identification of 701 genes that were up-regulated and 183 genes that were down-regulated in *Ndr*-null embryos. The complete microarray data will be available in the Gene Expression Omnibus once the manuscript has been submitted for publication. ***Paragraph provided by Tim Roloff.***

### ***ES cell isolation and cardiomyocyte differentiation***

Super-ovulated females were mated with males and sacrificed 2.5 days after plugging. Uteri were removed and flushed to obtain morulae. The zona pelucida was removed and naked morulae plated onto feeder layers of inactivated mouse embryonic fibroblasts. Upon confluency, aliquots were frozen until further use. Aliquots for genomic DNA extraction for geno- and gendertyping were plated without feeder cells. Geno- and gendertyping was performed as described above. Prior to cardiomyocyte differentiation, ES cells were passaged twice in the absence of feeder cells. Embryoid bodies were generated according to the screw cap method described by *Kurosawa et al. (125)*. In brief, 20 000 ES cells were incubated in 1ml of ES cell medium in 1.5 ml screw cap tubes (Sarstedt). After 5 days, embryoid bodies had formed and were plated in 24-well plates in the presence of 10  $\mu$ M PP2 to enhance the differentiation into cardiomyocytes as described by *Hakuno et al. (126)*. Four days after plating, the total number of beating foci per well was counted under the light microscope.

### 3.1.6 References

1. Cornils H, Stegert MR, Hergovich A, et al. Ablation of the kinase NDR1 predisposes mice to the development of T cell lymphoma. *Sci Signal.* 2010;3:ra47.
2. Devroe E, Erdjument-Bromage H, Tempst P, Silver PA. Human Mob proteins regulate the NDR1 and NDR2 serine-threonine kinases. *J Biol Chem.* 2004;279:24444-24451.
3. Stegert MR, Tamaskovic R, Bichsel SJ, Hergovich A, Hemmings BA. Regulation of NDR2 protein kinase by multi-site phosphorylation and the S100B calcium-binding protein. *J Biol Chem.* 2004;279:23806-23812.
4. Chiba S, Ikeda M, Katsunuma K, Ohashi K, Mizuno K. MST2- and Furry-mediated activation of NDR1 kinase is critical for precise alignment of mitotic chromosomes. *Curr Biol.* 2009;19:675-681.
5. Cornils H, Kohler RS, Hergovich A, Hemmings BA. Human NDR kinases control G1/S cell cycle transition by directly regulating p21 and c-myc stability. Thesis. Friedrich Miescher Institut, University of Basel 2010.
6. Hergovich A, Lamla S, Nigg EA, Hemmings BA. Centrosome-associated NDR kinase regulates centrosome duplication. *Mol Cell.* 2007;25:625-634.
7. Vichalkovski A, Gresko E, Cornils H, Hergovich A, Schmitz D, Hemmings BA. NDR kinase is activated by RASSF1A/MST1 in response to Fas receptor stimulation and promotes apoptosis. *Curr Biol.* 2008;18:1889-1895.
8. Harvey RP. Cardiac looping--an uneasy deal with laterality. *Semin Cell Dev Biol.* 1998;9:101-108.
9. Mercola M. Embryological basis for cardiac left-right asymmetry. *Semin Cell Dev Biol.* 1999;10:109-116.

10. Tamaskovic R, Bichsel SJ, Hemmings BA. NDR family of AGC kinases--essential regulators of the cell cycle and morphogenesis. *FEBS Lett.* 2003;546:73-80.
11. Hergovich A, Stegert MR, Schmitz D, Hemmings BA. NDR kinases regulate essential cell processes from yeast to humans. *Nat Rev Mol Cell Biol.* 2006;7:253-264.
12. Bidlingmaier S, Weiss EL, Seidel C, Drubin DG, Snyder M. The Cbk1p pathway is important for polarized cell growth and cell separation in *Saccharomyces cerevisiae*. *Mol Cell Biol.* 2001;21:2449-2462.
13. Geng W, He B, Wang M, Adler PN. The tricornered gene, which is required for the integrity of epidermal cell extensions, encodes the *Drosophila* nuclear DBF2-related kinase. *Genetics.* 2000;156:1817-1828.
14. Emoto K, He Y, Ye B, et al. Control of dendritic branching and tiling by the Tricornered-kinase/Furry signaling pathway in *Drosophila* sensory neurons. *Cell.* 2004;119:245-256.
15. Emoto K, Parrish JZ, Jan LY, Jan YN. The tumour suppressor Hippo acts with the NDR kinases in dendritic tiling and maintenance. *Nature.* 2006;443:210-213.
16. Gallegos ME, Bargmann CI. Mechanosensory neurite termination and tiling depend on SAX-2 and the SAX-1 kinase. *Neuron.* 2004;44:239-249.
17. Hergovich A, Bichsel SJ, Hemmings BA. Human NDR kinases are rapidly activated by MOB proteins through recruitment to the plasma membrane and phosphorylation. *Mol Cell Biol.* 2005;25:8259-8272.
18. Millward TA, Hess D, Hemmings BA. Ndr protein kinase is regulated by phosphorylation on two conserved sequence motifs. *J Biol Chem.* 1999;274:33847-33850.

19. Stegert MR, Hergovich A, Tamaskovic R, Bichsel SJ, Hemmings BA. Regulation of NDR protein kinase by hydrophobic motif phosphorylation mediated by the mammalian Ste20-like kinase MST3. *Mol Cell Biol.* 2005;25:11019-11029.
20. Tamaskovic R, Bichsel SJ, Rogniaux H, Stegert MR, Hemmings BA. Mechanism of Ca<sup>2+</sup>-mediated regulation of NDR protein kinase through autophosphorylation and phosphorylation by an upstream kinase. *J Biol Chem.* 2003;278:6710-6718.
21. Hergovich A, Kohler RS, Schmitz D, Vichalkovski A, Cornils H, Hemmings BA. The MST1 and hMOB1 tumor suppressors control human centrosome duplication by regulating NDR kinase phosphorylation. *Curr Biol.* 2009;19:1692-1702.
22. Oh S, Lee D, Kim T, et al. Crucial role for Mst1 and Mst2 kinases in early embryonic development of the mouse. *Mol Cell Biol.* 2009;29:6309-6320.
23. Song H, Mak KK, Topol L, et al. Mammalian Mst1 and Mst2 kinases play essential roles in organ size control and tumor suppression. *Proc Natl Acad Sci U S A.* 2010;107:1431-1436.
24. Dong Y, Du X, Ye J, et al. A cell-intrinsic role for Mst1 in regulating thymocyte egress. *J Immunol.* 2009;183:3865-3872.
25. Toyn JH, Araki H, Sugino A, Johnston LH. The cell-cycle-regulated budding yeast gene DBF2, encoding a putative protein kinase, has a homologue that is not under cell-cycle control. *Gene.* 1991;104:63-70.
26. Giaever G, Chu AM, Ni L, et al. Functional profiling of the *Saccharomyces cerevisiae* genome. *Nature.* 2002;418:387-391.
27. Kurischko C, Weiss G, Ottey M, Luca FC. A role for the *Saccharomyces cerevisiae* regulation of Ace2 and polarized morphogenesis signaling network in cell integrity. *Genetics.* 2005;171:443-455.



28. Hevner RF, Miyashita-Lin E, Rubenstein JL. Cortical and thalamic axon pathfinding defects in *Tbr1*, *Gbx2*, and *Pax6* mutant mice: evidence that cortical and thalamic axons interact and guide each other. *J Comp Neurol*. 2002;447:8-17.
29. Wikipedia. Notochord. Vol. 2010: Wikipedia; 2010.
30. Chiang C, Litingtung Y, Lee E, et al. Cyclopia and defective axial patterning in mice lacking Sonic hedgehog gene function. *Nature*. 1996;383:407-413.
31. Echelard Y, Epstein DJ, St-Jacques B, et al. Sonic hedgehog, a member of a family of putative signaling molecules, is implicated in the regulation of CNS polarity. *Cell*. 1993;75:1417-1430.
32. Ekker SC, McGrew LL, Lai CJ, et al. Distinct expression and shared activities of members of the hedgehog gene family of *Xenopus laevis*. *Development*. 1995;121:2337-2347.
33. Krauss S, Concordet JP, Ingham PW. A functionally conserved homolog of the *Drosophila* segment polarity gene *hh* is expressed in tissues with polarizing activity in zebrafish embryos. *Cell*. 1993;75:1431-1444.
34. Roelink H, Augsburger A, Heemskerk J, et al. Floor plate and motor neuron induction by *vhh-1*, a vertebrate homolog of hedgehog expressed by the notochord. *Cell*. 1994;76:761-775.
35. Chesley P. Development of the short-tailed mutant in the mouse house. *Journal of Experimental Zoology*. 1935;70:429-435.
36. Fujimoto H, Yanagisawa KO. Defects in the archenteron of mouse embryos homozygous for the T-mutation. *Differentiation*. 1983;25:44-47.
37. Gluecksohn-Schoenheimer S. The Development of Normal and Homozygous Brachy (T/T) Mouse Embryos in the Extraembryonic Coelom of the Chick. *Proc Natl Acad Sci U S A*. 1944;30:134-140.

38. Gruneberg H. Genetical studies on the skeleton of the mouse. XXIII. The development of brachyury and anury. *J Embryol Exp Morphol*. 1958;6:424-443.
39. Wilkinson DG, Bhatt S, Herrmann BG. Expression pattern of the mouse T gene and its role in mesoderm formation. *Nature*. 1990;343:657-659.
40. Kaufman HL. *The Atlas of Mouse Development (ed Revised)*. London: Academic Press; 1992.
41. Downs KM, Hellman ER, McHugh J, Barrickman K, Inman KE. Investigation into a role for the primitive streak in development of the murine allantois. *Development*. 2004;131:37-55.
42. Narla G, Heath KE, Reeves HL, et al. KLF6, a candidate tumor suppressor gene mutated in prostate cancer. *Science*. 2001;294:2563-2566.
43. Narla G, Kremer-Tal S, Matsumoto N, et al. In vivo regulation of p21 by the Kruppel-like factor 6 tumor-suppressor gene in mouse liver and human hepatocellular carcinoma. *Oncogene*. 2007;26:4428-4434.
44. Hendzel MJ, Wei Y, Mancini MA, et al. Mitosis-specific phosphorylation of histone H3 initiates primarily within pericentromeric heterochromatin during G2 and spreads in an ordered fashion coincident with mitotic chromosome condensation. *Chromosoma*. 1997;106:348-360.
45. Candia AF, Hu J, Crosby J, et al. Mox-1 and Mox-2 define a novel homeobox gene subfamily and are differentially expressed during early mesodermal patterning in mouse embryos. *Development*. 1992;116:1123-1136.
46. Mankoo BS, Skuntz S, Harrigan I, et al. The concerted action of Meox homeobox genes is required upstream of genetic pathways essential for the formation, patterning and differentiation of somites. *Development*. 2003;130:4655-4664.

47. Chapman DL, Agulnik I, Hancock S, Silver LM, Papaioannou VE. Tbx6, a mouse T-Box gene implicated in paraxial mesoderm formation at gastrulation. *Dev Biol.* 1996;180:534-542.
48. Watabe-Rudolph M, Schlautmann N, Papaioannou VE, Gossler A. The mouse rib-vertebrae mutation is a hypomorphic Tbx6 allele. *Mech Dev.* 2002;119:251-256.
49. White PH, Farkas DR, McFadden EE, Chapman DL. Defective somite patterning in mouse embryos with reduced levels of Tbx6. *Development.* 2003;130:1681-1690.
50. Wittler L, Shin EH, Grote P, et al. Expression of *Msgn1* in the presomitic mesoderm is controlled by synergism of WNT signalling and Tbx6. *EMBO Rep.* 2007;8:784-789.
51. Leimeister C, Bach A, Gessler M. Developmental expression patterns of mouse sFRP genes encoding members of the secreted frizzled related protein family. *Mech Dev.* 1998;75:29-42.
52. Rattner A, Hsieh JC, Smallwood PM, et al. A family of secreted proteins contains homology to the cysteine-rich ligand-binding domain of frizzled receptors. *Proc Natl Acad Sci U S A.* 1997;94:2859-2863.
53. Satoh W, Gotoh T, Tsunematsu Y, Aizawa S, Shimono A. *Sfrp1* and *Sfrp2* regulate anteroposterior axis elongation and somite segmentation during mouse embryogenesis. *Development.* 2006;133:989-999.
54. Zhang N, Gridley T. Defects in somite formation in lunatic fringe-deficient mice. *Nature.* 1998;394:374-377.
55. Hrabe de Angelis M, McIntyre J, 2nd, Gossler A. Maintenance of somite borders in mice requires the Delta homologue *Dll1*. *Nature.* 1997;386:717-721.

56. Kusumi K, Sun ES, Kerrebrock AW, et al. The mouse pudgy mutation disrupts Delta homologue Dll3 and initiation of early somite boundaries. *Nat Genet.* 1998;19:274-278.
57. Dunwoodie SL, Henrique D, Harrison SM, Beddington RS. Mouse Dll3: a novel divergent Delta gene which may complement the function of other Delta homologues during early pattern formation in the mouse embryo. *Development.* 1997;124:3065-3076.
58. Neidhardt LM, Kispert A, Herrmann BG. A mouse gene of the paired-related homeobox class expressed in the caudal somite compartment and in the developing vertebral column, kidney and nervous system. *Dev Genes Evol* 1997;207:330-339.
59. Dequeant ML, Pourquie O. Segmental patterning of the vertebrate embryonic axis. *Nat Rev Genet.* 2008;9:370-382.
60. Goldbeter A, Gonze D, Pourquie O. Sharp developmental thresholds defined through bistability by antagonistic gradients of retinoic acid and FGF signaling. *Dev Dyn.* 2007;236:1495-1508.
61. McCaffery P, Drager UC. Retinoic acid synthesizing enzymes in the embryonic and adult vertebrate. *Adv Exp Med Biol.* 1995;372:173-183.
62. Niederreither K, McCaffery P, Drager UC, Chambon P, Dolle P. Restricted expression and retinoic acid-induced downregulation of the retinaldehyde dehydrogenase type 2 (RALDH-2) gene during mouse development. *Mech Dev.* 1997;62:67-78.
63. Zhao D, McCaffery P, Ivins KJ, et al. Molecular identification of a major retinoic-acid-synthesizing enzyme, a retinaldehyde-specific dehydrogenase. *Eur J Biochem.* 1996;240:15-22.
64. Niederreither K, Fraulob V, Garnier JM, Chambon P, Dolle P. Differential expression of retinoic acid-synthesizing (RALDH) enzymes during fetal

- development and organ differentiation in the mouse. *Mech Dev.* 2002;110:165-171.
65. Crossley PH, Martin GR. The mouse *Fgf8* gene encodes a family of polypeptides and is expressed in regions that direct outgrowth and patterning in the developing embryo. *Development.* 1995;121:439-451.
  66. Dequeant ML, Glynn E, Gaudenz K, et al. A complex oscillating network of signaling genes underlies the mouse segmentation clock. *Science.* 2006;314:1595-1598.
  67. Copp AJ. Death before birth: clues from gene knockouts and mutations. *Trends Genet.* 1995;11:87-93.
  68. Harvey RP, Biben C, Elliott DA. Transcriptional control and pattern formation in the developing heart: studies on NK-2 class homeodomain factors. In: Harvey RP, Rosenthal N, eds. *Heart Development.* San Diego: Academic Press; 1999:111-129.
  69. Tam PP, Schoenwolf GC. Cardiac fate maps: lineage allocation, morphogenetic movement, and cell commitment In: Harvey RP, Rosenthal N, eds. *Heart Development.* San Diego: Academic Press; 1999:3-17.
  70. Navaratnam V, Kaufman MH, Skepper JN, Barton S, Guttridge KM. Differentiation of the myocardial rudiment of mouse embryos: an ultrastructural study including freeze-fracture replication. *J Anat.* 1986;146:65-85.
  71. Lucitti JL, Jones EA, Huang C, Chen J, Fraser SE, Dickinson ME. Vascular remodeling of the mouse yolk sac requires hemodynamic force. *Development.* 2007;134:3317-3326.
  72. Biben C, Harvey RP. Homeodomain factor *Nkx2-5* controls left/right asymmetric expression of bHLH gene *eHand* during murine heart development. *Genes Dev.* 1997;11:1357-1369.

73. Lyons I, Parsons LM, Hartley L, et al. Myogenic and morphogenetic defects in the heart tubes of murine embryos lacking the homeo box gene Nkx2-5. *Genes Dev.* 1995;9:1654-1666.
74. Stanley EG, Biben C, Elefanty A, et al. Efficient Cre-mediated deletion in cardiac progenitor cells conferred by a 3'UTR-ires-Cre allele of the homeobox gene Nkx2-5. *Int J Dev Biol.* 2002;46:431-439.
75. Gilbert SF. *Developmental Biology* (ed 9). Sunderland, Massachusetts: Sinauer Associates, Inc.; 2010.
76. Wang DZ, Reiter RS, Lin JL, et al. Requirement of a novel gene, Xin, in cardiac morphogenesis. *Development.* 1999;126:1281-1294.
77. Harper JW, Adami GR, Wei N, Keyomarsi K, Elledge SJ. The p21 Cdk-interacting protein Cip1 is a potent inhibitor of G1 cyclin-dependent kinases. *Cell.* 1993;75:805-816.
78. Hengst L, Dulic V, Slingerland JM, Lees E, Reed SI. A cell cycle-regulated inhibitor of cyclin-dependent kinases. *Proc Natl Acad Sci U S A.* 1994;91:5291-5295.
79. Polyak K, Kato JY, Solomon MJ, et al. p27Kip1, a cyclin-Cdk inhibitor, links transforming growth factor-beta and contact inhibition to cell cycle arrest. *Genes Dev.* 1994;8:9-22.
80. Slingerland JM, Hengst L, Pan CH, Alexander D, Stampfer MR, Reed SI. A novel inhibitor of cyclin-Cdk activity detected in transforming growth factor beta-arrested epithelial cells. *Mol Cell Biol.* 1994;14:3683-3694.
81. Bessho Y, Sakata R, Komatsu S, Shiota K, Yamada S, Kageyama R. Dynamic expression and essential functions of Hes7 in somite segmentation. *Genes Dev.* 2001;15:2642-2647.

82. Krebs LT, Iwai N, Nonaka S, et al. Notch signaling regulates left-right asymmetry determination by inducing Nodal expression. *Genes Dev.* 2003;17:1207-1212.
83. Dutcher SK. Elucidation of basal body and centriole functions in *Chlamydomonas reinhardtii*. *Traffic.* 2003;4:443-451.
84. Capdevila J, Vogan KJ, Tabin CJ, Izpisua Belmonte JC. Mechanisms of left-right determination in vertebrates. *Cell.* 2000;101:9-21.
85. Mercola M, Levin M. Left-right asymmetry determination in vertebrates. *Annu Rev Cell Dev Biol.* 2001;17:779-805.
86. Wright CV. Mechanisms of left-right asymmetry: what's right and what's left? *Dev Cell.* 2001;1:179-186.
87. Essner JJ, Vogan KJ, Wagner MK, Tabin CJ, Yost HJ, Brueckner M. Conserved function for embryonic nodal cilia. *Nature.* 2002;418:37-38.
88. Hamada H, Meno C, Watanabe D, Saijoh Y. Establishment of vertebrate left-right asymmetry. *Nat Rev Genet.* 2002;3:103-113.
89. Nonaka S, Shiratori H, Saijoh Y, Hamada H. Determination of left-right patterning of the mouse embryo by artificial nodal flow. *Nature.* 2002;418:96-99.
90. Tabin CJ, Vogan KJ. A two-cilia model for vertebrate left-right axis specification. *Genes Dev.* 2003;17:1-6.
91. Murcia NS, Richards WG, Yoder BK, Mucenski ML, Dunlap JR, Woychik RP. The Oak Ridge Polycystic Kidney (orp) disease gene is required for left-right axis determination. *Development.* 2000;127:2347-2355.
92. Nonaka S, Tanaka Y, Okada Y, et al. Randomization of left-right asymmetry due to loss of nodal cilia generating leftward flow of extraembryonic fluid in mice lacking KIF3B motor protein. *Cell.* 1998;95:829-837.

93. Okada Y, Nonaka S, Tanaka Y, Saijoh Y, Hamada H, Hirokawa N. Abnormal nodal flow precedes situs inversus in *iv* and *inv* mice. *Mol Cell*. 1999;4:459-468.
94. Okada Y, Takeda S, Tanaka Y, Belmonte JC, Hirokawa N. Mechanism of nodal flow: a conserved symmetry breaking event in left-right axis determination. *Cell*. 2005;121:633-644.
95. Takeda S, Yonekawa Y, Tanaka Y, Okada Y, Nonaka S, Hirokawa N. Left-right asymmetry and kinesin superfamily protein KIF3A: new insights in determination of laterality and mesoderm induction by *kif3A*<sup>-/-</sup> mice analysis. *J Cell Biol*. 1999;145:825-836.
96. Yokoyama T, Copeland NG, Jenkins NA, Montgomery CA, Elder FF, Overbeek PA. Reversal of left-right asymmetry: a situs inversus mutation. *Science*. 1993;260:679-682.
97. Fliegauf M, Benzing T, Omran H. When cilia go bad: cilia defects and ciliopathies. *Nat Rev Mol Cell Biol*. 2007;8:880-893.
98. Fisher SA, Langille BL, Srivastava D. Apoptosis during cardiovascular development. *Circ Res*. 2000;87:856-864.
99. Poelmann RE, Gittenberger-de Groot AC. Apoptosis as an instrument in cardiovascular development. *Birth Defects Res C Embryo Today*. 2005;75:305-313.
100. Tanaka M, Chen Z, Bartunkova S, Yamasaki N, Izumo S. The cardiac homeobox gene *Csx/Nkx2.5* lies genetically upstream of multiple genes essential for heart development. *Development*. 1999;126:1269-1280.
101. Kasahara H, Izumo S. Identification of the *in vivo* casein kinase II phosphorylation site within the homeodomain of the cardiac tissue-specifying homeobox gene product *Csx/Nkx2.5*. *Mol Cell Biol*. 1999;19:526-536.
102. Harvey RP. Patterning the vertebrate heart. *Nat Rev Genet*. 2002;3:544-556.



103. Buckingham M, Meilhac S, Zaffran S. Building the mammalian heart from two sources of myocardial cells. *Nat Rev Genet.* 2005;6:826-835.
104. Garry DJ, Olson EN. A common progenitor at the heart of development. *Cell.* 2006;127:1101-1104.
105. Shiratori H, Hamada H. The left-right axis in the mouse: from origin to morphology. *Development.* 2006;133:2095-2104.
106. Stalsberg H. The origin of heart asymmetry: right and left contributions to the early chick embryo heart. *Dev Biol.* 1969;19:109-127.
107. Linask KK, Han M, Cai DH, Brauer PR, Maisastry SM. Cardiac morphogenesis: matrix metalloproteinase coordination of cellular mechanisms underlying heart tube formation and directionality of looping. *Dev Dyn.* 2005;233:739-753.
108. Manasek FJ, Burnside MB, Waterman RE. Myocardial cell shape change as a mechanism of embryonic heart looping. *Dev Biol.* 1972;29:349-371.
109. Manasek FJ. Control of early embryonic heart morphogenesis: a hypothesis. *Ciba Found Symp.* 1983;100:4-19.
110. Itasaki N, Nakamura H, Sumida H, Yasuda M. Actin bundles on the right side in the caudal part of the heart tube play a role in dextro-looping in the embryonic chick heart. *Anat Embryol (Berl).* 1991;183:29-39.
111. Itasaki N, Nakamura H, Yasuda M. Changes in the arrangement of actin bundles during heart looping in the chick embryo. *Anat Embryol (Berl).* 1989;180:413-420.
112. Choi S, Gustafson-Wagner EA, Wang Q, et al. The intercalated disk protein, mXin $\alpha$ , is capable of interacting with beta-catenin and bundling actin filaments [corrected]. *J Biol Chem.* 2007;282:36024-36036.
113. Grosskurth SE, Bhattacharya D, Wang Q, Lin JJ. Emergence of Xin demarcates a key innovation in heart evolution. *PLoS One.* 2008;3:e2857.

114. Tsuda T, Philp N, Zile MH, Linask KK. Left-right asymmetric localization of flectin in the extracellular matrix during heart looping. *Dev Biol.* 1996;173:39-50.
115. Lu W, Seeholzer SH, Han M, et al. Cellular nonmuscle myosins NMHC-IIA and NMHC-IIB and vertebrate heart looping. *Dev Dyn.* 2008;237:3577-3590.
116. Pacholsky D, Vakeel P, Himmel M, et al. Xin repeats define a novel actin-binding motif. *J Cell Sci.* 2004;117:5257-5268.
117. Stork O, Zhdanov A, Kudersky A, Yoshikawa T, Obata K, Pape HC. Neuronal functions of the novel serine/threonine kinase Ndr2. *J Biol Chem.* 2004;279:45773-45781.
118. Racki WJ, Becam AM, Nasr F, Herbert CJ. Cbk1p, a protein similar to the human myotonic dystrophy kinase, is essential for normal morphogenesis in *Saccharomyces cerevisiae*. *EMBO J.* 2000;19:4524-4532.
119. Weiss EL, Kurischko C, Zhang C, Shokat K, Drubin DG, Luca FC. The *Saccharomyces cerevisiae* Mob2p-Cbk1p kinase complex promotes polarized growth and acts with the mitotic exit network to facilitate daughter cell-specific localization of Ace2p transcription factor. *J Cell Biol.* 2002;158:885-900.
120. Aulehla A, Wehrle C, Brand-Saberi B, et al. Wnt3a plays a major role in the segmentation clock controlling somitogenesis. *Dev Cell.* 2003;4:395-406.
121. Evrard YA, Lun Y, Aulehla A, Gan L, Johnson RL. lunatic fringe is an essential mediator of somite segmentation and patterning. *Nature.* 1998;394:377-381.
122. Mankoo BS, Collins NS, Ashby P, et al. Mox2 is a component of the genetic hierarchy controlling limb muscle development. *Nature.* 1999;400:69-73.
123. Herrmann BG. Expression pattern of the Brachyury gene in whole-mount TWis/TWis mutant embryos. *Development.* 1991;113:913-917.

124. Haramis AG, Brown JM, Zeller R. The limb deformity mutation disrupts the SHH/FGF-4 feedback loop and regulation of 5' HoxD genes during limb pattern formation. *Development*. 1995;121:4237-4245.
125. Kurosawa H, Imamura T, Koike M, Sasaki K, Amano Y. A simple method for forming embryoid body from mouse embryonic stem cells. *J Biosci Bioeng*. 2003;96:409-411.
126. Hakuno D, Takahashi T, Lammerding J, Lee RT. Focal adhesion kinase signaling regulates cardiogenesis of embryonic stem cells. *J Biol Chem*. 2005;280:39534-39544.

### **3.1.7 Acknowledgements**

The authors are grateful for the support provided by the FMI Facilities for Transgenic Mice, Genomics, Imaging and Histology. We thank Olivier Pourquie, Jacqueline Deschamps, Vassilis Pachnis and Bernhard Herrmann for freely providing various mRNA *in situ* hybridization probes and Hauke Cornils for critique of the manuscript.

### 3.1.8 Supplementary Materials

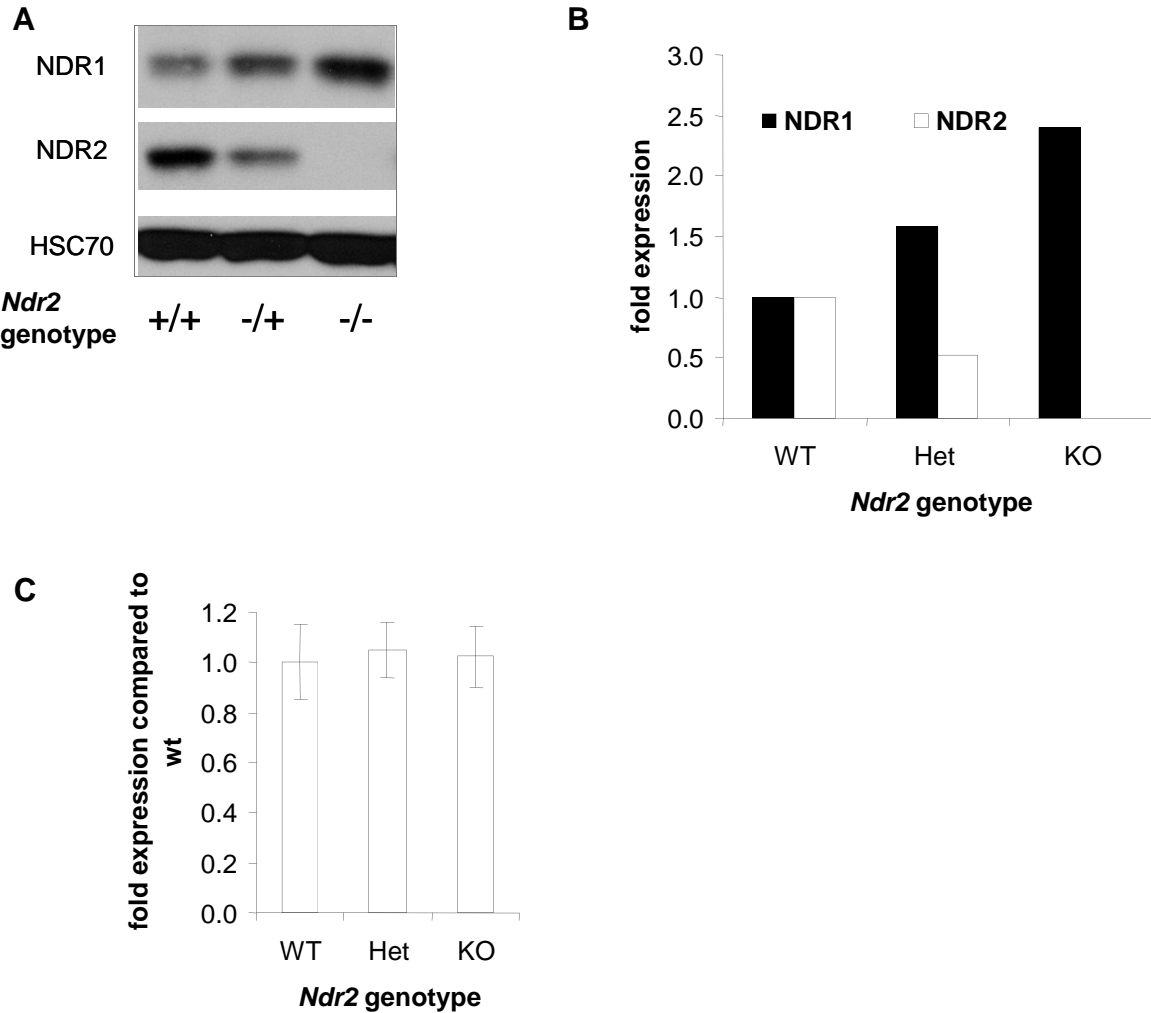


**Figure S1. mRNA levels of *Ndr1* remain unchanged in *Ndr2* knock-out colon.** **A** NDR1 and NDR2 protein levels in colon extracts of indicated genotype; HSC-70 served as loading control. Amount of protein loaded per lane: 1 mg. **B** Quantification of protein levels in **A**) by the LICOR system. **C** Corresponding *Ndr1* mRNA levels of tissues analyzed in **A**, determined by quantitative real-time PCR, normalized to GAPDH.

Tissue mRNA was extracted with Trizol (Invitrogen) according to the manual provided by the manufacturer and further purified via the Qiagen RNeasy columns (Qiagen). mRNA concentration and purity were determined on the nanodrop spectrometer (nd-1000, Thermo Scientific). cDNA synthesis was performed with the M-MuLV reverse transcriptase (NEB). Quantitative real time PCR was performed with the SYBR green PCR Master Mix (Applied Biosciences) on the ABI Prism 7000 (Applied Biosciences). *Ndr1* transcripts were detected using the following primers: fwd-<sup>5'</sup>cagacagtttggttg<sup>3'</sup> and rev-<sup>5'</sup>tcctctctgtcagagtac<sup>3'</sup>. Signals obtained for *Ndr1* were normalized to *Gapdh* transcript levels.

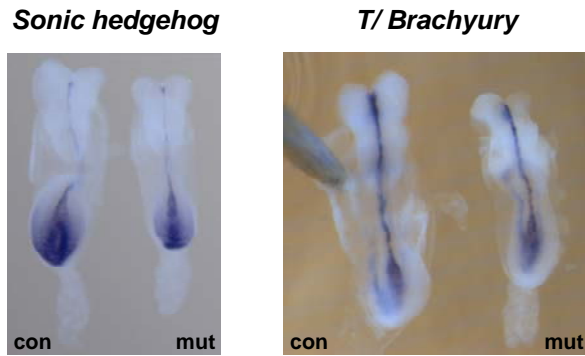


**Figure S2 . The notochord of *Ndr*-null embryos at E8.5 is intact.** Expression pattern of *Sonic hedgehog* (left) and *T/brachyury* (right) determined by mRNA *in situ* hybridization demonstrate that the notochord is continuous, indicating that loss of NDR does not negatively affect notochord development. Control embryos (con) are shown on the left, mutant embryos (mut) on the right.

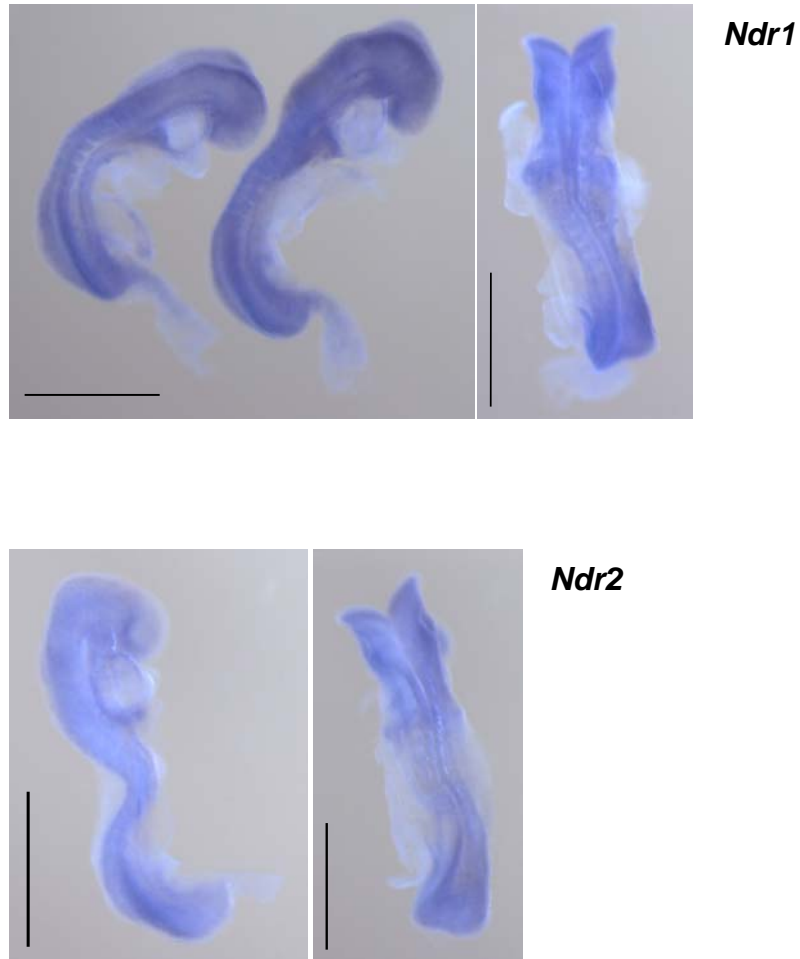


**Figure S3. *Ndr1* and *Ndr2* are broadly expressed in the mouse embryo at E8.5.** mRNA *in situ* hybridization with *Ndr1* and *Ndr2* probes. Both probes were designed to hybridize to the 3'UTR (sequences available upon request).

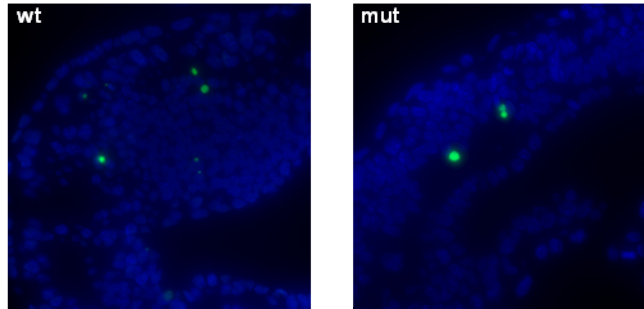


**Figure S4. Wildtype and *Ndr*-null embryos show low and comparable levels of apoptosis at E8.5.** This indicates that the small size of *Ndr*-null embryos is not due to increased levels of apoptosis. Apoptotic cells in wildtype (left) and *Ndr*-null (right) embryo labeled by the TUNEL method with FITC-labeled nucleotides. TUNEL analysis was performed on paraffin sections with the ApoAlert DNA Fragmentation Assay Kit. The protocol from the manufacturer was adapted for the Venata Biobench machine (S. Schultze), final washing steps were performed manually according to the protocol provided by the manufacturer.

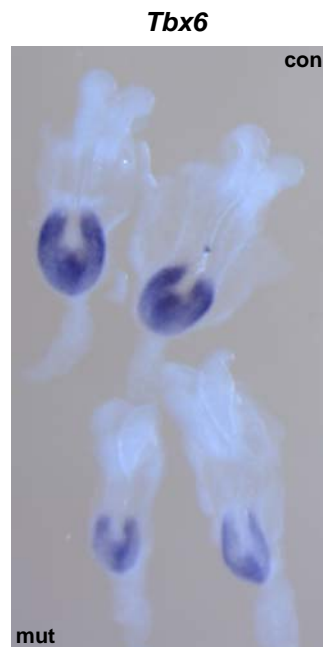


**Figure S5. *Tbx6* expression is decreased in *Ndr*-null embryos at E8.5.** Expression pattern of *Tbx6* in control (top) and *Ndr*-null embryos (bottom) determined by mRNA *in situ* hybridization. These data confirm the down-regulation of *Tbx6* observed in the microarray analysis

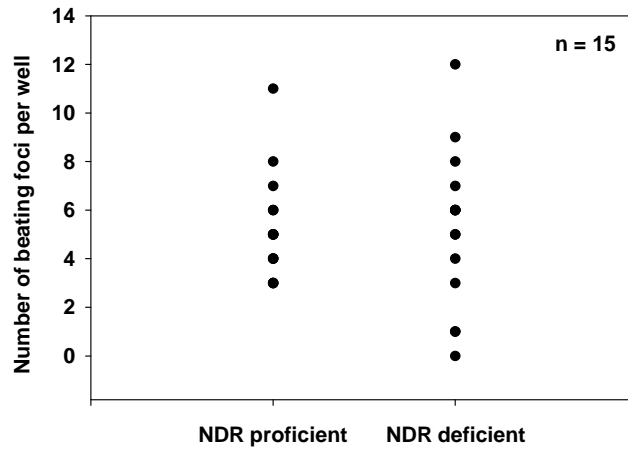


**Figure S6. NDR-deficient ES cells differentiate into cardiomyocytes.** These data show that NDR is dispensable for the formation of beating cardiomyocytes. ES cells pro- or deficient for NDR were differentiated into cardiomyocytes (see Materials and Methods for detailed protocol). Beating foci were counted four days after EB plating (15 wells of a 24-well plate per genotype)

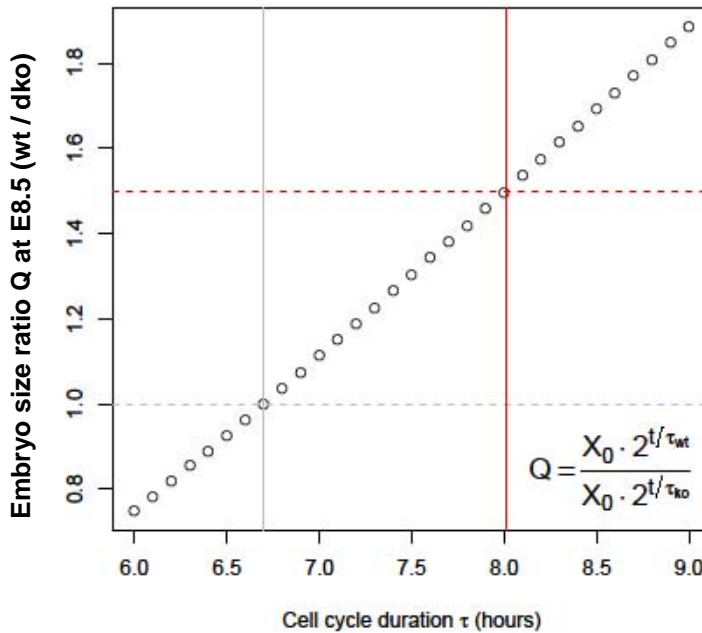


**Figure S7 Moderate increases of cell cycle duration over a short time period result in significant growth retardation of the mouse embryo at E8.5.** We generated a mathematical model to approximate the effect of an increase in cell cycle duration on embryo growth at E8.5. The model is based on the simplifying assumption that all cells in the embryo divide at the same, constant rate  $\tau_{wt}$  from E7.5 to E8.5. This leads to an exponential equation where  $X_t = X_0 \cdot 2^{t/\tau}$ .  $X_0$  is the total cell number of the embryo at  $t_0$ ,  $\tau$  is the cell cycle duration in hours and  $X_t$  the number of cells after  $t$  hours. We subsequently introduce the ratio “Q” of  $X_{t, \text{wild type}}$  over  $X_{t, \text{mutant}}$  to describe relative growth retardation as a function of the increase in  $\tau$  in the mutant. Q is plotted as a function of increasing cell cycle duration in the mutant after a period of 24 hours ( $t = 24$ ). We observed earlier that wildtype embryos were approximately 1.5 fold bigger than *Ndr* double-KO littermates at E8.5 (Figure 3). According to our model, an increase of cell cycle duration from 6.7h\* to 8h (intersection of dashed and solid red line) over 24 hours would suffice to generate a 1.5 fold difference at E8.5. \*approximate cell cycle duration at E7-7.5, taken from Snow, *J. Embryol. Exp. Morphol* 1977



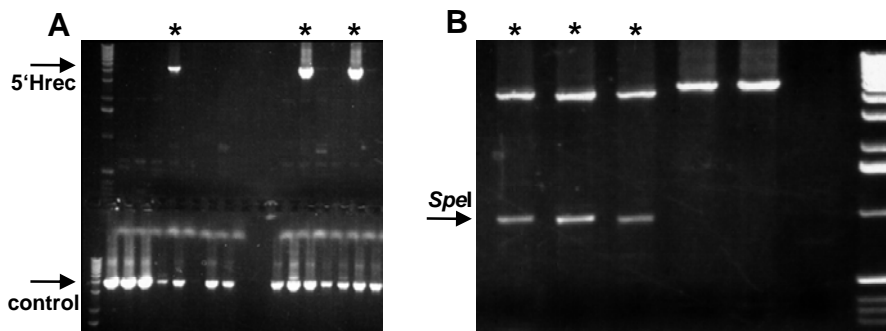


**Figure S8 ES cell screening by PCR.** G418-resistant ES cell clones were screened by two different PCR reactions for homologous recombination at the *Ndr2* locus. The over-all targeting strategy is described in Figure 1A and in Materials and Methods. All primer binding sites are indicated in Figure 1A. To identify clones that had correctly integrated the targeting vector at the 5' end of the locus, a PCR reaction with one forward primer (5'wt) that bound up-stream of the targeting vector homology region and two different reverse primers was set-up. The first reverse primer (3'Hrec) bound to a sequence in the Neo cassette of the targeting vector. Therefore, this PCR would only generate a product if the clone had integrated the targeting vector in the *Ndr2* locus. To control for the quality of genomic DNA and the PCR reaction, a second reverse primer (3'wt) was introduced that bound to an endogenous region in the *Ndr2* locus and was thus expected to yield a PCR product in the absence of target vector integration. Results of a 5' screening PCR are shown in **A**. The bands (5'Hrec) in the upper panel denote three clones (marked by asteriks) that have correctly integrated the targeting vector at the 5' end. The lower panel shows that the PCR reaction for the control fragment works in most clones, indicating that the risk of false negatives was rather low. Clones that were positive for the 5'Hrec fragment were tested with an analogous PCR on the 3' end of the vector integration site. The 3'Hrec fragment contained a *SpeI* restriction site that had been introduced adjacent to the *loxP* site that was farthest away from the Neo selection cassette. Therefore, 3'Hrec fragments were subjected to *SpeI* restriction digest to identify clones that had successfully integrated the *loxP* site, indicative of correct target vector integration. The result of a 3' PCR screen is shown in **B**. Three of the five clones (marked by an asteriks) that yielded a 3'Hrec fragment contained the *SpeI* site, suggesting that they had correctly integrated the most external *loxP* site.

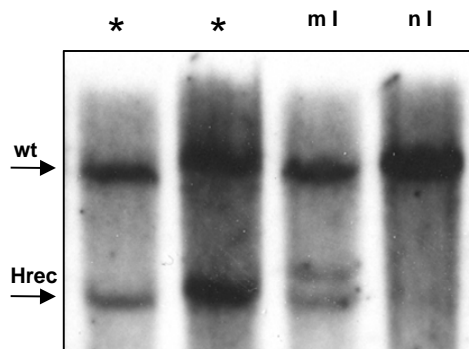


**Figure S9, Validation of single targeting vector integration.** 5' and 3' PCR reactions described in Figure S8 identified clones that had correctly integrated the targeting vector in the *Ndr2* locus. To exclude clones with multiple targeting vector integration events, Southern blot experiments were performed with an internal probe that bound immediately up-stream of the Neo cassette. The Figure shows the Southern blot result of two clones with unique targeting vector integration (denoted by an asteriks), one clone with multiple integration (m I) and one clone which did not integrate the targeting vector (n I).

<b><i>Ndr2</i></b>	<b>temp (C°)</b>	<b>duration (sec)</b>	
<b>initial denaturing</b>	94	120	
<b>denaturing</b>	94	45	<b>10 cycles</b>
<b>annealing</b>	initial 63 -0.5/cycle	30	
<b>elongation</b>	72	60	
<b>denaturing</b>	94	45	<b>25 cycles</b>
<b>annealing</b>	58	30	
<b>elongation</b>	72	60	
<b>final elongation</b>	72	300	
 <b>Gender</b>			
<b>initial denaturing</b>	94	180	
<b>denaturing</b>	94	45	<b>35 cycles</b>
<b>annealing</b>	65	30	
<b>elongation</b>	72	30	
<b>final elongation</b>	72	420	

**Figure S10. PCR cycling protocols for genotyping of the *Ndr2* locus** (as described in Materials and Methods) and **gender determination** (used for selection of embryos for microarray analysis as described in Materials and Methods)

### ***3.2 Complete Loss of NDR Kinases in the Intestinal Epithelium Induces Rectal Prolapse and Increases Susceptibility to Azoxymethane-induced Colon Carcinogenesis***

This part summarizes the work that has been done with the intestinal epithelium-specific *Ndr* double knock-out mouse line to address the role of NDR kinases in the context of colon carcinogenesis.

#### **Contributions**

**Deborah Hynx** performed the AOM injections and the weekly monitoring of experimental mice during the carcinogen studies. She also assisted with necropsies and dissections.

**David Restuccia** assisted with dissections and tissue embedding.

**Michael Stadler** performed Fisher's exact test to evaluate the statistical significance of colonic nodule development in NDR proficient versus NDR deficient mice (Figure 4).

All other work was performed by me.

The project is ongoing and will be continued in collaboration with Lei Zhang.

### 3.2.1 Introduction

Mammalian NDR kinases NDR1 and NDR2 are widely expressed and highly conserved (1-4). They positively regulate centrosome duplication, alignment of mitotic chromosomes, apoptosis and proliferation (1, 5-8). Several reports describe deregulated NDR levels in human malignancies (summarized in (9)). Importantly, aged mice with a targeted deletion of *Ndr1* develop T-cell lymphoma and tumors with low total NDR kinase levels display decreased levels of apoptosis, further supporting a positive role for NDR kinases in apoptosis induction (1). Moreover, these findings indicate that mammalian NDR has tumor suppressive properties.

We have recently generated a conditional targeted deletion of the *Ndr2* gene in the mouse (see section 3.1). Mice that completely lack functional NDR2 protein are phenotypically normal and do not display increased susceptibility to tumor development. However, similar to the *Ndr1* knock-out (KO) mouse, protein levels of NDR1 are increased in tissues with high endogenous NDR2 levels which might mask the tumor suppressive function of NDR kinases. To exclude potential compensation by the remaining NDR isoform, we generated the *Ndr1/Ndr2* double KO mouse line. Complete loss of *Ndr1* and *Ndr2* results in embryonic lethality at mid-gestation (section 3.1), precluding the evaluation of the tumor suppressive function of NDR in the systemic *Ndr1/2* double KO. Therefore, we decided to make use of the conditionally targeted *Ndr2* gene to study the tumor suppressive function of NDR kinases in a tissue-specific *Ndr*-null mouse line.

NDR2 protein levels are particularly high in the murine colon ((1), section 3.1). The turn-over of cells in the intestinal epithelium ranges among the fastest in the human

body (10). Colorectal cancer (CRC) originates in this tissue. NDR1 protein levels are particularly high in organs of the immune system and loss of *Ndr1* results in T-cell lymphoma (1). Conversely, NDR2 levels are highest in the colon. Therefore, we hypothesized that ablation of *Ndr2* in the colon could contribute to CRC formation. To eliminate isoform compensation by NDR1, we specifically ablated *Ndr2* in the intestinal epithelium of *Ndr1*-null mice. Spontaneous colon cancer in rodents is very rare. In addition to genetic models such as the APC<sup>min</sup> mouse (11), carcinogen models have been established to study factors thought to play a role in tumor initiation and / or tumor progression in the colon (12). Azoxymethane (AOM)-induced tumors in mice resemble human CRC. They are characterized by aberrant APC expression, altered  $\beta$ -catenin localization and K-ras mutations (13). Therefore, we treated conditional *Ndr1/2* double KO mice with AOM to study the potential tumor-suppressive function of NDR kinases in the colon.

We find that NDR2 protein is highly expressed in the colonic epithelium. Mice that lack both *Ndr1* and *Ndr2* (*Ndr1*<sup>-/-</sup>*Ndr2* <sup>$\Delta/\Delta$ VilCre</sup>) in the intestinal epithelium are viable and fertile. However, homozygous *Ndr1*<sup>-/-</sup>*Ndr2* <sup>$\Delta/\Delta$ VilCre</sup> mice develop rectal prolapse, a symptom of chronic colonic inflammation. We do not observe spontaneous colon cancer development, but *Ndr1*<sup>-/-</sup>*Ndr2* <sup>$\Delta/\Delta$ VilCre</sup> mice seem to be more susceptible to AOM-induced colon carcinogenesis. Therefore, *Ndr1*<sup>-/-</sup>*Ndr2* <sup>$\Delta/\Delta$ VilCre</sup> mice could represent a new model to study CRC development in the context of chronic inflammation.

### 3.2.2 Results

#### ***NDR2 is expressed in the colonic epithelium***

Initial lesions that develop into colorectal cancer (CRC) arise in the colonic epithelium (reviewed in (14)). The colon is constituted of four tissue layers, namely the serosa, the muscularis externa, the submucosa and the mucosa which comprises the lamina muscularis mucosae, the lamina propria and the epithelium (15). Although Westernblot data show high NDR2 protein levels in whole colon tissue extracts (section 3.1, Figure 2), they do not indicate where the protein is localized. Therefore, we determined NDR2 localization in the murine colon by immuno-histochemistry using an NDR2 specific antibody (1). Colon from a *Ndr2*-null littermate served as negative control. NDR2 protein was detected in all layers of the murine colon with highest expression in the epithelium (Figure 1), consistent with a putative role as a tumor suppressor in CRC.

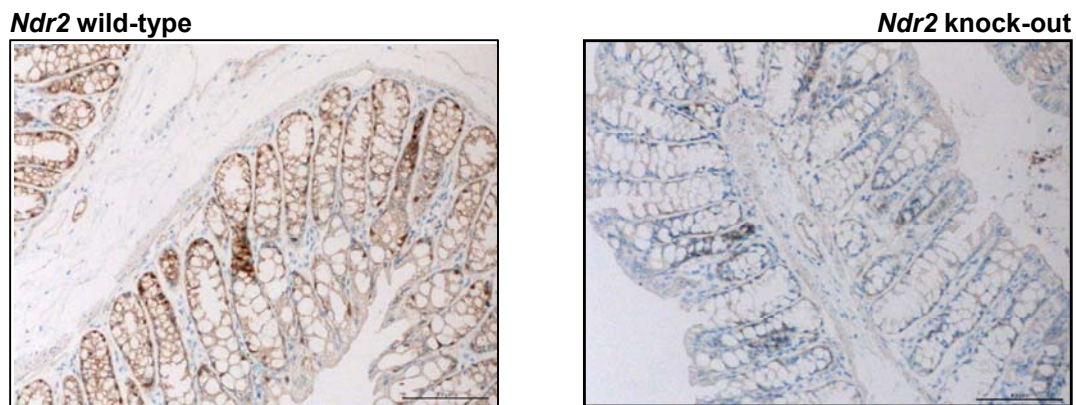


**Figure 1. NDR2 is strongly expressed in the colonic epithelium.** Colon sections of *Ndr2* wild type (A) and *Ndr2* knock-out (B) littermate males (4 months old) were stained with the isoform-specific NDR2 antibody; magnification: 200x

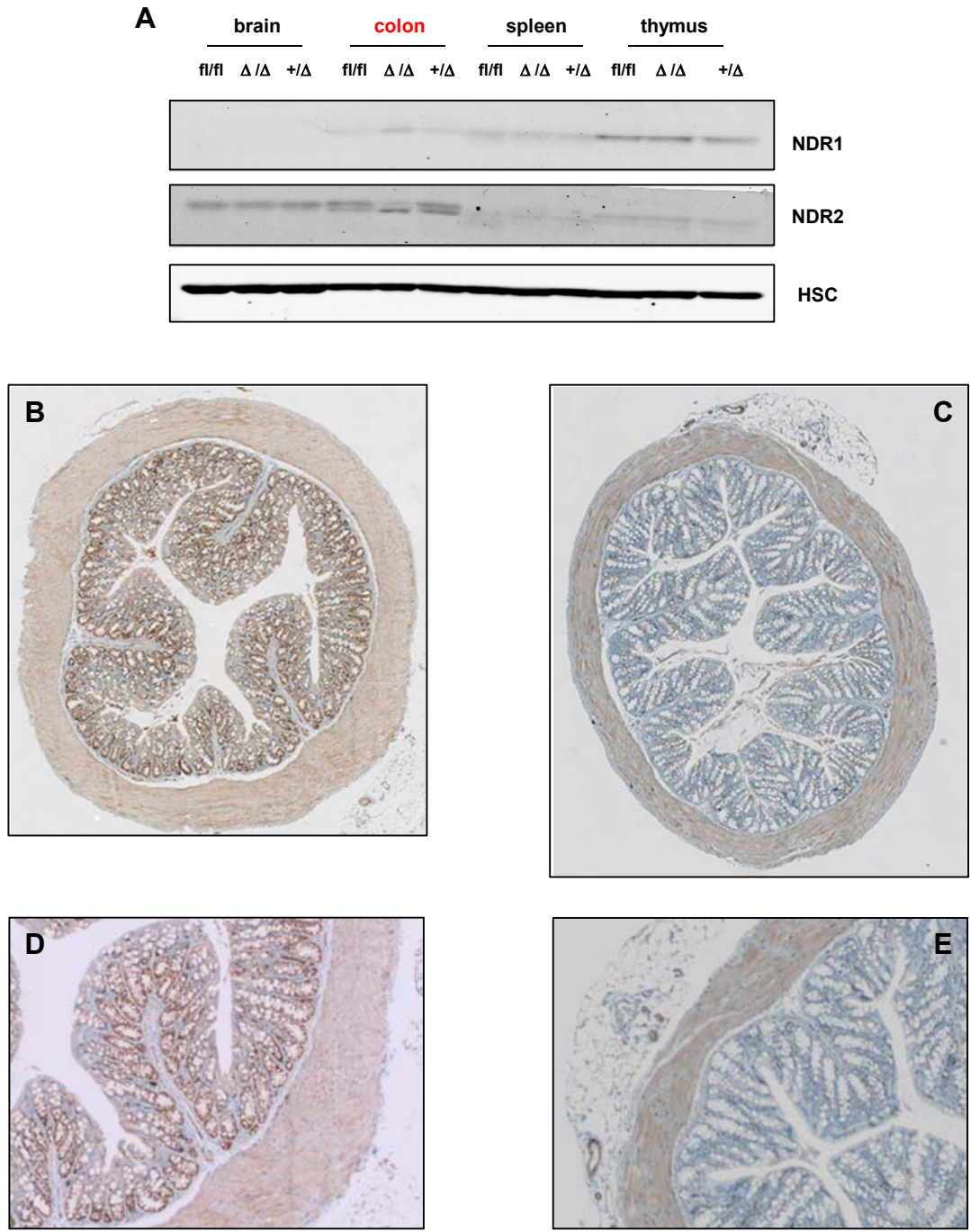


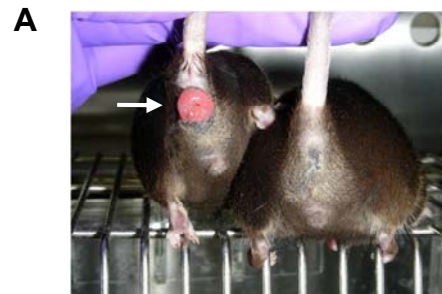
**Figure 2. Specific ablation of NDR2 protein in the colonic epithelium.** **A** Western blot analysis of Ndr2 flox/flox (fl/fl), flox/flox Vil-Cre ( $\Delta/\Delta$ ) and +/flox Vil-Cre (+/ $\Delta$ ) tissues. HSC70 served as loading control. Cre-recombinase should only be expressed in intestinal epithelium. As expected, NDR2 levels are specifically decreased in the colon of  $\Delta/\Delta$  mice, but not in the colon of control mice. NDR2 levels remain constant in other tissues of  $\Delta/\Delta$  mice, indicating that Cre is specifically expressed in the colon. **B-E** Immunohistochemical detection of NDR2. **B, D:** colon sections of fl/fl mouse, 40x and 200x, respectively. **C, E:** colon sections of  $\Delta/\Delta$  mouse, 40x and 200x, respectively. The data confirm that NDR2 is specifically ablated in epithelium but not in other layers of the colon

***Tissue-specific deletion of Ndr2 in the intestinal epithelium of Ndr1-null mice induces colonic prolapse***

As reported earlier, NDR kinase isoforms mutually compensate for each other and the systemic *Ndr1/2* double KO is embryonic lethal ((1), section 3.1). Therefore, we made use of the conditionally targeted *Ndr2* gene to establish a mouse line with an intestinal-epithelium specific deletion of *Ndr1/2* (*Ndr1<sup>-/-</sup>Ndr2<sup>Δ/ΔVilCre</sup>*). To that end, we crossed conditional *Ndr1/2* double KO (*Ndr1<sup>-/-</sup>Ndr2<sup>flox/flox</sup>*) mice with the Villin-Cre deleter strain. The villin promoter drives Cre expression in the intestinal epithelium from E12.5 (16). Westernblot analysis of *Ndr1<sup>+/-</sup>Ndr2<sup>Δ/ΔVilCre</sup>* tissues showed that NDR2 levels were decreased in the colon but not in the brain or the thymus (Figure 2A). Subsequent immuno-histochemical analysis confirmed that NDR2 protein was lost specifically in the colonic epithelium but not in other layers of the colon (Figure 2C,E). At weaning, *Ndr1<sup>-/-</sup>Ndr2<sup>Δ/ΔVilCre</sup>* mice were indistinguishable from control littermates that retained one or both *Ndr2* alleles in the intestinal epithelium. In particular, crypt morphology in *Ndr1<sup>-/-</sup>Ndr2<sup>Δ/ΔVilCre</sup>* colons was not changed (data not shown). However, 90% of male and 40% of female homozygous *Ndr1<sup>-/-</sup>Ndr2<sup>Δ/ΔVilCre</sup>* mice developed rectal prolapse (Figure 3B). Significantly, neither male nor female heterozygous *Ndr1<sup>-/-</sup>Ndr2<sup>+/ΔVilCre</sup>* mice developed prolapse, indicating that prolapse incidence was not linked to unspecific Cre activity but resulted from loss of NDR2 protein. Moreover, loss of *Ndr2* alone in *Ndr1* wild type mice was not sufficient to induce colonic prolapse, suggesting that increased levels of NDR1 functionally compensated for loss of NDR2. We did not observe spontaneous colon cancer formation in either heterozygous or homozygous *Ndr1<sup>-/-</sup>Ndr2<sup>Δ/ΔVilCre</sup>* mice. Importantly, mice with prolapse did not display any signs of weight loss, malaise or



untimely morbidity, indicating that the prolapsed rectum did not impair gastro-intestinal function.



**B** Naïve mice

<i>Ndr2</i> GT	$\Delta/\Delta$ Cre	$+/\Delta$ Cre	$-/-$
male	10/11	0/20	0/20
female	4/10	0/21	0/26

**C** AOM-treated mice

<i>Ndr2</i> GT	$\Delta/\Delta$ Cre	$+/\Delta$ Cre	$-/-$
male	5/8	1/9	0/3
female	7/8	0/10	0/2

**Figure 4. Rectal prolapsed incidence in *Ndr2*  $\Delta/\Delta$  Cre mice.** **A** Male with rectal prolapsed (white arrow, left) and control littermate (right). **B** Rectal prolapse incidence in naïve mice older than 150 days. *Ndr2*  $\Delta/\Delta$  Cre and *Ndr2*  $+/\Delta$  Cre mice are on an *Ndr1*-null background,  $-/-$  mice are NDR1 proficient. Male *Ndr2*  $\Delta/\Delta$  Cre mice develop prolapse with nearly complete penetrance, females are less affected. Loss of *Ndr2* in NDR1-proficient mice does not cause prolapse. **C** Rectal prolapse incidence in AOM (Azoxymethane) treated mice. AOM treatment induces rectal prolapse in *Ndr2*  $\Delta/\Delta$  Cre females but not in *Ndr2*  $+/\Delta$  Cre or  $-/-$  control mice. GT: genotype. *Picture in A taken by D. Hynx.*

As described in detail below, homozygous *Ndr1*<sup>-/-</sup>*Ndr2* <sup>$\Delta/\Delta$ VilCre</sup> and control mice were treated with azoxymethane (AOM) to induce colon cancer formation. Importantly, AOM treatment increased the incidence of rectal prolapse in *Ndr1*<sup>-/-</sup>*Ndr2* <sup>$\Delta/\Delta$ VilCre</sup> females to 88% (Figure 3C). AOM treatment did not induce rectal prolapse in either male or female heterozygous *Ndr1*<sup>-/-</sup>*Ndr2* <sup>$+/\Delta$ VilCre</sup> control mice. In summary, complete loss of NDR kinases in the intestinal epithelium predisposes male mice to rectal prolapse. *Ndr1*<sup>-/-</sup>*Ndr2* <sup>$\Delta/\Delta$ VilCre</sup> females are moderately resistant to rectal prolapse unless treated with the carcinogen AOM. Loss of NDR is not sufficient to induce colon cancer formation. How

NDR kinases protect against rectal prolapse and why males and females display differences in prolapse susceptibility remains to be addressed.

***Combined loss of Ndr1 and Ndr2 in the intestinal epithelium increases the frequency of AOM induced nodule formation in the colon***

As combined loss of *Ndr1* and *Ndr2* in the intestinal epithelium was not sufficient to induce colon carcinogenesis, we treated homozygous *Ndr1*<sup>-/-</sup>*Ndr2*<sup>Δ/ΔVilCre</sup> and control mice with the colon carcinogen AOM according to a protocol established by *Neufert et al.* (13) (detailed in Materials and Methods). In a pilot experiment, we noticed significantly higher treatment-related mortality than predicted by the protocol, particularly in females with low bodyweight. Moreover, we did not observe robust nodule formation after 30 weeks as indicated in the protocol. Therefore, we only included mice with a bodyweight superior to 20 g into the following studies and increased the study duration to 37 - 41 weeks. The changes decreased treatment-related mortality and resulted in macroscopic nodule formation. Results for AOM study 6, 7 and 8 are summarized in Supplementary Materials (Table 1). One or more nodules were detected in 25% of *Ndr2* wild type (*Ndr1*<sup>-/-</sup>*Ndr2*<sup>+/+VilCre</sup>), 43% of heterozygous (*Ndr1*<sup>-/-</sup>*Ndr2*<sup>+/<sup>Δ</sup>VilCre</sup>) and 78% of homozygous (*Ndr1*<sup>-/-</sup>*Ndr2*<sup>Δ/ΔVilCre</sup>) mice (Figure 4). However, due to unexpected losses of control mice, the observed differences exhibit rather high P-values, namely 0.23 when all three genotypes are compared and 0.09 (Fisher exact test) when *Ndr2* pro- versus *Ndr2* deficient animals are compared. In summary, our data suggest that NDR kinases might act as tumor suppressors in the colonic epithelium. Additional studies have to be performed to confirm the statistical significance of our findings.

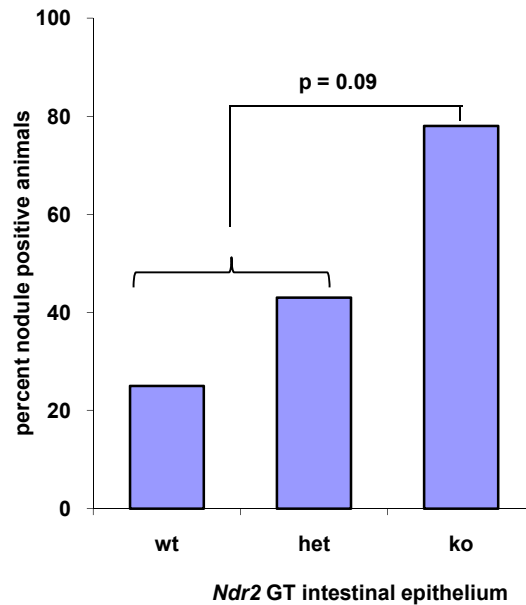


**Figure 4. Colonic nodule formation in mice treated with AOM.** Animals which had developed one or more macroscopic nodules in the colon were counted as positive. The *Ndr2* genotype in the intestinal epithelium is indicated on the x-axis. All mice were on an *Ndr1*-null background. Mouse numbers in the three groups: wt = 4; het = 7; ko = 9. The indicated p-value describes the statistical significance of nodule development in NDR2 proficient (wt and het) versus NDR2 deficient (ko) mice. If all three *Ndr2* genotype groups are compared separately, the p-value is 0.23. A detailed summary of experimental conditions including exact treatment duration, age and gender is shown in Table S1 (Supplementary Materials).

### 3.2.3 Discussion

Mammalian NDR kinases are implicated in centrosome duplication, mitotic chromosome alignment, proliferation and apoptosis (1, 5-8). Loss of *Ndr1* in the mouse leads to T-cell lymphoma (1). NDR isoforms mutually compensate for each other and combined loss of *Ndr1/2* in the mouse is embryonic lethal (section 3.1). NDR2 protein is highly expressed in the colonic epithelium (Figure 1, 2). Therefore, we have generated an intestinal epithelium-specific *Ndr1/Ndr2* double KO mouse model (*Ndr1*<sup>-/-</sup>*Ndr2*<sup>Δ/ΔVilCre</sup>) to study the potential tumor suppressive function of NDR kinases in colon cancer. We find that NDR2 protein is efficiently and specifically deleted in the colonic epithelium of *Ndr1*<sup>-/-</sup>

*Ndr2*<sup>Δ/ΔVilCre</sup> mice (Figure 2). *Ndr1*<sup>-/-</sup>*Ndr2*<sup>Δ/ΔVilCre</sup> mice are viable and fertile but develop rectal prolapse starting from around 4 months of age (Figure 3). Males are significantly more susceptible to prolapse development than females (90% versus 40%, Figure 3B). However, *Ndr1*<sup>-/-</sup>*Ndr2*<sup>Δ/ΔVilCre</sup> females also develop rectal prolapse with almost complete penetrance if treated with the colon carcinogen AOM (Figure 3C).

In experimental mouse models, rectal prolapse is often associated with a deregulation of the immune system and inflammation. It has been reported in mice deficient for interleukin 2 (IL-2), IL-10, or TCRα/β (17-19). Similarly, transgenic over-expression of hepatocyte growth factor (HGF) in mice results in decreased IL-2 levels and rectal prolapse (20). In the IL-2, IL-10 and TCRα/β models, prolapse incidence is significantly decreased when mice are housed under germ-free conditions, indicating that prolapse might be caused by an infection of the immuno-compromised host (21-23). We did not detect common mouse pathogens in the *Ndr1*<sup>-/-</sup>*Ndr2*<sup>Δ/ΔVilCre</sup> colony, indicating that prolapse development in *Ndr1*<sup>-/-</sup>*Ndr2*<sup>Δ/ΔVilCre</sup> mice is independent of infection status. Mice carrying the Δ14 APC mutation develop tumors in the distal colon and the rectum, more closely resembling human CRC (24). In this model, prolapse incidence correlates with the severity of colorectal carcinogenesis and inflammatory cells are present both in lesions and in the prolapsed tissue (24). In summary, these data suggest that deregulated immune function in the colon contributes to rectal prolapse formation. NDR1 is highly expressed in organs of the immune system and loss of *Ndr1* results in T-cell lymphoma (1). Therefore, rectal prolapse in *Ndr1*<sup>-/-</sup>*Ndr2*<sup>Δ/ΔVilCre</sup> mice could arise from the combination of a general defect of the immune system due to systemic loss of *Ndr1* and a local defect in the colonic epithelium due to loss of *Ndr2*. Detailed

characterization of tissue morphology and inflammation status in prolapsed rectum are warranted to confirm this hypothesis. Importantly, patients suffering from chronic inflammation of the colon are at increased risk for developing CRC (25). However, we did not observe spontaneous CRC formation in *Ndr1<sup>-/-</sup>Ndr2<sup>Δ/ΔVilCre</sup>* mice. Therefore, we treated *Ndr1<sup>-/-</sup>Ndr2<sup>Δ/ΔVilCre</sup>* and *Ndr1<sup>-/-</sup>Ndr2<sup>+/<sup>Δ</sup>VilCre</sup>* control mice with AOM to induce CRC formation. Although additional studies have to be performed to confirm the statistical significance of our data, *Ndr1<sup>-/-</sup>Ndr2<sup>Δ/ΔVilCre</sup>* mice appear to be more susceptible to AOM induced CRC (Figure 4). As none of the *Ndr1<sup>-/-</sup>Ndr2<sup>+/<sup>Δ</sup>VilCre</sup>* control mice developed rectal prolapse (Figure 3) we cannot discriminate whether NDR kinases function as conventional tumor suppressors in this context or whether increased CRC susceptibility is a secondary effect of chronic inflammation.

In summary, we show that NDR2 kinase is prominently expressed in the colonic epithelium. Combined loss of NDR1 and NDR2 in the intestinal epithelium leads to rectal prolapse formation with almost complete penetrance in male mice. We hypothesize that rectal prolapse is the result of an abnormal inflammatory response in the colonic epithelium of *Ndr1<sup>-/-</sup>Ndr2<sup>Δ/ΔVilCre</sup>* mice. Histological and inflammatory marker analyses of prolapsed rectum are warranted to confirm this hypothesis. *Ndr1<sup>-/-</sup>Ndr2<sup>Δ/ΔVilCre</sup>* mice do not develop spontaneous CRC but appear to be more susceptible to AOM induced CRC. Assuming that future AOM studies confirm the observed trend, *Ndr1<sup>-/-</sup>Ndr2<sup>Δ/ΔVilCre</sup>* mice could constitute a new model system to study the molecular mechanisms that underlie the increased risk of CRC formation in patients with chronic colonic inflammation.

### 3.2.4 Materials and Methods

#### ***Immuno-histochemical detection of NDR2 protein in murine colon sections***

Colons were dissected out, cleaned in PBS and fixed with 4% PFA over night at 4°C. Subsequently, colons were washed in PBS and dehydrated for 30 min in 50%EtOH/PBS, then 70%EtOH/PBS. Paraffin embedding was performed in a Medite Tissue Processor TPC 15 (Medite) according to the standard protocol of the manufacturer. Paraffin blocks were sectioned at 5 µm and mounted on poly-lysine coated slides. Sections were pre-treated with CC1 buffer (Ventana) for 30 minutes to unmask epitopes. NDR2 protein was detected with a polyclonal rabbit antibody (1) at a 1:100 dilution using the DAB detection method on the Discovery XT system (Ventana). After the staining procedure, slides were extensively washed, dehydrated, cleared in Ultraclear (Medite) and mounted with Ultrakitt mounting medium (J.T.Baker). Sections were analyzed on a Nikon Eclipse E600 microscope.

#### ***Generation of the $Ndr1^{-/-}Ndr2^{\Delta/\Delta VilCre}$ mouse line***

The Villin-Cre deleter strain ((16), B6.SJL-Tg(Vil-cre)997Gum/J) was obtained from Jackson Laboratories. Genotyping of the cre transgene was performed according to the protocol provided by Jackson Laboratories.  $Ndr1^{-/-}Ndr2^{lox/lox}$  mice (described in 3.1) were crossed with Vil-Cre mice to generate the  $Ndr1^{-/-}Ndr2^{\Delta/\Delta VilCre}$  mouse line. Mice were maintained on a mixed C57BL/6 background.

### **AOM colon carcinogenesis**

AOM colon carcinogenesis was performed according to the protocol by *Neufert et al.* (13) with some modifications. Experimental mice between 6 and 8 weeks of age and a bodyweight of at least 20 g were injected weekly with AOM (SIGMA) at 10 mg/kg bodyweight for 6 consecutive weeks. Animals were monitored weekly for weight loss and signs of malaise. At the end of the study, 37 – 41 weeks after the first injection, mice were sacrificed. Following gross general organ analysis, the colon was removed, washed in PBS and cut open longitudinally to assess and count nodule formation. Subsequently, colons fixed and paraffin embedded as described above. All AOM carcinogenesis experiments were performed under Tumor license 2044.

### **3.2.5 References**

1. Cornils H, Stegert MR, Hergovich A, et al. Ablation of the kinase NDR1 predisposes mice to the development of T cell lymphoma. *Sci Signal.* 2010;3:ra47.
2. Devroe E, Erdjument-Bromage H, Tempst P, Silver PA. Human Mob proteins regulate the NDR1 and NDR2 serine-threonine kinases. *J Biol Chem.* 2004;279:24444-24451.
3. Hergovich A, Stegert MR, Schmitz D, Hemmings BA. NDR kinases regulate essential cell processes from yeast to humans. *Nat Rev Mol Cell Biol.* 2006;7:253-264.

4. Stegert MR, Hergovich A, Tamaskovic R, Bichsel SJ, Hemmings BA. Regulation of NDR protein kinase by hydrophobic motif phosphorylation mediated by the mammalian Ste20-like kinase MST3. *Mol Cell Biol.* 2005;25:11019-11029.
5. Chiba S, Ikeda M, Katsunuma K, Ohashi K, Mizuno K. MST2- and Furry-mediated activation of NDR1 kinase is critical for precise alignment of mitotic chromosomes. *Curr Biol.* 2009;19:675-681.
6. Cornils H, Kohler RS, Hergovich A, Hemmings BA. Human NDR kinases control G1/S cell cycle transition by directly regulating p21 and c-myc stability. Thesis. Friedrich Miescher Institut, University of Basel 2010.
7. Hergovich A, Lamla S, Nigg EA, Hemmings BA. Centrosome-associated NDR kinase regulates centrosome duplication. *Mol Cell.* 2007;25:625-634.
8. Vichalkovski A, Gresko E, Cornils H, Hergovich A, Schmitz D, Hemmings BA. NDR kinase is activated by RASSF1A/MST1 in response to Fas receptor stimulation and promotes apoptosis. *Curr Biol.* 2008;18:1889-1895.
9. Hergovich A, Cornils H, Hemmings BA. Mammalian NDR protein kinases: from regulation to a role in centrosome duplication. *Biochim Biophys Acta.* 2008;1784:3-15.
10. Radtke F, Clevers H. Self-renewal and cancer of the gut: two sides of a coin. *Science.* 2005;307:1904-1909.
11. Moser AR, Pitot HC, Dove WF. A dominant mutation that predisposes to multiple intestinal neoplasia in the mouse. *Science.* 1990;247:322-324.
12. Rosenberg DW, Giardina C, Tanaka T. Mouse models for the study of colon carcinogenesis. *Carcinogenesis.* 2009;30:183-196.



13. Neufert C, Becker C, Neurath MF. An inducible mouse model of colon carcinogenesis for the analysis of sporadic and inflammation-driven tumor progression. *Nat Protoc.* 2007;2:1998-2004.
14. Fearon ER, Vogelstein B. A genetic model for colorectal tumorigenesis. *Cell.* 1990;61:759-767.
15. Fritsch H, Kuehnel W eds. *Color Atlas of Human Anatomy. Vol. 2; Internal Organs (ed 5th): Thieme; 2008.*
16. Madison BB, Dunbar L, Qiao XT, Braunstein K, Braunstein E, Gumucio DL. Cis elements of the villin gene control expression in restricted domains of the vertical (crypt) and horizontal (duodenum, cecum) axes of the intestine. *J Biol Chem.* 2002;277:33275-33283.
17. Kuhn R, Lohler J, Rennick D, Rajewsky K, Muller W. Interleukin-10-deficient mice develop chronic enterocolitis. *Cell.* 1993;75:263-274.
18. Mombaerts P, Mizoguchi E, Grusby MJ, Glimcher LH, Bhan AK, Tonegawa S. Spontaneous development of inflammatory bowel disease in T cell receptor mutant mice. *Cell.* 1993;75:274-282.
19. Sadlack B, Merz H, Schorle H, Schimpl A, Feller AC, Horak I. Ulcerative colitis-like disease in mice with a disrupted interleukin-2 gene. *Cell.* 1993;75:253-261.
20. Takayama H, Takagi H, Larochelle WJ, Kapur RP, Merlino G. Ulcerative proctitis, rectal prolapse, and intestinal pseudo-obstruction in transgenic mice overexpressing hepatocyte growth factor/scatter factor. *Lab Invest.* 2001;81:297-305.

21. Dianda L, Hanby AM, Wright NA, Sebesteny A, Hayday AC, Owen MJ. T cell receptor-alpha beta-deficient mice fail to develop colitis in the absence of a microbial environment. *Am J Pathol.* 1997;150:91-97.
22. Schultz M, Tonkonogy SL, Sellon RK, et al. IL-2-deficient mice raised under germfree conditions develop delayed mild focal intestinal inflammation. *Am J Physiol.* 1999;276:G1461-1472.
23. Specht S, Arriens S, Hoerauf A. Induction of chronic colitis in IL-10 deficient mice requires IL-4. *Microbes Infect.* 2006;8:694-703.
24. Colnot S, Niwa-Kawakita M, Hamard G, et al. Colorectal cancers in a new mouse model of familial adenomatous polyposis: influence of genetic and environmental modifiers. *Lab Invest.* 2004;84:1619-1630.
25. Itzkowitz SH, Yio X. Inflammation and cancer IV. Colorectal cancer in inflammatory bowel disease: the role of inflammation. *Am J Physiol Gastrointest Liver Physiol.* 2004;287:G7-17.

### 3.2.6 Supplementary Material Table S1

mouse ID	ko:NDR1	cko:NDR2	tg:ViICre	Gender	study #	tx duration	age at tx 0	prolapse	nodule(s)	comments
NDR-ViICre-0343	-/-	+/+	tg/+	female	6	265	77	-	-	
NDR-ViICre-0476	-/-	+/+	tg/+	female	7	286	69	-	-	
NDR-ViICre-0480	-/-	+/+	tg/+	female	7	265	69	-	-	
NDR-ViICre-0556	-/-	+/+	tg/+	male	8	258	82	+	2 very small nodules	
NDR-ViICre-0340	-/-	fl/fl	tg/+	female	6	265	77	-	-	
NDR-ViICre-0477	-/-	fl/fl	tg/+	female	7	286	69	+	nodules	
NDR-ViICre-0491	-/-	fl/fl	tg/+	female	7	259	69	-	-	
NDR-ViICre-0571	-/-	fl/fl	tg/+	female	8	258	81	-	-	
NDR-ViICre-0561	-/-	fl/fl	tg/+	female	8	258	82	-	-	
NDR-ViICre-0482	-/-	fl/fl	tg/+	male	7	286	69	+	nodules	
NDR-ViICre-0579	-/-	fl/fl	tg/+	male	8	258	79	+	1 very small nodule	
NDR-ViICre-0342	-/-	fl/fl	tg/+	female	6	265	77	+	nodules	
NDR-ViICre-0346	-/-	fl/fl	tg/+	female	6	265	77	+	thickening rectal end	
NDR-ViICre-0417	-/-	fl/fl	tg/+	female	6	265	50	+	nodules	
NDR-ViICre-0593	-/-	fl/fl	tg/+	female	8	258	77	+	7 nodules in a lump	
NDR-ViICre-0595	-/-	fl/fl	tg/+	female	8	258	77	+	12 nodules in a lump	
NDR-ViICre-0473	-/-	fl/fl	tg/+	male	7	286	69	+	nodules	
NDR-ViICre-0581	-/-	fl/fl	tg/+	male	8	258	79	+	-	
NDR-ViICre-0373	-/-	fl/fl	tg/+	male	6	265	74	+	nodules	
NDR-ViICre-0350	-/-	fl/fl	tg/+	male	6	265	77	+	nodules	

**Summary of AOM studies 6, 7 and 8.** Animals were treated with AOM as detailed in Materials and Methods. Included are only mice that were sacrificed and analyzed between 258 and 286 days after the first treatment. Gender and *Ndr1* and *Ndr2* genotypes are indicated. Each mouse carried one allele of the ViI-Cre transgene. Treatment duration (tx) and age at first AOM injection (tx 0) are indicated. Prolapse and nodule development are documented and briefly commented

## 4 General Discussion

The aim of this thesis was to identify *in vivo* functions of mammalian NDR kinases in general and their impact on tumorigenesis in particular. Using mouse models for combined *Ndr1/Ndr2* deficiency we can show that NDR kinases are essential for embryonic survival beyond E10. They positively regulate embryonic growth, somitogenesis and heart development. Tissue-specific ablation of *Ndr1/Ndr2* in the intestinal epithelium appears to sensitize mice to AOM induced colon carcinogenesis.

Mammalian NDR kinases function in centrosome duplication, mitotic chromosome alignment, apoptosis and proliferation (27, 36-38). However, the majority of the studies that led to the identification of these roles were performed in transformed tissue cultured cell lines (27, 37, 38). Therefore, it was important to generate an *in vivo* model to address the physiological relevance of these functions. Given that MST1/2 kinases function as up-stream regulators of mammalian NDR kinases, similar phenotypes could be expected for the respective knock-out mouse models. Both NDR1 and MST1 are highly abundant in lymphoid tissue (36, 115). *Ndr1*-null mice are morphologically indistinguishable from normal littermates at weaning, but develop T-cell lymphoma at old age (36). Similarly, loss of *Mst1* specifically affects T-cell development (113, 115). Moreover, loss of *Ndr2* or *Mst2* does not cause any overt morphological phenotype (Section 1, Figure 1; (105-107)). A single allele of either *Ndr1/2* or *Mst1/2* is sufficient for normal embryonic development, but complete loss of *Ndr1/2* or *Mst1/2* is embryonic lethal, indicating that both NDR1/2 and MST1/2 can efficiently compensate for each other (Section 1, Table 1 and 2; (105-107)). Detailed comparison of mutant *Ndr1/2* and *Mst1/2* embryos reveals that their respective phenotypes are also generally similar. Both

*Ndr1/2* and *Mst1/2*-null embryos are growth retarded and developmentally delayed at E8.5 (Section 1, Figure 3; (105-107)). By E9.5 mutant embryos show pericardial edema and their yolk sac vasculature has failed to undergo remodeling, indicating cardiac insufficiency (Section 1, Figure 4; (105-107)). While we specifically observe arrested heart development in *Ndr1/2* mutant embryos at the onset of cardiac looping (Section 1, Figure 10), specific heart defects are not reported in any of the *Mst1/2* double KO studies (105-107). However, pericardial edema and un-remodeled yolk sac vasculature of *Mst1/2*-null embryos suggest that cardiac development is equally affected by loss of MST1/2. MST1/2 kinases are core components of the mammalian Hippo pathway. At present, the majority of studies addressing mammalian Hippo signaling designates LATS1/2 kinases as main substrates and down-stream effectors of MST1/2 (99, 116, 117). However, *Lats2*-null mice die only around E12.5 (118) and *Lats1* KO mice are still detected in the expected Mendelian ratio at E18.5 (119). Taken together, these findings suggest that NDR kinases rather than LATS kinases are important down-stream effectors of MST1/2 signaling during organogenesis.

The first obvious defect of *Ndr*-null embryos is their reduced size at E8.5. Microarray analysis revealed that the CDK inhibitors *p21* and *p27* are up-regulated in mutant embryos (Section 1, Table 3), suggesting that NDR kinases positively regulate proliferation. An independent study recently found that NDR kinases regulate G1/S transition in HeLa cells (10). They do so by directly phosphorylating *p21* which results in its destabilization and subsequently decreased *p21* levels. Moreover, the study shows that NDR stabilizes c-myc protein in a kinase-independent manner (10). C-myc was shown to repress *p21* and *p27* at the transcriptional level (120). Therefore, it is tempting to speculate that the increased

levels of *p21* and *p27* in *Ndr*-null embryos reflect that NDR kinases regulate proliferation *in vivo* by means of controlling G1/S transition. Alternatively, loss of NDR could potentially affect cell size. Although we do not detect gross cell size difference by visual examination of the embryo sections, further analyses are required to exclude that loss of NDR negatively affects cell growth. Mutant embryos do not show signs of over-proliferation, indicating that the role of NDR kinases in apoptosis induction is not essential for embryonic development prior to E10. Although technically challenging, it would be interesting to analyze centrosome and chromosome status of cells in NDR-deficient embryos, because loss of NDR was shown to interfere with centrosome duplication (37) and mitotic chromosome alignment (38). Primary mouse embryonic fibroblasts with a conditional deletion of *Ndr1/2* represent a valuable tool to address the role of NDR kinases in the regulation of cell cycle progression in future studies. Moreover, they can be used to identify substrates of NDR kinases using the NDR-Shokat mutant generated by R. Kohler (unpublished work).

*Ndr*-null embryos display small and irregularly shaped somites (Section 1, Figure 6, 7) and arrest heart development at the onset of cardiac looping (Figure 10), revealing previously unknown roles for mammalian NDR kinases as positive regulators of somitogenesis and heart development. Importantly, members of the Notch pathway that are implicated in somitogenesis are asymmetrically expressed in the presomitic mesoderm of *Ndr*-null embryos at E8.5 (Section 1, Figure 9). Both somitogenesis and cardiac looping depend on properly established symmetry axes in the embryo (121-123). Therefore, a symmetry defect could be the common underlying cause for abnormal somitogenesis and arrested cardiac development in

NDR-deficient embryos. Retinoic acid (RA), a derivative of vitamin A, is indispensable for symmetric somitogenesis (124-127). Transcript levels of *Raldh2*, an essential enzyme for RA synthesis in the embryo (128), are down-regulated 1.3 fold in *Ndr*-null embryos (Section 3.1, Table 3B). However, we do not detect changes in *Raldh2* expression patterns as reported for a mouse mutant with a somite symmetry defect due to impaired RA signaling (129). Moreover, *Lunatic fringe* (*Lnfg*) expression domains are asymmetrically shifted in this mutant while we observe asymmetric loss of *Lnfg* expression in NDR-deficient embryos ((129) and Section 3.1, Figure 8). Therefore, the symmetry defects observed in *Ndr*-null mutants are most likely not due to impaired RA signaling. Conversely, our microarray data indicate that several members of the Notch pathway are down-regulated in *Ndr*-null embryos at E8.5 (Section 1, Table 3B). On the one hand, these proteins are essential for proper somitogenesis (130-133), as reflected by altered somite morphology of mutant embryos (Section 1, Figure 6 and 7). On the other hand, Notch signaling is essential for left-side specific expression of *Nodal* (134), the initial molecular manifestation of the left / right axis in the embryo. Interestingly, the intracellular domain of all four Notch receptors (NICD) contains a putative phosphorylation site for NDR kinases (R.Tamaskovic, unpublished observation), representing a potential entry point for NDR kinases to impact on Notch signaling. Moreover, NDR kinases are required for centriole duplication (37), providing an additional putative link to the establishment of left / right symmetry up-stream of left-sided *Nodal* expression. Modified centrioles, so-called basal bodies are a core component of primary cilia (135). Therefore, loss of NDR might result in defective primary cilia. Primary cilia in the node generate leftward flow of extra-embryonic fluid which induces left-restricted expression of *Nodal* (136-

142). Impaired primary cilia function results in laterality defects in mice (143-148) and humans (summarized in (149)). Primary cilia are absent from cells in the node of mice that lack intraflagellar transport proteins, such as KIF3A, KIF3B or Ift88. These mice show random heart looping and die by mid-gestation due to cardiovascular malformation (143, 144, 147). Therefore, future studies will analyze the expression patterns of symmetry markers (*Nodal*, *Lefty-2*) in *Ndr*-null embryos to address whether NDR kinases play a role in the establishment of left / right symmetry. Moreover, we will determine whether NDR can phosphorylate the Notch receptor as suggested by bioinformatic phospho-site prediction. Alternatively, NDR kinases could mediate cardiac looping more directly via interactions with the actin cytoskeleton. Although the exact mechanism that drives rightward looping of the heart tube is unknown, one line of evidence attributes an important role to the actin cytoskeleton (150-153). Mammalian NDR2 was shown to directly bind actin (154), and Cbk1, the NDR homolog in yeast, interacts with the cytoskeleton to control polarized growth (19, 28, 155). In summary, NDR kinases are essential for cardiac looping, arguably their most relevant function for survival of the developing embryo. Based on our observations, NDR kinases might contribute to establish left / right symmetry in the embryo, a prerequisite for rightward cardiac looping. Alternatively, they could mediate morphogenic looping by modulating cytoskeleton architecture. However, both hypotheses remain speculative and have to be evaluated in future studies of heart-specific *Ndr* knock-out mice.

While the complete *Ndr1/2* double KO strategy has revealed previously unknown roles of NDR kinases in cardiac development and somitogenesis, early embryonic lethality precludes the analysis of other functions in development and



tumorigenesis. As described earlier, *Ndr* homologs in worm and fly orchestrate dendritic tiling, a process that ensures complete but non-redundant dendritic coverage of receptive fields (31, 33). Importantly, abnormal dendritic tiling has been linked to neurological and neurodevelopmental disorders in humans (156). NDR2 is the major isoform expressed in murine brain (Section 3.1, Figure 2). Contrary to other tissues with high intrinsic NDR2 levels, NDR1 levels are not up-regulated in brains of adult mice. The adult brain is thus the only tissue that does not counteract total loss of NDR protein. Studies in *Drosophila* indicate that Trc, the fly homolog of NDR, is essential for dendritic tiling but dispensable for dendrite maintenance (32). Similarly, NDR levels might only be required for earlier stages of neural development in mice. Therefore, compensatory up-regulation of NDR1 in brains of *Ndr2*-null mice might be transient and no longer detectable in adult mice. Nevertheless, *Ndr2*-null mice should be subjected to standard behavioral tests such as fear conditioning to assess whether loss of NDR2 affects brain function. Experimental evidence for a role of mammalian NDR kinases in neuronal development comes from our observation that *pax6* levels are down-regulated 1.5 fold in *Ndr*-null embryos at E8.5. The Pax6 transcription factor controls the development of the eye and other sensory organs (157). Importantly, Pax6 KO mice display axonal wiring defects (158). A collaboration with the group of Jeroen Pasterkamp at the UMC Utrecht has been initiated to generate neuron-specific *Ndr1/2* KO models to specifically study the role of mammalian NDR kinases in the brain.

In addition to investigating the roles of mammalian NDR kinases in normal development, we have also made use of the *Ndr1/2* double KO model to study the

impact of NDR kinases on tumorigenesis. Several lines of evidence suggest that mammalian NDR kinases play a role in cancer development. However, while certain reports describe up-regulated *Ndr* transcript levels in a particular cancer which would suggest an oncogenic function, others report down-regulated *Ndr* transcript levels, reflecting a tumor suppressive role (summarized in (90)). This controversy is mirrored by the different functions of mammalian NDR kinases, namely the positive regulation of centrosome duplication (37) and proliferation (10) which could provide oncogenic properties as opposed to its role in apoptosis induction (27, 36), endowing the kinase with tumor suppressive qualities. Moreover, aged *Ndr1*-null mice develop T-cell lymphoma (36). Although this last observation would favor a tumor suppressive function of NDR1, the concurrent robust up-regulation of NDR2 levels in thymus, spleen and lymph nodes obviates this straightforward conclusion. Furthermore, data obtained in the context of the present study indicate that MOB2 levels are significantly down-regulated in thymus, spleen and lymph nodes by an unknown mechanism when *Ndr1* is ablated (data not shown). As MOB2 was recently shown to function as a negative regulator of NDR kinases (16), this could indicate an alternative scenario, namely that unrestricted activation of NDR2 induces T-cell lymphoma in the absence of NDR1, in line with an oncogenic role of NDR kinases. To study the role of NDR kinases in colorectal cancer (CRC) and to circumvent the effect of compensatory up-regulation of the remaining NDR isoform, we have generated an intestinal-epithelium specific *Ndr1/2* double KO mouse line (*Ndr1*<sup>-/-</sup> *Ndr2*<sup>Δ/ΔVilCre</sup>). *Ndr1*<sup>-/-</sup> *Ndr2*<sup>Δ/ΔVilCre</sup> mice are initially indistinguishable from control littermates, but develop rectal prolapse at around five months of age (Section 3.2, Figure 3). Rectal prolapse has been reported in the context of deregulated immune

function (159-162). NDR1 is highly expressed in organs of the immune system and loss of *Ndr1* results in abnormal T-cell development ((36), Section 3.1, Figure 2). Therefore, rectal prolapse in *Ndr1*<sup>-/-</sup>*Ndr2*<sup>Δ/ΔVilCre</sup> mice could arise from the combination of a general defect of the immune system due to systemic loss of *Ndr1* and a local defect in the colonic epithelium due to loss of *Ndr2*. Detailed characterization of tissue morphology and inflammation status in prolapsed rectum are warranted to confirm this hypothesis. Importantly, patients suffering from chronic inflammation of the colon are at increased risk for developing CRC (163). As we did not observe spontaneous CRC formation in *Ndr1*<sup>-/-</sup>*Ndr2*<sup>Δ/ΔVilCre</sup> mice, we treated *Ndr1*<sup>-/-</sup>*Ndr2*<sup>Δ/ΔVilCre</sup> and *Ndr1*<sup>-/-</sup>*Ndr2*<sup>+/<sup>ΔVilCre</sup> control mice with AOM to induce CRC formation. Although additional studies have to be performed to confirm the statistical significance of our data, *Ndr1*<sup>-/-</sup>*Ndr2*<sup>Δ/ΔVilCre</sup> mice appear to be more susceptible to AOM induced CRC (Section 3.2, Figure 4). As none of the *Ndr1*<sup>-/-</sup>*Ndr2*<sup>+/<sup>ΔVilCre</sup> control mice developed rectal prolapse (Section 3.2, Figure 3) we cannot discriminate whether NDR kinases function as conventional tumor suppressors in this context or whether increased CRC susceptibility is a secondary effect of chronic inflammation. Taken together, our initial data from the study of tissue-specific ablation of *Ndr1/2* in the intestinal epithelium add yet another layer of complexity to the role of NDR kinases in the context of tumorigenesis. *Ndr1*<sup>-/-</sup>*Ndr2*<sup>Δ/ΔVilCre</sup> mice do not contribute a decisive argument to the tumor suppressor versus oncogene debate. However, they could represent a new model system to study the molecular mechanisms that underlie the increased risk of CRC formation in patients with chronic colonic inflammation. Although time constraints have restricted the use of the conditional *Ndr1/2* mouse model, tissue-specific deletion of NDR kinases in other organ systems is warranted. MST1/2, the</sup></sup>

mammalian hippo homologs (see General Introduction, Figure 8) were shown to regulate quiescence and tumor suppression in the liver via a currently unknown YAP-kinase that is distinct from LATS (105). Therefore, conditional ablation of *Ndr1/2* in the liver could provide insights into the putative role of NDR kinases in liver tumorigenesis.

In summary, the mouse model for combined *Ndr1/Ndr2* deficiency generated in the context of this thesis demonstrates for the first time that NDR kinases play essential roles in mammalian biology. It establishes NDR kinases as physiological regulators of growth and cardiac development. Moreover, the conditional *Ndr1/Ndr2* double knock-out mouse line represents a valuable tool for future research addressing the roles of NDR kinases in normal physiology and disease.

## 5 General References

1. Millward T, Cron P, Hemmings BA. Molecular cloning and characterization of a conserved nuclear serine(threonine) protein kinase. *Proc Natl Acad Sci U S A*. 1995;92:5022-5026.
2. Berg MB, Tymoczko JL, Stryer L. *Biochemistry* (ed 6th edition). New York: Sara Tenney; 2007.
3. Manning G, Whyte DB, Martinez R, Hunter T, Sudarsanam S. The protein kinase complement of the human genome. *Science*. 2002;298:1912-1934.
4. Hanks SK, Hunter T. Protein kinases 6. The eukaryotic protein kinase superfamily: kinase (catalytic) domain structure and classification. *FASEB J*. 1995;9:576-596.
5. Remy I, Montmarquette A, Michnick SW. PKB/Akt modulates TGF-beta signalling through a direct interaction with Smad3. *Nat Cell Biol*. 2004;6:358-365.
6. Kim M, Lee JH, Koh H, et al. Inhibition of ERK-MAP kinase signaling by RSK during *Drosophila* development. *EMBO J*. 2006;25:3056-3067.
7. Jiang X, Yang P, Ma L. Kinase activity-independent regulation of cyclin pathway by GRK2 is essential for zebrafish early development. *Proc Natl Acad Sci U S A*. 2009;106:10183-10188.
8. Kim S, Gailite I, Moussian B, et al. Kinase-activity-independent functions of atypical protein kinase C in *Drosophila*. *J Cell Sci*. 2009;122:3759-3771.
9. Lee YG, Lee SW, Sin HS, Kim EJ, Um SJ. Kinase activity-independent suppression of p73alpha by AMP-activated kinase alpha (AMPKalpha). *Oncogene*. 2009;28:1040-1052.
10. Cornils H, Kohler RS, Hergovich A, Hemmings BA. Human NDR kinases control G1/S cell cycle transition by directly regulating p21 and c-myc stability. *Friedrich Miescher Institut*. Basel: Basel; 2010.
11. Pearce LR, Komander D, Alessi DR. The nuts and bolts of AGC protein kinases. *Nat Rev Mol Cell Biol*. 2010;11:9-22.
12. Bichsel SJ, Tamaskovic R, Stegert MR, Hemmings BA. Mechanism of activation of NDR (nuclear Dbf2-related) protein kinase by the hMOB1 protein. *J Biol Chem*. 2004;279:35228-35235.

13. Hergovich A, Stegert MR, Schmitz D, Hemmings BA. NDR kinases regulate essential cell processes from yeast to humans. *Nat Rev Mol Cell Biol.* 2006;7:253-264.
14. Hou MC, Salek J, McCollum D. Mob1p interacts with the Sid2p kinase and is required for cytokinesis in fission yeast. *Curr Biol.* 2000;10:619-622.
15. Hou MC, Wiley DJ, Verde F, McCollum D. Mob2p interacts with the protein kinase Orb6p to promote coordination of cell polarity with cell cycle progression. *J Cell Sci.* 2003;116:125-135.
16. Kohler RS, Schmitz D, Cornils H, Hemmings BA, Hergovich A. Differential NDR/LATS Interactions with the Human MOB Family Reveal a Negative Role for hMOB2 in the Regulation of Human NDR Kinases. *Mol Cell Biol.* 2010.
17. Komarnitsky SI, Chiang YC, Luca FC, et al. DBF2 protein kinase binds to and acts through the cell cycle-regulated MOB1 protein. *Mol Cell Biol.* 1998;18:2100-2107.
18. Mah AS, Jang J, Deshaies RJ. Protein kinase Cdc15 activates the Dbf2-Mob1 kinase complex. *Proc Natl Acad Sci U S A.* 2001;98:7325-7330.
19. Weiss EL, Kurischko C, Zhang C, Shokat K, Drubin DG, Luca FC. The *Saccharomyces cerevisiae* Mob2p-Cbk1p kinase complex promotes polarized growth and acts with the mitotic exit network to facilitate daughter cell-specific localization of Ace2p transcription factor. *J Cell Biol.* 2002;158:885-900.
20. Devroe E, Erdjument-Bromage H, Tempst P, Silver PA. Human Mob proteins regulate the NDR1 and NDR2 serine-threonine kinases. *J Biol Chem.* 2004;279:24444-24451.
21. Hergovich A, Bichsel SJ, Hemmings BA. Human NDR kinases are rapidly activated by MOB proteins through recruitment to the plasma membrane and phosphorylation. *Mol Cell Biol.* 2005;25:8259-8272.
22. Millward TA, Hess D, Hemmings BA. Ndr protein kinase is regulated by phosphorylation on two conserved sequence motifs. *J Biol Chem.* 1999;274:33847-33850.
23. Stegert MR, Hergovich A, Tamaskovic R, Bichsel SJ, Hemmings BA. Regulation of NDR protein kinase by hydrophobic motif phosphorylation

- mediated by the mammalian Ste20-like kinase MST3. *Mol Cell Biol.* 2005;25:11019-11029.
24. Stegert MR, Tamaskovic R, Bichsel SJ, Hergovich A, Hemmings BA. Regulation of NDR2 protein kinase by multi-site phosphorylation and the S100B calcium-binding protein. *J Biol Chem.* 2004;279:23806-23812.
  25. Tamaskovic R, Bichsel SJ, Rogniaux H, Stegert MR, Hemmings BA. Mechanism of Ca<sup>2+</sup>-mediated regulation of NDR protein kinase through autophosphorylation and phosphorylation by an upstream kinase. *J Biol Chem.* 2003;278:6710-6718.
  26. Hergovich A, Kohler RS, Schmitz D, Vichalkovski A, Cornils H, Hemmings BA. The MST1 and hMOB1 tumor suppressors control human centrosome duplication by regulating NDR kinase phosphorylation. *Curr Biol.* 2009;19:1692-1702.
  27. Vichalkovski A, Gresko E, Cornils H, Hergovich A, Schmitz D, Hemmings BA. NDR kinase is activated by RASSF1A/MST1 in response to Fas receptor stimulation and promotes apoptosis. *Curr Biol.* 2008;18:1889-1895.
  28. Bidlingmaier S, Weiss EL, Seidel C, Drubin DG, Snyder M. The Cbk1p pathway is important for polarized cell growth and cell separation in *Saccharomyces cerevisiae*. *Mol Cell Biol.* 2001;21:2449-2462.
  29. Tamaskovic R, Bichsel SJ, Hemmings BA. NDR family of AGC kinases--essential regulators of the cell cycle and morphogenesis. *FEBS Lett.* 2003;546:73-80.
  30. Geng W, He B, Wang M, Adler PN. The tricornered gene, which is required for the integrity of epidermal cell extensions, encodes the *Drosophila* nuclear DBF2-related kinase. *Genetics.* 2000;156:1817-1828.
  31. Emoto K, He Y, Ye B, et al. Control of dendritic branching and tiling by the Tricornered-kinase/Furry signaling pathway in *Drosophila* sensory neurons. *Cell.* 2004;119:245-256.
  32. Emoto K, Parrish JZ, Jan LY, Jan YN. The tumour suppressor Hippo acts with the NDR kinases in dendritic tiling and maintenance. *Nature.* 2006;443:210-213.

33. Gallegos ME, Bargmann CI. Mechanosensory neurite termination and tiling depend on SAX-2 and the SAX-1 kinase. *Neuron*. 2004;44:239-249.
34. Zallen JA, Kirch SA, Bargmann CI. Genes required for axon pathfinding and extension in the *C. elegans* nerve ring. *Development*. 1999;126:3679-3692.
35. Zallen JA, Peckol EL, Tobin DM, Bargmann CI. Neuronal cell shape and neurite initiation are regulated by the Ndr kinase SAX-1, a member of the Orb6/COT-1/warts serine/threonine kinase family. *Mol Biol Cell*. 2000;11:3177-3190.
36. Cornils H, Stegert MR, Hergovich A, et al. Ablation of the kinase NDR1 predisposes mice to the development of T cell lymphoma. *Sci Signal*. 2010;3:ra47.
37. Hergovich A, Lamla S, Nigg EA, Hemmings BA. Centrosome-associated NDR kinase regulates centrosome duplication. *Mol Cell*. 2007;25:625-634.
38. Chiba S, Ikeda M, Katsunuma K, Ohashi K, Mizuno K. MST2- and Furry-mediated activation of NDR1 kinase is critical for precise alignment of mitotic chromosomes. *Curr Biol*. 2009;19:675-681.
39. Chiang C, Litingtung Y, Lee E, et al. Cyclopia and defective axial patterning in mice lacking Sonic hedgehog gene function. *Nature*. 1996;383:407-413.
40. Schachter KA, Krauss RS. Murine models of holoprosencephaly. *Curr Top Dev Biol*. 2008;84:139-170.
41. Teglund S, Toftgard R. Hedgehog beyond medulloblastoma and basal cell carcinoma. *Biochim Biophys Acta*. 2010;1805:181-208.
42. Lints TJ, Parsons LM, Hartley L, Lyons I, Harvey RP. Nkx-2.5: a novel murine homeobox gene expressed in early heart progenitor cells and their myogenic descendants. *Development*. 1993;119:419-431.
43. Akazawa H, Komuro I. Cardiac transcription factor Csx/Nkx2-5: Its role in cardiac development and diseases. *Pharmacol Ther*. 2005;107:252-268.
44. Benson DW, Silberbach GM, Kavanaugh-McHugh A, et al. Mutations in the cardiac transcription factor NKX2.5 affect diverse cardiac developmental pathways. *J Clin Invest*. 1999;104:1567-1573.



45. Elliott DA, Kirk EP, Yeoh T, et al. Cardiac homeobox gene NKX2-5 mutations and congenital heart disease: associations with atrial septal defect and hypoplastic left heart syndrome. *J Am Coll Cardiol.* 2003;41:2072-2076.
46. Goldmuntz E. The epidemiology and genetics of congenital heart disease. *Clin Perinatol.* 2001;28:1-10.
47. Gutierrez-Roelens I, Sluysmans T, Gewillig M, Devriendt K, Vikkula M. Progressive AV-block and anomalous venous return among cardiac anomalies associated with two novel missense mutations in the CSX/NKX2-5 gene. *Hum Mutat.* 2002;20:75-76.
48. McElhinney DB, Geiger E, Blinder J, Benson DW, Goldmuntz E. NKX2.5 mutations in patients with congenital heart disease. *J Am Coll Cardiol.* 2003;42:1650-1655.
49. Schott JJ, Benson DW, Basson CT, et al. Congenital heart disease caused by mutations in the transcription factor NKX2-5. *Science.* 1998;281:108-111.
50. Conway SJ, Kruzynska-Frejtag A, Kneer PL, Machnicki M, Koushik SV. What cardiovascular defect does my prenatal mouse mutant have, and why? *Genesis.* 2003;35:1-21.
51. Copp AJ. Death before birth: clues from gene knockouts and mutations. *Trends Genet.* 1995;11:87-93.
52. Cross JC, Werb Z, Fisher SJ. Implantation and the placenta: key pieces of the development puzzle. *Science.* 1994;266:1508-1518.
53. Santamaria D, Barriere C, Cerqueira A, et al. Cdk1 is sufficient to drive the mammalian cell cycle. *Nature.* 2007;448:811-815.
54. Bultman S, Gebuhr T, Yee D, et al. A Brg1 null mutation in the mouse reveals functional differences among mammalian SWI/SNF complexes. *Mol Cell.* 2000;6:1287-1295.
55. Morham SG, Kluckman KD, Voulomanos N, Smithies O. Targeted disruption of the mouse topoisomerase I gene by camptothecin selection. *Mol Cell Biol.* 1996;16:6804-6809.
56. Tsuzuki T, Fujii Y, Sakumi K, et al. Targeted disruption of the Rad51 gene leads to lethality in embryonic mice. *Proc Natl Acad Sci U S A.* 1996;93:6236-6240.

57. Nishioka N, Inoue K, Adachi K, et al. The Hippo signaling pathway components Lats and Yap pattern Tead4 activity to distinguish mouse trophectoderm from inner cell mass. *Dev Cell*. 2009;16:398-410.
58. Cross JC. Genetic insights into trophoblast differentiation and placental morphogenesis. *Semin Cell Dev Biol*. 2000;11:105-113.
59. Rossant J, Cross JC. Placental development: lessons from mouse mutants. *Nat Rev Genet*. 2001;2:538-548.
60. Simon C, Frances A, Piquette GN, et al. Embryonic implantation in mice is blocked by interleukin-1 receptor antagonist. *Endocrinology*. 1994;134:521-528.
61. Nagy A, Gertsenstein M, Vintersten K, Behringer K. *Manipulating the Mouse Embryo Vol. (ed 3rd)*. Cold Spring Harbor, New York Cold Spring Harbor Laboratory Press 2003
62. George EL, Georges-Labouesse EN, Patel-King RS, Rayburn H, Hynes RO. Defects in mesoderm, neural tube and vascular development in mouse embryos lacking fibronectin. *Development*. 1993;119:1079-1091.
63. Yang JT, Rayburn H, Hynes RO. Embryonic mesodermal defects in alpha 5 integrin-deficient mice. *Development*. 1993;119:1093-1105.
64. Goldie LC, Nix MK, Hirschi KK. Embryonic vasculogenesis and hematopoietic specification. *Organogenesis*. 2008;4:257-263.
65. Carmeliet P, Ferreira V, Breier G, et al. Abnormal blood vessel development and lethality in embryos lacking a single VEGF allele. *Nature*. 1996;380:435-439.
66. Shalaby F, Rossant J, Yamaguchi TP, et al. Failure of blood-island formation and vasculogenesis in Flk-1-deficient mice. *Nature*. 1995;376:62-66.
67. Lucitti JL, Jones EA, Huang C, Chen J, Fraser SE, Dickinson ME. Vascular remodeling of the mouse yolk sac requires hemodynamic force. *Development*. 2007;134:3317-3326.
68. Bonifer C, Faust N, Geiger H, Muller AM. Developmental changes in the differentiation capacity of haematopoietic stem cells. *Immunol Today*. 1998;19:236-241.

69. Baribault H, Price J, Miyai K, Oshima RG. Mid-gestational lethality in mice lacking keratin 8. *Genes Dev.* 1993;7:1191-1202.
70. Jacks T, Fazeli A, Schmitt EM, Bronson RT, Goodell MA, Weinberg RA. Effects of an Rb mutation in the mouse. *Nature.* 1992;359:295-300.
71. Lee EY, Chang CY, Hu N, et al. Mice deficient for Rb are nonviable and show defects in neurogenesis and haematopoiesis. *Nature.* 1992;359:288-294.
72. Mucenski ML, McLain K, Kier AB, et al. A functional c-myc gene is required for normal murine fetal hepatic hematopoiesis. *Cell.* 1991;65:677-689.
73. DeRuiter MC, Poelmann RE, VanderPlas-de Vries I, Mentink MM, Gittenberger-de Groot AC. The development of the myocardium and endocardium in mouse embryos. Fusion of two heart tubes? *Anat Embryol (Berl).* 1992;185:461-473.
74. Adamo L, Naveiras O, Wenzel PL, et al. Biomechanical forces promote embryonic haematopoiesis. *Nature.* 2009;459:1131-1135.
75. Buckingham M, Meilhac S, Zaffran S. Building the mammalian heart from two sources of myocardial cells. *Nat Rev Genet.* 2005;6:826-835.
76. Bruneau BG, Logan M, Davis N, et al. Chamber-specific cardiac expression of Tbx5 and heart defects in Holt-Oram syndrome. *Dev Biol.* 1999;211:100-108.
77. Cai CL, Liang X, Shi Y, et al. Isl1 identifies a cardiac progenitor population that proliferates prior to differentiation and contributes a majority of cells to the heart. *Dev Cell.* 2003;5:877-889.
78. Lin Q, Schwarz J, Bucana C, Olson EN. Control of mouse cardiac morphogenesis and myogenesis by transcription factor MEF2C. *Science.* 1997;276:1404-1407.
79. Lyons I, Parsons LM, Hartley L, et al. Myogenic and morphogenetic defects in the heart tubes of murine embryos lacking the homeo box gene Nkx2-5. *Genes Dev.* 1995;9:1654-1666.
80. Riley P, Anson-Cartwright L, Cross JC. The Hand1 bHLH transcription factor is essential for placentation and cardiac morphogenesis. *Nat Genet.* 1998;18:271-275.

81. Srivastava D, Thomas T, Lin Q, Kirby ML, Brown D, Olson EN. Regulation of cardiac mesodermal and neural crest development by the bHLH transcription factor, dHAND. *Nat Genet.* 1997;16:154-160.
82. von Both I, Silvestri C, Erdemir T, et al. Foxh1 is essential for development of the anterior heart field. *Dev Cell.* 2004;7:331-345.
83. Charron J, Malynn BA, Fisher P, et al. Embryonic lethality in mice homozygous for a targeted disruption of the N-myc gene. *Genes Dev.* 1992;6:2248-2257.
84. Chen Z, Friedrich GA, Soriano P. Transcriptional enhancer factor 1 disruption by a retroviral gene trap leads to heart defects and embryonic lethality in mice. *Genes Dev.* 1994;8:2293-2301.
85. Jacks T, Shih TS, Schmitt EM, Bronson RT, Bernards A, Weinberg RA. Tumour predisposition in mice heterozygous for a targeted mutation in Nf1. *Nat Genet.* 1994;7:353-361.
86. Moens CB, Stanton BR, Parada LF, Rossant J. Defects in heart and lung development in compound heterozygotes for two different targeted mutations at the N-myc locus. *Development.* 1993;119:485-499.
87. Sucov HM, Dyson E, Gumeringer CL, Price J, Chien KR, Evans RM. RXR alpha mutant mice establish a genetic basis for vitamin A signaling in heart morphogenesis. *Genes Dev.* 1994;8:1007-1018.
88. Culver JC, Dickinson ME. The effects of hemodynamic force on embryonic development. *Microcirculation.* 2010;17:164-178.
89. Watson ED, Cross JC. Development of structures and transport functions in the mouse placenta. *Physiology (Bethesda).* 2005;20:180-193.
90. Hergovich A, Cornils H, Hemmings BA. Mammalian NDR protein kinases: from regulation to a role in centrosome duplication. *Biochim Biophys Acta.* 2008;1784:3-15.
91. Xu T, Wang W, Zhang S, Stewart RA, Yu W. Identifying tumor suppressors in genetic mosaics: the *Drosophila* lats gene encodes a putative protein kinase. *Development.* 1995;121:1053-1063.
92. Bothos J, Tuttle RL, Ottey M, Luca FC, Halazonetis TD. Human LATS1 is a mitotic exit network kinase. *Cancer Res.* 2005;65:6568-6575.

93. Hergovich A, Schmitz D, Hemmings BA. The human tumour suppressor LATS1 is activated by human MOB1 at the membrane. *Biochem Biophys Res Commun.* 2006;345:50-58.
94. Hao Y, Chun A, Cheung K, Rashidi B, Yang X. Tumor suppressor LATS1 is a negative regulator of oncogene YAP. *J Biol Chem.* 2008;283:5496-5509.
95. Ota M, Sasaki H. Mammalian Tead proteins regulate cell proliferation and contact inhibition as transcriptional mediators of Hippo signaling. *Development.* 2008;135:4059-4069.
96. Zhao B, Wei X, Li W, et al. Inactivation of YAP oncoprotein by the Hippo pathway is involved in cell contact inhibition and tissue growth control. *Genes Dev.* 2007;21:2747-2761.
97. Bertini E, Oka T, Sudol M, Strano S, Blandino G. YAP: at the crossroad between transformation and tumor suppression. *Cell Cycle.* 2009;8:49-57.
98. Zeng Q, Hong W. The emerging role of the hippo pathway in cell contact inhibition, organ size control, and cancer development in mammals. *Cancer Cell.* 2008;13:188-192.
99. Zhao B, Li L, Lei Q, Guan KL. The Hippo-YAP pathway in organ size control and tumorigenesis: an updated version. *Genes Dev.* 2010;24:862-874.
100. Oh H, Irvine KD. Yorkie: the final destination of Hippo signaling. *Trends Cell Biol.* 2010;20:410-417.
101. Camargo FD, Gokhale S, Johnnidis JB, et al. YAP1 increases organ size and expands undifferentiated progenitor cells. *Curr Biol.* 2007;17:2054-2060.
102. Fernandez LA, Northcott PA, Dalton J, et al. YAP1 is amplified and up-regulated in hedgehog-associated medulloblastomas and mediates Sonic hedgehog-driven neural precursor proliferation. *Genes Dev.* 2009;23:2729-2741.
103. Wang Y, Dong Q, Zhang Q, Li Z, Wang E, Qiu X. Overexpression of yes-associated protein contributes to progression and poor prognosis of non-small-cell lung cancer. *Cancer Sci.* 2010;101:1279-1285.
104. Xu MZ, Yao TJ, Lee NP, et al. Yes-associated protein is an independent prognostic marker in hepatocellular carcinoma. *Cancer.* 2009;115:4576-4585.

105. Zhou D, Conrad C, Xia F, et al. Mst1 and Mst2 maintain hepatocyte quiescence and suppress hepatocellular carcinoma development through inactivation of the Yap1 oncogene. *Cancer Cell*. 2009;16:425-438.
106. Oh S, Lee D, Kim T, et al. Crucial role for Mst1 and Mst2 kinases in early embryonic development of the mouse. *Mol Cell Biol*. 2009;29:6309-6320.
107. Song H, Mak KK, Topol L, et al. Mammalian Mst1 and Mst2 kinases play essential roles in organ size control and tumor suppression. *Proc Natl Acad Sci U S A*. 2010;107:1431-1436.
108. Ganem NJ, Godinho SA, Pellman D. A mechanism linking extra centrosomes to chromosomal instability. *Nature*. 2009;460:278-282.
109. D'Assoro AB, Lingle WL, Salisbury JL. Centrosome amplification and the development of cancer. *Oncogene*. 2002;21:6146-6153.
110. Lengauer C, Kinzler KW, Vogelstein B. Genetic instability in colorectal cancers. *Nature*. 1997;386:623-627.
111. Nigg EA. Centrosome aberrations: cause or consequence of cancer progression? *Nat Rev Cancer*. 2002;2:815-825.
112. Sluder G, Nordberg JJ. The good, the bad and the ugly: the practical consequences of centrosome amplification. *Curr Opin Cell Biol*. 2004;16:49-54.
113. Dong Y, Du X, Ye J, et al. A cell-intrinsic role for Mst1 in regulating thymocyte egress. *J Immunol*. 2009;183:3865-3872.
114. Goldie LC, Lucitti JL, Dickinson ME, Hirschi KK. Cell signaling directing the formation and function of hemogenic endothelium during murine embryogenesis. *Blood*. 2008;112:3194-3204.
115. Zhou D, Medoff BD, Chen L, et al. The Nore1B/Mst1 complex restrains antigen receptor-induced proliferation of naive T cells. *Proc Natl Acad Sci U S A*. 2008;105:20321-20326.
116. Badouel C, Garg A, McNeill H. Herding Hippos: regulating growth in flies and man. *Curr Opin Cell Biol*. 2009;21:837-843.
117. Saucedo LJ, Edgar BA. Filling out the Hippo pathway. *Nat Rev Mol Cell Biol*. 2007;8:613-621.

118. McPherson JP, Tamblyn L, Elia A, et al. Lats2/Kpm is required for embryonic development, proliferation control and genomic integrity. *EMBO J.* 2004;23:3677-3688.
119. St John MA, Tao W, Fei X, et al. Mice deficient of Lats1 develop soft-tissue sarcomas, ovarian tumours and pituitary dysfunction. *Nat Genet.* 1999;21:182-186.
120. Yang W, Shen J, Wu M, et al. Repression of transcription of the p27(Kip1) cyclin-dependent kinase inhibitor gene by c-Myc. *Oncogene.* 2001;20:1688-1702.
121. Dequeant ML, Pourquie O. Segmental patterning of the vertebrate embryonic axis. *Nat Rev Genet.* 2008;9:370-382.
122. Harvey RP. Cardiac looping--an uneasy deal with laterality. *Semin Cell Dev Biol.* 1998;9:101-108.
123. Shiratori H, Hamada H. The left-right axis in the mouse: from origin to morphology. *Development.* 2006;133:2095-2104.
124. Kawakami Y, Raya A, Raya RM, Rodriguez-Esteban C, Belmonte JC. Retinoic acid signalling links left-right asymmetric patterning and bilaterally symmetric somitogenesis in the zebrafish embryo. *Nature.* 2005;435:165-171.
125. Sirbu IO, Duester G. Retinoic-acid signalling in node ectoderm and posterior neural plate directs left-right patterning of somitic mesoderm. *Nat Cell Biol.* 2006;8:271-277.
126. Vermot J, Gallego Llamas J, Fraulob V, Niederreither K, Chambon P, Dolle P. Retinoic acid controls the bilateral symmetry of somite formation in the mouse embryo. *Science.* 2005;308:563-566.
127. Vermot J, Pourquie O. Retinoic acid coordinates somitogenesis and left-right patterning in vertebrate embryos. *Nature.* 2005;435:215-220.
128. Niederreither K, Vermot J, Messaddeq N, Schuhbaur B, Chambon P, Dolle P. Embryonic retinoic acid synthesis is essential for heart morphogenesis in the mouse. *Development.* 2001;128:1019-1031.
129. Vilhais-Neto GC, Maruhashi M, Smith KT, et al. Rere controls retinoic acid signalling and somite bilateral symmetry. *Nature.* 2010;463:953-957.

130. Bessho Y, Sakata R, Komatsu S, Shiota K, Yamada S, Kageyama R. Dynamic expression and essential functions of Hes7 in somite segmentation. *Genes Dev.* 2001;15:2642-2647.
131. Dunwoodie SL, Henrique D, Harrison SM, Beddington RS. Mouse Dll3: a novel divergent Delta gene which may complement the function of other Delta homologues during early pattern formation in the mouse embryo. *Development.* 1997;124:3065-3076.
132. Hrabe de Angelis M, McIntyre J, 2nd, Gossler A. Maintenance of somite borders in mice requires the Delta homologue Dll1. *Nature.* 1997;386:717-721.
133. Kusumi K, Sun ES, Kerrebrock AW, et al. The mouse pudgy mutation disrupts Delta homologue Dll3 and initiation of early somite boundaries. *Nat Genet.* 1998;19:274-278.
134. Krebs LT, Iwai N, Nonaka S, et al. Notch signaling regulates left-right asymmetry determination by inducing Nodal expression. *Genes Dev.* 2003;17:1207-1212.
135. Dutcher SK. Elucidation of basal body and centriole functions in *Chlamydomonas reinhardtii*. *Traffic.* 2003;4:443-451.
136. Capdevila J, Vogon KJ, Tabin CJ, Izpisua Belmonte JC. Mechanisms of left-right determination in vertebrates. *Cell.* 2000;101:9-21.
137. Mercola M, Levin M. Left-right asymmetry determination in vertebrates. *Annu Rev Cell Dev Biol.* 2001;17:779-805.
138. Wright CV. Mechanisms of left-right asymmetry: what's right and what's left? *Dev Cell.* 2001;1:179-186.
139. Essner JJ, Vogon KJ, Wagner MK, Tabin CJ, Yost HJ, Brueckner M. Conserved function for embryonic nodal cilia. *Nature.* 2002;418:37-38.
140. Hamada H, Meno C, Watanabe D, Saijoh Y. Establishment of vertebrate left-right asymmetry. *Nat Rev Genet.* 2002;3:103-113.
141. Nonaka S, Shiratori H, Saijoh Y, Hamada H. Determination of left-right patterning of the mouse embryo by artificial nodal flow. *Nature.* 2002;418:96-99.
142. Tabin CJ, Vogon KJ. A two-cilia model for vertebrate left-right axis specification. *Genes Dev.* 2003;17:1-6.



143. Murcia NS, Richards WG, Yoder BK, Mucenski ML, Dunlap JR, Woychik RP. The Oak Ridge Polycystic Kidney (orpk) disease gene is required for left-right axis determination. *Development*. 2000;127:2347-2355.
144. Nonaka S, Tanaka Y, Okada Y, et al. Randomization of left-right asymmetry due to loss of nodal cilia generating leftward flow of extraembryonic fluid in mice lacking KIF3B motor protein. *Cell*. 1998;95:829-837.
145. Okada Y, Nonaka S, Tanaka Y, Saijoh Y, Hamada H, Hirokawa N. Abnormal nodal flow precedes situs inversus in iv and inv mice. *Mol Cell*. 1999;4:459-468.
146. Okada Y, Takeda S, Tanaka Y, Belmonte JC, Hirokawa N. Mechanism of nodal flow: a conserved symmetry breaking event in left-right axis determination. *Cell*. 2005;121:633-644.
147. Takeda S, Yonekawa Y, Tanaka Y, Okada Y, Nonaka S, Hirokawa N. Left-right asymmetry and kinesin superfamily protein KIF3A: new insights in determination of laterality and mesoderm induction by kif3A<sup>-/-</sup> mice analysis. *J Cell Biol*. 1999;145:825-836.
148. Yokoyama T, Copeland NG, Jenkins NA, Montgomery CA, Elder FF, Overbeek PA. Reversal of left-right asymmetry: a situs inversus mutation. *Science*. 1993;260:679-682.
149. Fliegauf M, Benzing T, Omran H. When cilia go bad: cilia defects and ciliopathies. *Nat Rev Mol Cell Biol*. 2007;8:880-893.
150. Choi S, Gustafson-Wagner EA, Wang Q, et al. The intercalated disk protein, mXin $\alpha$ , is capable of interacting with beta-catenin and bundling actin filaments [corrected]. *J Biol Chem*. 2007;282:36024-36036.
151. Grosskurth SE, Bhattacharya D, Wang Q, Lin JJ. Emergence of Xin demarcates a key innovation in heart evolution. *PLoS One*. 2008;3:e2857.
152. Wang DZ, Reiter RS, Lin JL, et al. Requirement of a novel gene, Xin, in cardiac morphogenesis. *Development*. 1999;126:1281-1294.
153. Wang Q, Lin JL, Reinking BE, et al. Essential roles of an intercalated disc protein, mXin $\beta$ , in postnatal heart growth and survival. *Circ Res*. 2010;106:1468-1478.

154. Stork O, Zhdanov A, Kudersky A, Yoshikawa T, Obata K, Pape HC. Neuronal functions of the novel serine/threonine kinase Ndr2. *J Biol Chem.* 2004;279:45773-45781.
155. Racki WJ, Becam AM, Nasr F, Herbert CJ. Cbk1p, a protein similar to the human myotonic dystrophy kinase, is essential for normal morphogenesis in *Saccharomyces cerevisiae*. *EMBO J.* 2000;19:4524-4532.
156. Jan YN, Jan LY. Branching out: mechanisms of dendritic arborization. *Nat Rev Neurosci.* 2010;11:316-328.
157. Callaerts P, Halder G, Gehring WJ. PAX-6 in development and evolution. *Annu Rev Neurosci.* 1997;20:483-532.
158. Hevner RF, Miyashita-Lin E, Rubenstein JL. Cortical and thalamic axon pathfinding defects in *Tbr1*, *Gbx2*, and *Pax6* mutant mice: evidence that cortical and thalamic axons interact and guide each other. *J Comp Neurol.* 2002;447:8-17.
159. Kuhn R, Lohler J, Rennick D, Rajewsky K, Muller W. Interleukin-10-deficient mice develop chronic enterocolitis. *Cell.* 1993;75:263-274.
160. Mombaerts P, Mizoguchi E, Grusby MJ, Glimcher LH, Bhan AK, Tonegawa S. Spontaneous development of inflammatory bowel disease in T cell receptor mutant mice. *Cell.* 1993;75:274-282.
161. Sadlack B, Merz H, Schorle H, Schimpl A, Feller AC, Horak I. Ulcerative colitis-like disease in mice with a disrupted interleukin-2 gene. *Cell.* 1993;75:253-261.
162. Takayama H, Takagi H, Larochelle WJ, Kapur RP, Merlino G. Ulcerative proctitis, rectal prolapse, and intestinal pseudo-obstruction in transgenic mice overexpressing hepatocyte growth factor/scatter factor. *Lab Invest.* 2001;81:297-305.
163. Itzkowitz SH, Yio X. Inflammation and cancer IV. Colorectal cancer in inflammatory bowel disease: the role of inflammation. *Am J Physiol Gastrointest Liver Physiol.* 2004;287:G7-17.

## 6 Appendix

### ***Co-authorships and Contributions to Publications***

In the following section I have listed the publications I contributed to in the context of my PhD studies. As detailed below, I have significantly contributed to the paper

**“Differential NDR/LATS Interactions with the Human MOB Family Reveal a Negative Role for Human MOB2 in the Regulation of Human NDR Kinases”**  
***(Kohler et al.)***

The complete manuscript is included in the appendix. Contributions to other publications were less extensive. Therefore, I have only included the respective abstracts followed by a brief description of my contribution.

## **A. 1. Differential NDR/LATS Interactions with the Human MOB Family Reveal a Negative Role for hMOB2 in the Regulation of Human NDR Kinases**

*Kohler RS, **Schmitz D**, Cornils H, Hemmings BA, Hergovich A*

Published in *Molecular and Cellular Biology*. 2010 Sep;30(18):4507-20

“MOB proteins are integral components of signaling pathways controlling important cellular processes, such as mitotic exit, centrosome duplication, apoptosis, and cell proliferation in eukaryotes. The human MOB protein family consists of six distinct members (human MOB1A [hMOB1A], -1B, -2, -3A, -3B, and -3C), with hMOB1A/B the best studied due to their putative tumor-suppressive functions through the regulation of NDR/LATS kinases. The roles of the other MOB proteins are less well defined. Accordingly, we characterized all six human MOB proteins in the context of NDR/LATS binding and their abilities to activate NDR/LATS kinases. hMOB3A/B/C proteins neither bind nor activate any of the four human NDR/LATS kinases. We found that both hMOB2 and hMOB1A bound to the N-terminal region of NDR1. However, our data suggest that the binding modes differ significantly. Our work revealed that hMOB2 competes with hMOB1A for NDR binding. hMOB2, in contrast to hMOB1A/B, is bound to unphosphorylated NDR. Moreover, RNA interference (RNAi) depletion of hMOB2 resulted in increased NDR kinase activity. Consistent with these findings, hMOB2 overexpression interfered with the functional roles of NDR in death receptor signaling and centrosome overduplication. In summary, our data indicate that hMOB2 is a negative regulator of human NDR kinases in biochemical and biological settings.”

*I significantly contributed to the overall design of the study. Moreover, I designed and cloned various NDR mutants and performed co-immunoprecipitation experiments. Figure XY has been done by me. I also instructed and supervised a summer-internship student that performed experiments in the context of this study. Finally, I contributed to the editing of the manuscript. The complete manuscript is printed below (see next page).*

## Differential NDR/LATS Interactions with the Human MOB Family Reveal a Negative Role for Human MOB2 in the Regulation of Human NDR Kinases<sup>∇</sup>

Reto S. Kohler, Debora Schmitz, Hauke Cornils, Brian A. Hemmings,\* and Alexander Hergovich\*

*Friedrich Miescher Institute for Biomedical Research, Maulbeerstrasse 66, 4058 Basel, Switzerland*

Received 5 February 2010/Returned for modification 11 April 2010/Accepted 22 June 2010

**MOB proteins are integral components of signaling pathways controlling important cellular processes, such as mitotic exit, centrosome duplication, apoptosis, and cell proliferation in eukaryotes. The human MOB protein family consists of six distinct members (human MOB1A [hMOB1A], -1B, -2, -3A, -3B, and -3C), with hMOB1A/B the best studied due to their putative tumor-suppressive functions through the regulation of NDR/LATS kinases. The roles of the other MOB proteins are less well defined. Accordingly, we characterized all six human MOB proteins in the context of NDR/LATS binding and their abilities to activate NDR/LATS kinases. hMOB3A/B/C proteins neither bind nor activate any of the four human NDR/LATS kinases. We found that both hMOB2 and hMOB1A bound to the N-terminal region of NDR1. However, our data suggest that the binding modes differ significantly. Our work revealed that hMOB2 competes with hMOB1A for NDR binding. hMOB2, in contrast to hMOB1A/B, is bound to unphosphorylated NDR. Moreover, RNA interference (RNAi) depletion of hMOB2 resulted in increased NDR kinase activity. Consistent with these findings, hMOB2 overexpression interfered with the functional roles of NDR in death receptor signaling and centrosome overduplication. In summary, our data indicate that hMOB2 is a negative regulator of human NDR kinases in biochemical and biological settings.**

The first MOB (Mps one binder) protein was identified in *Saccharomyces cerevisiae* more than a decade ago (22, 25). Since then, members of the MOB protein family have been found in unicellular organisms to mammals. Initially, the biological roles of MOB proteins were mainly investigated using budding and fission yeasts, revealing that Mob1p plays a vital role in the control of mitotic exit (3, 8, 23). *Drosophila* MOB1 (dMOB1)/Mats (MOB as tumor suppressor) emerged as an integral part of the Hippo tumor-suppressing pathway controlling cell proliferation and apoptosis from recent work in *Drosophila melanogaster* (24, 37). Interestingly, the functions of MOB proteins seem to be evolutionarily conserved, since the lethality and overgrowth phenotypes in *Drosophila mats* mutants can be rescued by the human homolog human MOB1A (hMOB1A) (24). This suggests that the Hippo signaling pathway is highly conserved from flies to humans (9, 12, 30, 31, 40). However, the biological roles of hMOB1A/B seem to be more diverse, as they function in cellular proliferation (29), apoptosis (36), and centrosome duplication (13). Mob2p in budding and fission yeasts is an essential part of a signaling network responsible for polarized cell growth and transcriptional asymmetry (6, 20, 38). In flies, the biological functions of dMOB2 and dMOB3 are less understood. However, dMOB2 seems to

play a role in wing hair morphogenesis (10). In mammals, the biological roles of MOB2 proteins have so far proved elusive.

A conserved property of MOB proteins is the association with and activation of the NDR (nuclear-Dbf2-related) kinases of the AGC family (16, 28). In yeast, Mob1p binds to and is necessary for the activation of Dbf2/Dbf20 and Sid2 kinases (19, 22, 26). Similarly, Mob2p binds to and activates Cbk1 and Orb6 (20, 38). Furthermore, yeast MOB proteins and NDR kinases form restricted heterodimers of signaling complexes in which the subunits are not interchangeable (18, 20). In contrast, in multicellular organisms, the binding of MOB proteins is not restricted to a unique NDR kinase. For example, three MOB proteins exist in flies: dMOB1/Mats, dMOB2, and dMOB3 (10). dMOB1/Mats was shown to interact physically with warts, the fly homolog of human LATS1/2, and to be necessary for warts activity (24, 37). Moreover, dMOB1/Mats also genetically interacts with the second NDR kinase in flies, tricorned (*trc*) (10). Furthermore, it was shown in coimmunoprecipitation experiments that dMOB2 physically associates with *trc* (10).

The molecular mechanisms by which MOB proteins bind to and activate NDR kinases are best understood in mammals. hMOB1A binds to and activates human NDR1/2 kinases by stimulating autophosphorylation on the activation segment (2). Similarly, hMOB1A also binds to and activates LATS1 and -2 (4, 15, 39). In contrast, hMOB2 was shown to bind to NDR1 and NDR2, but not to LATS1 (4, 15). Importantly, hMOB1A/B are also required for efficient phosphorylation of the hydrophobic motif (T444/442) of NDR1/2 kinases by MST1 kinase (mammalian STE-20-like 1) (13, 36). Spatial relocalization of NDR kinases seems to be a further level of regulation, because membrane targeting of hMOB1 proteins leads to rapid activation of NDR1/2 and LATS1 kinases (11, 15). Indeed, mem-

\* Corresponding author. Mailing address for Brian A. Hemmings: Friedrich Miescher Institute for Biomedical Research, Maulbeerstrasse 66, CH-4058 Basel, Switzerland. Phone: 41 61 697 4872. Fax: 41 61 697 3976. E-mail: brian.hemmings@fmi.ch. Present address for Alexander Hergovich: UCL Cancer Institute, University College of London, London WC1E 6BT, United Kingdom. Phone: 44 20 7679 0723. Fax: 44 20 7679 6817. E-mail: a.hergovich@cancer.ucl.ac.uk.

<sup>∇</sup> Published ahead of print on 12 July 2010.

brane targeting of dMOB1/Mats in *Drosophila* activates warts kinase and inhibits tissue growth by increasing apoptosis and reducing proliferation (17). Further, membrane-targeted tricorned kinase rescues the dendritic tiling defect in *trc* mutant flies (21). These observations indicate that activation of NDR kinases by relocalization to the plasma membrane is an important step in NDR/LATS kinase activation and function.

Here, we study for the first time all six human MOB proteins (hMOB1A/B, hMOB2, and hMOB3A/B/C) with respect to their abilities to bind and activate all four human NDR kinases. Surprisingly, we found that three out of the six MOBs neither bind to nor activate human NDR1/2 or LATS1/2 kinases. By focusing on the NDR1/2-specific binder hMOB2, we found that hMOB2 competes with hMOB1A/B for NDR binding. Furthermore, we provide evidence that overexpression of hMOB2 impairs NDR1/2 activation in a binding-dependent manner and affects functions of NDR, such as centrosome duplication and apoptotic signaling. Significantly, RNA interference (RNAi)-mediated reduction of the hMOB2 protein resulted in increased NDR kinase activity. These data indicate that hMOB2, in contrast to hMOB1A/B, plays an inhibitory role in the regulation of human NDR1/2 kinases.

#### MATERIALS AND METHODS

**Construction of plasmids.** Human NDR1 and NDR2 and hMOB1A, hMOB1B, hMOB2, hMOB3A, hMOB3B, and hMOB3C cDNAs were subcloned into pcDNA3, pGEX-4T1, or pMal-2c using BamHI and XhoI restriction sites. Accession numbers for hMOB3 reference cDNAs are 3A, NM\_130807; 3B, NM\_024761; and 3C, NM\_201403. The cloning of hMOB3 cDNAs has been described previously (13). Plasmids containing human LATS1 and LATS2 were described elsewhere (14). pcDNA3 derivatives contained a hemagglutinin (HA) or a myc epitope alone or the myristoylation/palmitoylation motif of the Lck tyrosine kinase (MGCVCSSN) combined with a myc epitope (mp-myc). Mutants of NDR1 and hMOB2 were generated by site-directed mutagenesis according to the manufacturer's instructions (Stratagene). Deletion mutants of NDR1 were cloned via PCR. Individual PCR products were digested with BamHI and XhoI and cloned into pcDNA3 derivatives. To generate a construct expressing the N terminus of NDR1 or NDR2 with a C-terminal tag, the coding sequences for amino acids 1 to 83 of NDR1/2 were amplified by PCR, digested by NheI and KpnI, and cloned into pcDNA3.1-myc-RFP as described elsewhere (27). To generate hMOB3 proteins containing a C-terminal myc tag, hMOB3A/B/C cDNAs were cloned into pcDNA3.1-myc-RFP as described above, and the red fluorescent protein (RFP) was removed by PCR. To generate tetracycline-regulated mammalian expression vectors, cDNAs encoding myc-hMOB2(wt) or myc-hMOB2(H157A) were digested with KpnI and XhoI and ligated into pENTR 3C (Invitrogen). N-terminally tagged hMOB2 cDNAs were finally inserted into pT-Rex-DEST30 using Gateway technology (Invitrogen). To obtain pTER-shMOB2 vectors that express short hairpin RNAs (shRNAs) against human MOB2, the following oligonucleotide pairs were inserted into pTER using BglII and HindIII: 5'-GATCCCGCTGGTGACGGATGAGGA CTTCAAGAGAGTCCATCCGTCACCAGCTTTTGGAAA-3' (targeting sequences of the hMOB2 coding sequence are underlined) and 5'-AGC TTTTCAAAAAGCTGGTGACGGATGAGGACTCTTTGAAGTCCT CATCCGTCACCAGCGG-3'. The generation of the pTER-shLuc control vector has been described previously (14). All constructs were confirmed by sequence analysis.

**Cell culture, transfections, and chemicals.** COS-7, HEK 293, U2-OS, and HeLa cells were maintained in Dulbecco's modified Eagle's medium (DMEM) supplemented with 10% fetal calf serum. Exponentially growing COS-7 cells were plated at consistent confluence ( $1 \times 10^6$  cells/10-cm dish) and transfected the next day using Fugene 6 (Roche) as described by the manufacturer. Exponentially growing HEK 293 cells were transfected in solution at consistent confluence ( $5 \times 10^6$  cells/10-cm dish) using jetPEI (PolyPlus Transfections) according to the manufacturer's instruction. Exponentially growing U2-OS cells were plated at consistent confluence and transfected the next day using Lipofectamine 2000 (Invitrogen) as described by the manufacturer. Aphidicolin was from Calbiochem, and okadaic acid (OA) was purchased from Alexis Biochemicals (Enzo

Life Sciences). Apoptosis of U2-OS cells was induced by the addition of activating anti-Fas antibody clone CH-11 (0.5  $\mu$ g/ml) in combination with cycloheximide (CHX) (10  $\mu$ g/ml).

**Generation of stable cell lines.** To generate inducible cell lines, U2-OS T-Rex cells were transfected with pT-Rex-DEST30 vectors encoding hMOB2 variants. Cell clones were selected by growth in the presence of 1 mg/ml G418 (Gibco) and 50  $\mu$ g/ml hygromycin B (Invivogen). Stable transformants were maintained in DMEM supplemented with 0.5 mg/ml G418 and 50  $\mu$ g/ml hygromycin B. Expression of myc-hMOB2 variants was induced by the addition of 2  $\mu$ g/ml tetracycline.

**Antibodies.** The generation and purification of anti-T444-P, anti-S281-P, anti-NDR2, anti-NDR<sub>NT</sub>, anti-NDR<sub>CTD</sub>, and anti-hMOB1A/B antibodies has been described previously (13, 14, 35, 36). It is important to note that the anti-T444-P antibody recognizes the phosphorylated hydrophobic motifs of both NDR isoforms, NDR1 (T444-P) and NDR2 (T442-P). Anti-HA 12CA5 and 42F13, anti-myc 9E10, and anti- $\alpha$ -tubulin YL1/2 were used as hybridoma supernatants. Further, anti-HA antibody (Y-11) and anti- $\beta$ -actin were purchased from Santa Cruz and anti-Fas (CH-11) from Millipore. Anti-LATS1 antibody was purchased from Cell Signaling and anti-cleaved poly(ADP-ribose) polymerase (PARP) from BD Bioscience. Anti-p63(G1/296) antibody was from Alexis Biochemicals (Enzo Life Sciences). Anti-hMOB2 antibody was raised against purified, bacterially produced full-length hMOB2 fused C terminally to maltose-binding protein (MBP). Rabbit injections and bleed collections were done by Eurogentec. Anti-protein antibody was purified by preabsorbing the bleeds against  $\sim 10$  mg of immobilized MBP and then binding them to 5 to 10 mg of GST-hMOB2 covalently coupled to glutathione-Sepharose 4B beads. Antibodies were eluted with 0.2 M glycine (pH 2.2).

**Immunoblotting and immunoprecipitation.** Immunoblotting experiments were performed as described previously (11). For immunoprecipitation, cells were harvested, pelleted at  $1,000 \times g$  for 3 min, and washed with cold phosphate-buffered saline (PBS) before lysis in immunoprecipitation (IP) buffer (20 mM Tris, 150 mM NaCl, 10% glycerol, 1% NP-40, 5 mM EDTA, 0.5 mM EGTA, 20 mM  $\beta$ -glycerophosphate, 50 mM NaF, 1 mM Na<sub>3</sub>VO<sub>4</sub>, 1 mM benzamide, 4  $\mu$ M leupeptin, 0.5 mM phenylmethylsulfonyl fluoride [PMSF], 1  $\mu$ M microcystine, and 1 mM dithiothreitol [DTT] at pH 8.0). Lysates were centrifuged for 10 min at  $16,000 \times g$  at 4°C before being precleared with protein A-Sepharose. The beads were washed twice with IP buffer, once with IP buffer containing 1 M NaCl, and finally once with IP buffer before samples were analyzed by SDS-PAGE. To analyze the association of NDR1/2 or LATS1/2 and hMOB species by coimmunoprecipitation, cells coexpressing HA-NDR or HA-LATS and myc-hMOB species were subjected to immunoprecipitation using anti-HA 12CA5 antibody as described above, omitting the wash with 1 M NaCl IP buffer, before analysis by SDS-PAGE and immunoblotting. For immunoprecipitation of endogenous proteins, cells were processed for immunoprecipitation as described above. Lysates were preincubated with control rabbit IgG, anti-hMOB2, anti-NDR2, anti-LATS1, or anti-T444-P antibody overnight, and then protein A-Sepharose was added for 3 h and the beads were washed four times in IP buffer containing 150 mM NaCl before analysis by SDS-PAGE. To analyze the association of NDR1 mutants and hMOB2, coimmunoprecipitation experiments were performed as described above, including one wash with IP buffer containing 1 M NaCl. Characterization of hMOB2 mutants by IP was performed in low-stringency buffer (30 mM HEPES, pH 7.4, 20 mM  $\beta$ -glycerophosphate, 20 mM KCl, 1 mM EGTA, 2 mM NaF, 1 mM Na<sub>3</sub>VO<sub>4</sub>, 1% TX-100) supplemented with protease inhibitors.

**HA-NDR kinase assay and HA-LATS kinase assay.** Analysis of HA-NDR or HA-LATS kinase activities after immunoprecipitation was performed as described previously (11, 15).

**HA-LATS autophosphorylation assay.** Analysis of immunoprecipitated HA-LATS autophosphorylation was also carried out as reported previously (15).

**Fractionation of cells.** Cytosolic and membrane-associated proteins were separated by S100/P100 fractionation as described previously (11).

**Immunofluorescence microscopy.** Cells were processed for immunofluorescence analysis as defined elsewhere (14).

## RESULTS

**Human NDR and LATS kinases do not interact with hMOB3A, -B, or -C protein.** MOB proteins are evolutionarily highly conserved from yeast to humans. Unfortunately, human MOB proteins have been named inconsistently in the literature (Table 1). Alignments, as well as phylogenetic analysis of the human MOB family (data not shown), revealed a close rela-

TABLE 1. Human MOB proteins

Protein	% identity	No. of amino acids	Alternative names
hMOB1A	100	216	MOB1 $\alpha$ , MOBKL1B, MOBK1B, MOB4B, hMats1
hMOB1B	95	216	MOB1 $\beta$ , MOBKL1A, MOB4A, hMats2, MOB1
hMOB2	38	237	HCCA2, hMOB3
hMOB3A	50	217	MOBKL2A, MOB-LAK, MOB1C, hMOB2A
hMOB3B	51	216	MOBKL2B, MOB1D, hMOB2B
hMOB3C	49	216	MOBKL2C, MOB1E, hMOB2C

tionship of hMOB3 proteins with hMOB1A. Many biochemical properties of hMOB1A and -B have been described (2, 11, 15), suggesting that hMOB3A/B or -C proteins might display some of these properties. In order to test whether hMOB3 proteins can physically interact with human NDR or LATS kinases, HA-NDR1/2 or HA-LATS1/2 were coexpressed with N-terminally myc-tagged hMOB proteins prior to being processed for immunoprecipitation and subsequent immunoblotting (Fig. 1). As expected, we observed interactions between HA-NDR1 and myc-hMOB2 (Fig. 1A, top, lane 1) as well as HA-NDR2 and myc-hMOB2 (Fig. 1B, top, lane 1). To our surprise, none of the hMOB3 proteins interacted with HA-NDR1 (Fig. 1A, top, lanes 2 to 4) or HA-NDR2 (Fig. 1B, top, lanes 2 to 4) in these settings. In addition, hMOB3A, -B, and -C did not associate with HA-LATS1 or HA-LATS2 (Fig. 1C and D, top, lanes 2 to 4). In full agreement with the existing literature (4, 15), we confirmed that HA-LATS1 and myc-MOB2 do not interact in cells (Fig. 1C, top, lane 5) and also

demonstrated that myc-hMOB2 cannot associate with HA-LATS2 (Fig. 1D, top, lane 5), thus illustrating that hMOB2 is a specific binder of NDR1/2. Significantly, these data were fully confirmed using hMOB proteins containing a C-terminal myc tag (data not shown).

**Membrane-targeted variants of hMOB3 proteins do not activate human NDR and LATS kinases.** We have demonstrated that hMOB3A, -B, and -C do not bind to NDR1/2 or LATS1/2 in our settings (Fig. 1). In order to exclude possible postlysis effects we applied a second experimental setting as described previously (11, 15). Briefly, fusion of the myristoylation/palmitoylation motif (mp) from the Lck kinase to the N terminus of myc-tagged hMOB1A (mp-myc-hMOB1A) led to efficient plasma membrane localization. Importantly, the resulting activation of NDR/LATS is dependent on hMOB1A-NDR/LATS interaction and takes place within the cells before subsequent manipulations, such as cell lysis and immunoprecipitation. To address whether membrane-targeted variants of hMOB3 proteins are able to activate either human NDR1/2 or LATS1/2 kinases, we transfected HEK 293 cells with the respective NDR/LATS kinase and membrane-targeted hMOBs. As reported previously (11), mp-myc-MOB1A robustly activated HA-NDR1, as reflected in increased Thr444 phosphorylation at the hydrophobic motif of NDR1 (Fig. 2A, top, lane 2), paralleled by increased kinase activity (Fig. 2B, lane 2). Coexpressing membrane-targeted hMOB3 variants produced no increase in phosphorylation (Fig. 2A, top panel, lanes 3 to 5) or kinase activity (Fig. 2B, lanes 3 to 5). Comparable results were obtained when cells were transfected with HA-NDR2 and mp-myc-hMOB3A, -B, or -C (Fig. 2C, top, lanes 3 to 5, and D, lanes 3 to 5). This is consistent with the coimmunoprecipitation

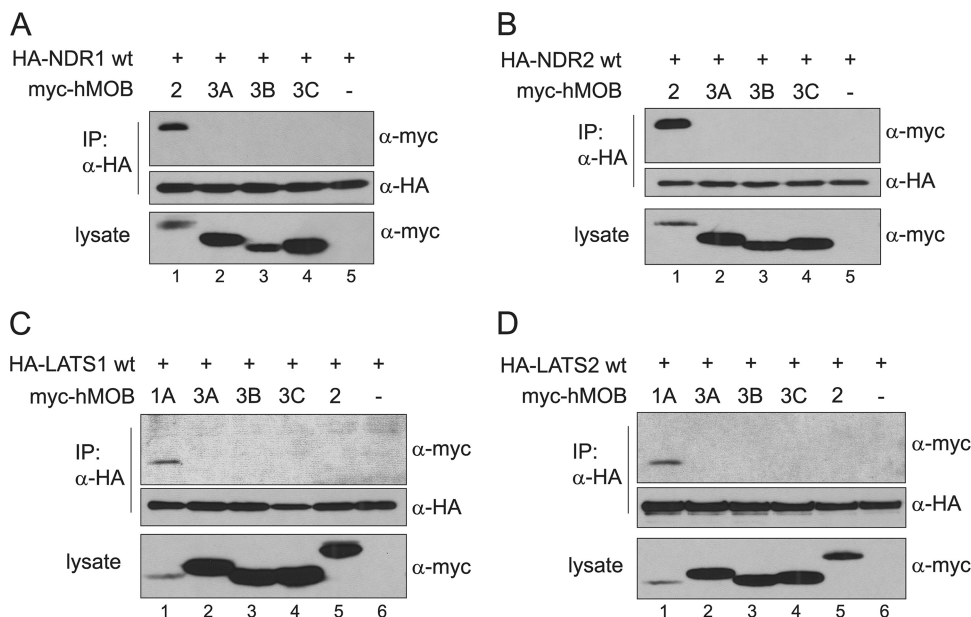


FIG. 1. Human NDR and LATS kinases do not interact with hMOB3A/B/C proteins. (A and B) Lysates of HEK 293 cells coexpressing the indicated combinations of HA-tagged NDR1 wild-type (wt), HA-tagged NDR2(wt), and myc-tagged hMOB species were analyzed by IP using anti-HA 12CA5 antibody. Complexes were assayed by immunoblotting using anti-myc antibody (top) or anti-HA antibody (middle). Input lysates were analyzed by immunoblotting using anti-myc antibody (bottom). hMOB2 served as a positive control. (C and D) Lysates of HEK 293 cells coexpressing the indicated HA-tagged LATS1(wt) or LATS2(wt) and myc-tagged human MOB species were analyzed as described for panels A and B, except that hMOB1A served as the positive control and hMOB2 as the negative control.

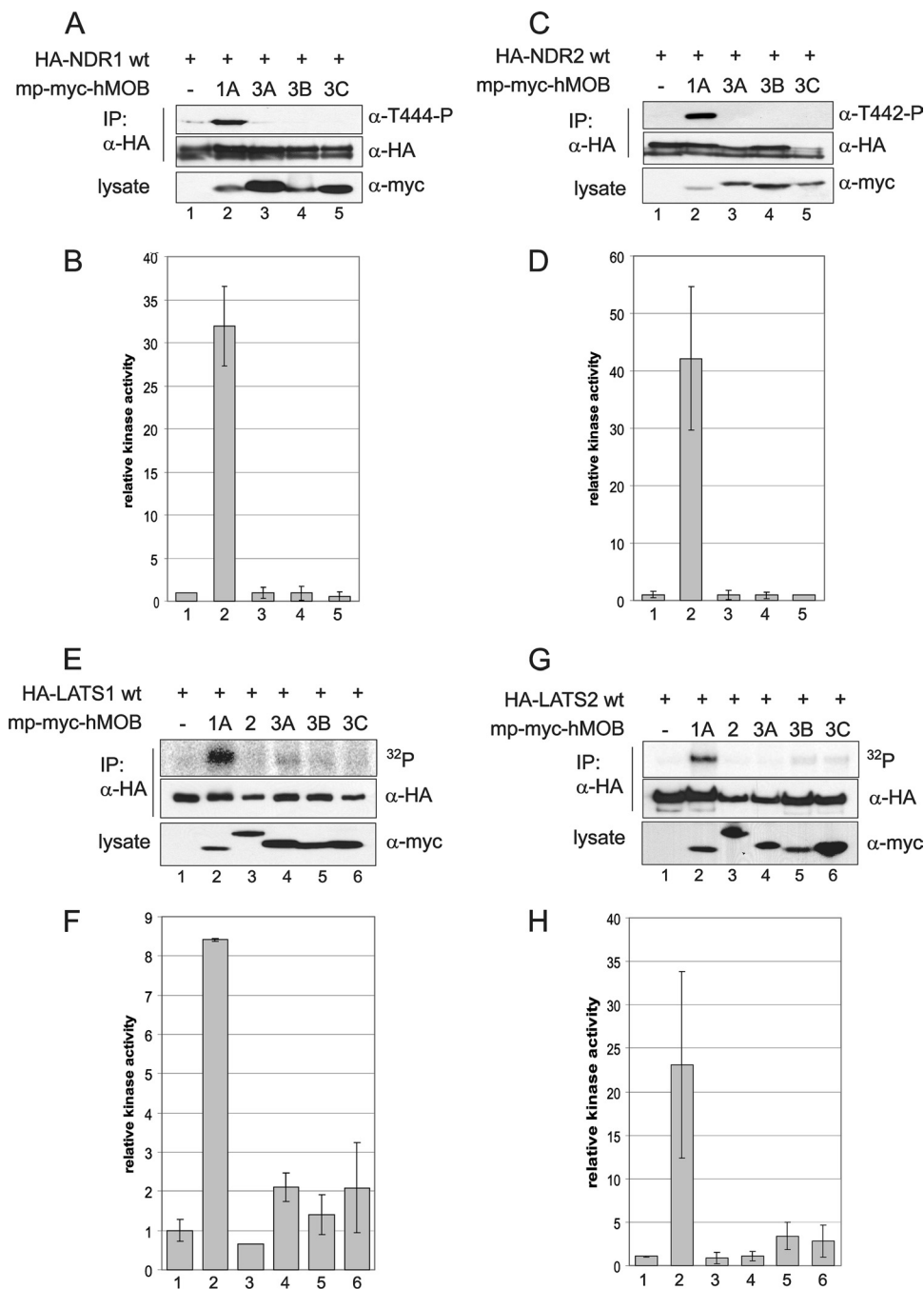


FIG. 2. Membrane-targeted variants of hMOB3A/B/C do not activate human NDR and LATS kinases. (A) Lysates of HEK 293 cells coexpressing the indicated combinations of HA-tagged NDR1(wt) and membrane-targeted human MOB proteins (mp-myc-hMOB) were analyzed by IP using anti-HA 12CA5 antibody. Complexes were assayed by immunoblotting using anti-T444-P antibody (top) or anti-HA antibody (middle). Input lysates were immunoblotted with anti-myc antibody (bottom). (B) In parallel, complexes were subjected to kinase assays. The results of two independent experiments are shown. The error bars indicate standard deviations. (C) Lysates of HEK 293 cells coexpressing the indicated combinations of HA-tagged NDR2(wt) and mp-myc-hMOB proteins were analyzed as described for panel A. (D) In parallel, complexes were subjected to kinase assays as described for panel B. (E) Lysates of HEK 293 cells coexpressing the indicated combinations of HA-tagged LATS1(wt) and mp-myc-hMOB species were analyzed by IP using anti-HA 12CA5 antibody before being assayed by immunoblotting using anti-HA antibody (middle) or an autophosphorylation assay (top). Input lysates were analyzed by immunoblotting with anti-myc antibody. (F) In parallel, complexes were subjected to peptide kinase assays. The result from one representative experiment performed in duplicate is shown. (G) Lysates of HEK 293 cells coexpressing the indicated combinations of HA-tagged LATS2(wt) and mp-myc-hMOB species were analyzed as described above for panel E. (H) In parallel, complexes were subjected to peptide kinase assays. The results from two independent experiments are shown. The error bars indicate standard deviations.



experiments (Fig. 1A and B) and indicates that hMOB3s cannot interact with human NDR1/2 kinases in cultured mammalian cells despite the significant similarity to hMOB1A. Furthermore, we addressed whether membrane-targeted hMOB3 variants are able to activate HA-LATS1 or HA-LATS2 (Fig. 2E to H). As already reported (15), HA-LATS1 was substantially activated by mp-myc-hMOB1A (Fig. 2E and F, lanes 2), as illustrated by increased autophosphorylation and kinase activity, whereas mp-hMOB3 proteins were unable to activate HA-LATS1 (Fig. 2E and F, lanes 4 to 6). We observed similar results in the case of HA-LATS2 (Fig. 2G and H). In combination with the coimmunoprecipitation experiments (Fig. 1), these findings strongly suggest that none of the three hMOB3 proteins physically interacts with or activates human NDR1/2 or LATS1/2 kinases.

**hMOB2 binds to the amino terminus of human NDR1/2 kinases in a mode distinct from hMOB1A/B binding.** We have shown that hMOB3s do not associate with human NDR1/2 kinases (Fig. 1 and 2), despite their higher degree of similarity to hMOB1A/B than to hMOB2 (Table 1). Interestingly, hMOB2 appears to be an NDR-specific binder, since it did not bind to human LATS1 (4, 15) or LATS2 (Fig. 1 and 2) but readily bound to NDR1 and 2 (Fig. 1). Therefore, we investigated the interaction of hMOB2 with NDR1/2 in more detail using a series of NDR1 mutants (Fig. 3A and Table 2). We deleted the N or C terminus of NDR1 to determine which region was necessary for the interaction with hMOB2 (Fig. 3B). NDR1(wt) and NDR1(1-380) coprecipitated hMOB2 (Fig. 3B, top, lanes 2 and 4), whereas NDR1 lacking the conserved N-terminal regulatory domain (NTR), HA-NDR1( $\Delta$ NTR), did not (Fig. 3B, top, lane 3). Conversely, we addressed whether the N terminus of NDR (amino acids 1 to 83) was sufficient for association with hMOB2. Indeed, NDR1(1-83)-myc-RFP interacted with HA-hMOB2 (Fig. 3C, top, lane 2), and NDR2(1-83)-myc-RFP also bound HA-hMOB2 (Fig. 3D, top, lane 2). Remarkably, hMOB1A/B binds to the same N-terminal region of NDR (2). Therefore, since the key residues essential for interaction between NDR1/LATS1 kinases and hMOB1A have been described (2, 15), we investigated whether hMOB2 utilized the same conserved binding motif. Interestingly, point mutations in the NDR1 N terminus that abolish or diminish the interaction with hMOB1A did not impair binding of hMOB2 (Fig. 3E, top, lanes 5 and 6, and Table 2). Since hMOB2 appeared to bind to NDR separately from hMOB1A, we aimed to define the N-terminal region on human NDR1 necessary for the hMOB2 interaction via N-terminal mutagenesis of NDR1 (Fig. 3F). We observed that NDR1 lacking the first 26 amino acids [NDR1( $\Delta$ 26)] still interacted with hMOB2 (Fig. 3F, top, lane 3), whereas an NDR1 mutant lacking the first 33 residues [NDR1( $\Delta$ 33)] was no longer able to bind to hMOB2 (Fig. 3F, top, lane 2), arguing that the amino acids between residues 27 and 33 of human NDR1 are necessary for the interaction. We sought to further analyze this region and mutated 5 residues within this stretch to alanines (HA-NDR1 5A: Leu27, Glu28, Asn29, Phe30, and Ser32, respectively) and examined whether this mutant was still able to bind to hMOB2 (Fig. 3G). Unexpectedly, the NDR1 mutant carrying 5 point mutations bound to hMOB2 but lost the ability to bind to hMOB1A (Fig. 3G, top, lanes 4 and 5). Neither single point mutations in this stretch nor multiple mutations led to the loss

of hMOB2 interaction (Table 2). Therefore, we attempted to create an NDR1 mutant incapable of binding to hMOB2 by mutating residues in the N terminus that differ significantly from the N-terminal region of LATS1. However, this effort remained ineffective, since all tested mutants bound to hMOB2 (Table 2), leaving a defined binding motif of hMOB2 on NDR1 yet to be determined. Nevertheless, these data demonstrate that while hMOB2 and hMOB1 proteins utilize identical regions of human NDR1/2 kinases to bind, the interactions differ significantly between these two hMOB isoforms.

**hMOB2 competes with hMOB1A for binding to NDR and interferes with the activation of endogenous NDR by okadaic acid.** We showed that hMOB2, like hMOB1A, binds to the N terminus of NDR (Fig. 3), suggesting that hMOB1A and hMOB2 might function competitively in binding NDR kinases. Thus, we examined whether the coimmunoprecipitation of myc-tagged hMOB1A by HA-NDR1 is affected by expressing increasing amounts of myc-hMOB2 (Fig. 4A). In the absence of myc-hMOB2, a substantial amount of myc-hMOB1A coimmunoprecipitated with HA-NDR1 (Fig. 4A, top, lane 2). On the other hand, coexpression of increasing amounts of myc-hMOB2 led to a significant decrease in myc-hMOB1A coimmunoprecipitating with HA-NDR1 (Fig. 4A, lanes 3 to 6), despite the fact that the overall amount of expressed myc-hMOB1A was not changed (Fig. 4A, bottom, lanes 2 to 6). Interestingly, hMOB2 displaced hMOB1A even though it was expressed at a lower level than hMOB1A (Fig. 4A, lanes 3 and 4). This indicates that hMOB2 can efficiently compete with hMOB1A for binding to NDR1.

Activation of NDR kinases by the protein phosphatase 2A inhibitor OA was shown to depend on intact interaction of NDR1/2 and hMOB1 proteins (2). Since hMOB2 is able to partially displace hMOB1A from NDR, we investigated the effect of hMOB2 expression on OA-induced activation of endogenous NDR species (Fig. 4B and C). As expected, treatment of HEK293 cells with OA strongly increased Thr-444 phosphorylation of NDR (Fig. 4B, top, lane 3) and elevated the kinase activity of endogenous NDR2 (Fig. 4C, lane 3). Interestingly, expression of hMOB2(wt) impaired NDR phosphorylation (Fig. 4B, top, lane 4) and led to an ~50% reduction in endogenous NDR2 activity (Fig. 4C, lane 4). Overall, these data suggest that hMOB2 competes with hMOB1 for NDR binding and interferes with OA-induced activation of NDR, in contrast to hMOB1, which was previously shown to enhance OA-induced activation (2).

**hMOB2 interferes with the activation of ectopic and endogenous NDR kinases by membrane-targeted hMOB1A in a binding-dependent manner.** Next, we investigated whether the competition with hMOB1 and the inhibitory effect on NDR activation by hMOB2 depended on an intact NDR-hMOB2 interaction. For this, we generated an hMOB2 variant deficient in NDR binding (Fig. 5A). Mutating His157 to alanine abolished binding to NDR1 and -2 despite similar expression levels (Fig. 5A, top, compare lanes 2 and 3, 5 and 6). Subsequently, we investigated whether hMOB2 can interfere with the activation of NDR by membrane-targeted hMOB1A in an interaction-dependent manner (Fig. 5B and C). As previously reported (11), mp-myc-hMOB1A potently activates HA-NDR1 (Fig. 5B and C). Intriguingly, myc-tagged hMOB2(wt) expression almost completely abolished the activation of HA-NDR1

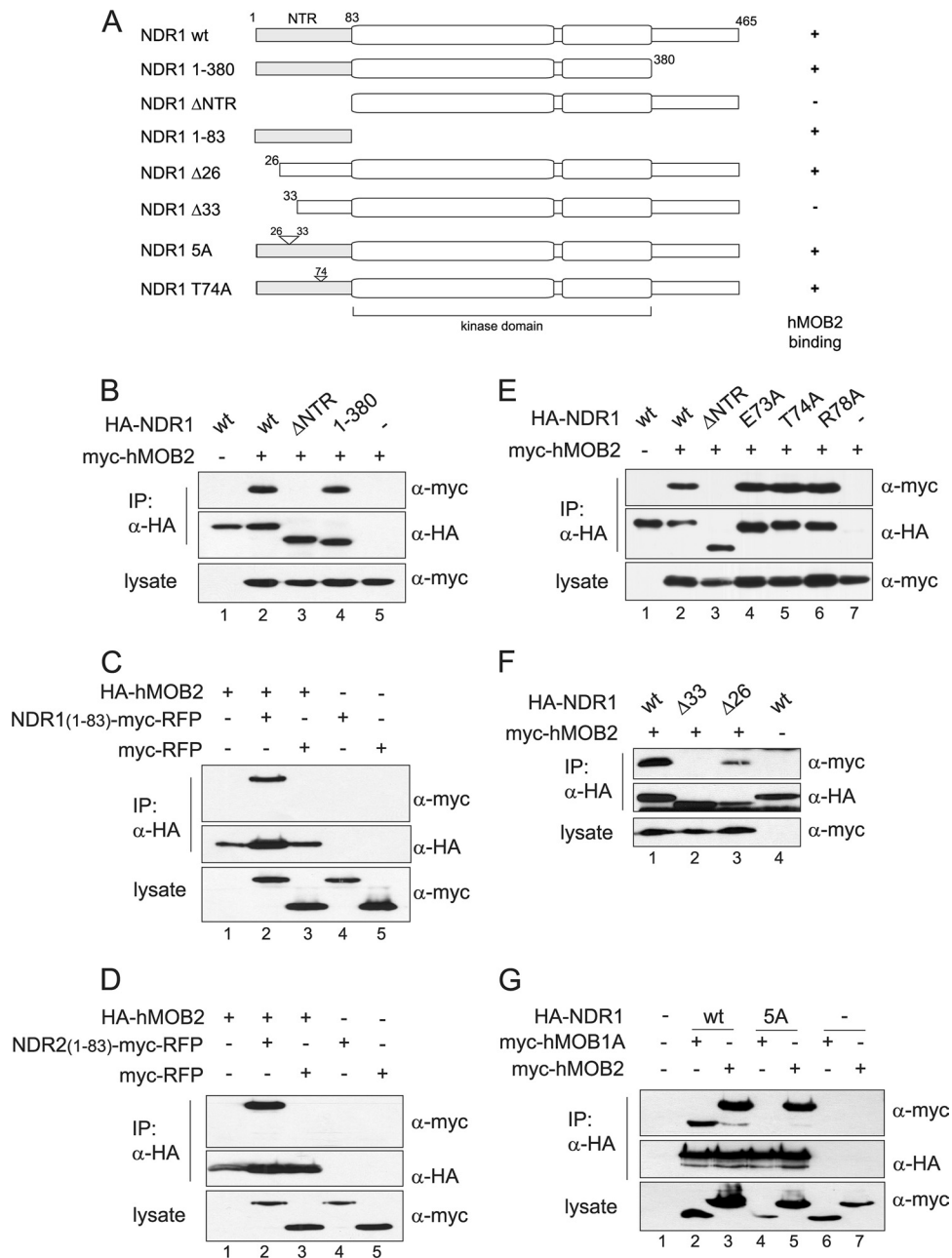


FIG. 3. hMOB2 binds to the N terminus of NDR but in a manner distinct from that for hMOB1A/B. (A) Primary structures of human NDR1 and overview of HA-tagged NDR1 mutant derivatives. (B) Lysates of COS-7 cells containing the indicated combinations of HA-tagged NDR1 forms and myc-tagged hMOB2(wt) were analyzed by IP using anti-HA antibody. Complexes were analyzed by immunoblotting using anti-myc (top) or anti-HA (middle) antibody. Input lysates were analyzed using anti-myc antibody.  $\Delta$ NTR denotes deletion of amino acids 1 to 83 of NDR1, the NTR (N-terminal regulatory domain). (C) Lysates of HEK 293 cells coexpressing the indicated combinations of HA-tagged hMOB2(wt), the N terminus of NDR1 (amino acids 1 to 83) fused N terminally to myc-RFP, or myc-RFP alone were analyzed by IP using anti-HA antibody. Complexes were assayed by immunoblotting using anti-myc (top) and anti-HA (middle) antibodies. The lysates were analyzed using anti-myc antibody. (D) Lysates of HEK 293 cells coexpressing combinations of HA-tagged hMOB2(wt), the N terminus of NDR2 (amino acids 1 to 83) containing a C-terminal myc-RFP tag, or myc-RFP alone were analyzed as described for panel C. (E) Lysates of COS-7 cells coexpressing HA-tagged NDR1 (wt), NDR1( $\Delta$ NTR), NDR1(E73A), NDR1(T74A), NDR1(R78A), and myc-tagged hMOB2(wt) were analyzed by IP using anti-HA antibody. Complexes were analyzed by immunoblotting using anti-myc or anti-HA antibody. Input lysates were assayed by immunoblotting using anti-myc antibody. (F) Lysates of HEK 293 cells coexpressing HA-tagged NDR1(wt), NDR1 containing a deletion of amino acids 1 to 33 [NDR1( $\Delta$ 33)], NDR1( $\Delta$ 26), and myc-tagged hMOB2(wt) were analyzed by IP using anti-HA antibody. Complexes were assayed using anti-myc or anti-HA antibody. Input lysates were assayed by immunoblotting using anti-myc antibody. (G) Lysates of HEK 293 cells containing the indicated combinations of HA-tagged NDR1(wt), NDR1 5A mutant, myc-tagged hMOB1A, or hMOB2 were analyzed by IP using anti-HA antibody. NDR1 5A mutant denotes mutation of amino acids Leu27, Glu28, Asn29, Phe30, and Ser32 to alanine. Complexes were assayed by immunoblotting using anti-myc (top) or anti-HA (middle) antibody. Input lysates were assayed by immunoblotting using anti-myc antibody (bottom).

TABLE 2. Summary of coimmunoprecipitation experiments

NDR1 mutation	Binding to <sup>a</sup> :	
	hMOB2	hMOB1A
Y31A	+	-
R41A	+	-
R44A	+	(+)
T74A	+	-
R78A	+	-
K24A	+	+
T26A	+	ND
T26F	+	ND
L27A	+	ND
E28A	+	+
N29A	+	ND
F30A	+	ND
S32A	+	ND
A36K	+	ND
E40A	+	+
V51E	+	ND
E54R	+	ND
D59A	+	ND
E60A	+	+
E61A	+	+
R63A	+	+
E73A	+	+
TVT23/25/26FFF	+	ND
FY30/31HV	+	ND
EE39/40AA	+	ND
Q45K/K47Q	+	ND
EEE53-55RRR	+	ND
EEKR60-63AAAA	+	ND
KRR62/63/65QDM	+	ND
H69D/R71D	+	ND
SAHAR67-71KMLCQ	+	ND

<sup>a</sup> HA-tagged NDR1 mutants were coexpressed with either myc-hMOB2 or myc-hMOB1A in HEK 293 or COS7 cells before coimmunoprecipitation experiments were performed. +, interaction; -, no interaction; (+), impaired interaction; ND, not determined.

by mp-myc-hMOB1A (Fig. 5B and C, lanes 3), even though the expression of mp-myc-hMOB1A remained unchanged (Fig. 5B, bottom, lane 3). However, coexpression of myc-tagged hMOB2(H157A), which cannot bind to NDR1/2 kinases, did not interfere with mp-myc-hMOB1A-driven activation of HA-NDR1 (Fig. 5B and C, lanes 4). In conclusion, the negative effect of hMOB2 on NDR1 activation by membrane-targeted hMOB1A is likely to be binding dependent.

We have previously shown that expression of membrane-targeted hMOB1A in U2OS cells leads to the membrane recruitment and activation of endogenous NDR1 species (11). To address the effect of hMOB2 on membrane recruitment and activation of endogenous NDR species, HEK 293 cells transfected with mp-myc-hMOB1A, myc-hMOB2(wt), or myc-hMOB2(H157A) were separated into cytoplasmic and membranous fractions prior to analysis by immunoblotting (Fig. 5D). While in untransfected cells native phospho-T444/442 proteins were found almost exclusively in the cytoplasmic fraction (Fig. 5D, lane 1), in cells expressing mp-myc-hMOB1A NDR, phosphospecies were enriched at the membrane (Fig. 5D, lane 4). Congruently, endogenous NDR1/2 was recruited to the membrane by mp-myc-hMOB1A (Fig. 5D, lane 4). Upon coexpression of myc-tagged hMOB2(wt) the phosphosignal of endogenous NDR species at the membrane disappeared (Fig. 5D, lane 6), although we still observed residual

NDR2 in the membranous fraction (Fig. 5D, lane 6). To address whether this effect was dependent on the interaction between hMOB2 and endogenous NDR species, we coexpressed NDR binding-deficient hMOB2(H157A) with mp-myc-hMOB1A. Confirming the result with overexpressed HA-NDR1 (Fig. 5B), myc-hMOB2(H157A) did not interfere with

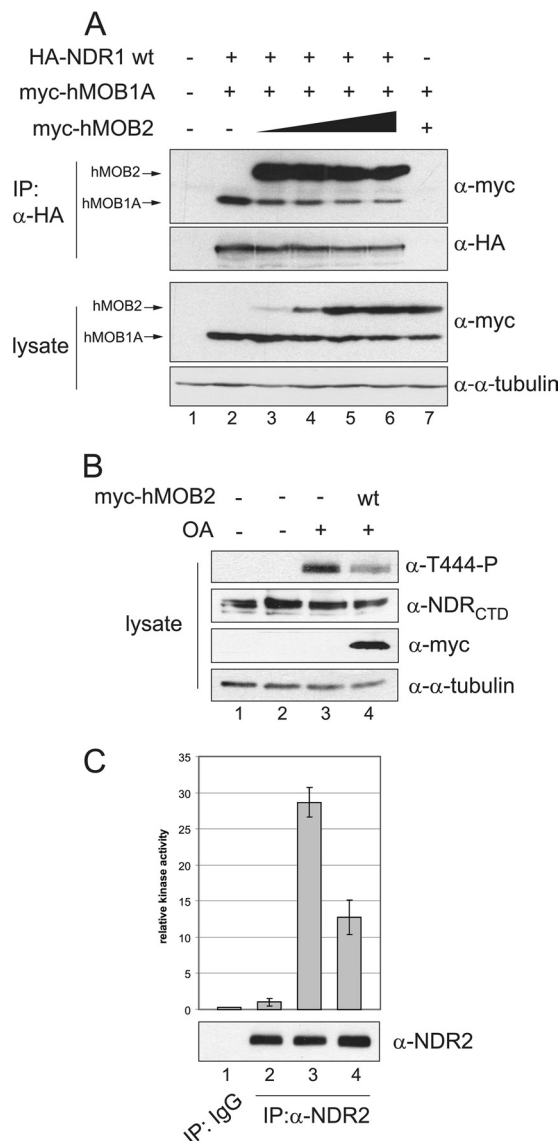


FIG. 4. hMOB2 competes with hMOB1A and interferes with okadaic acid-induced activation of endogenous NDR kinases. (A) hMOB1A-NDR1 and hMOB2-NDR1 interactions are mutually exclusive. Lysates of HEK 293 cells coexpressing HA-tagged NDR1(wt) and myc-tagged hMOB1A and hMOB2 were analyzed by IP using anti-HA antibody. Complexes were assayed by immunoblotting using anti-myc (top) and anti-HA (middle) antibodies. Input lysates were analyzed by immunoblotting using anti-myc antibody. (B) HEK 293 cells transfected with empty vector (-) or hMOB2(wt) were treated with 1 μM OA for 45 min before input lysates were processed for immunoblotting with the indicated antibodies. (C) In parallel, samples were subjected to immunoprecipitation using rabbit IgG or anti-NDR2 antibody before peptide kinase assays were performed. Data from at least two independent experiments with two replicates per experiment are shown. The error bars represent standard deviations.

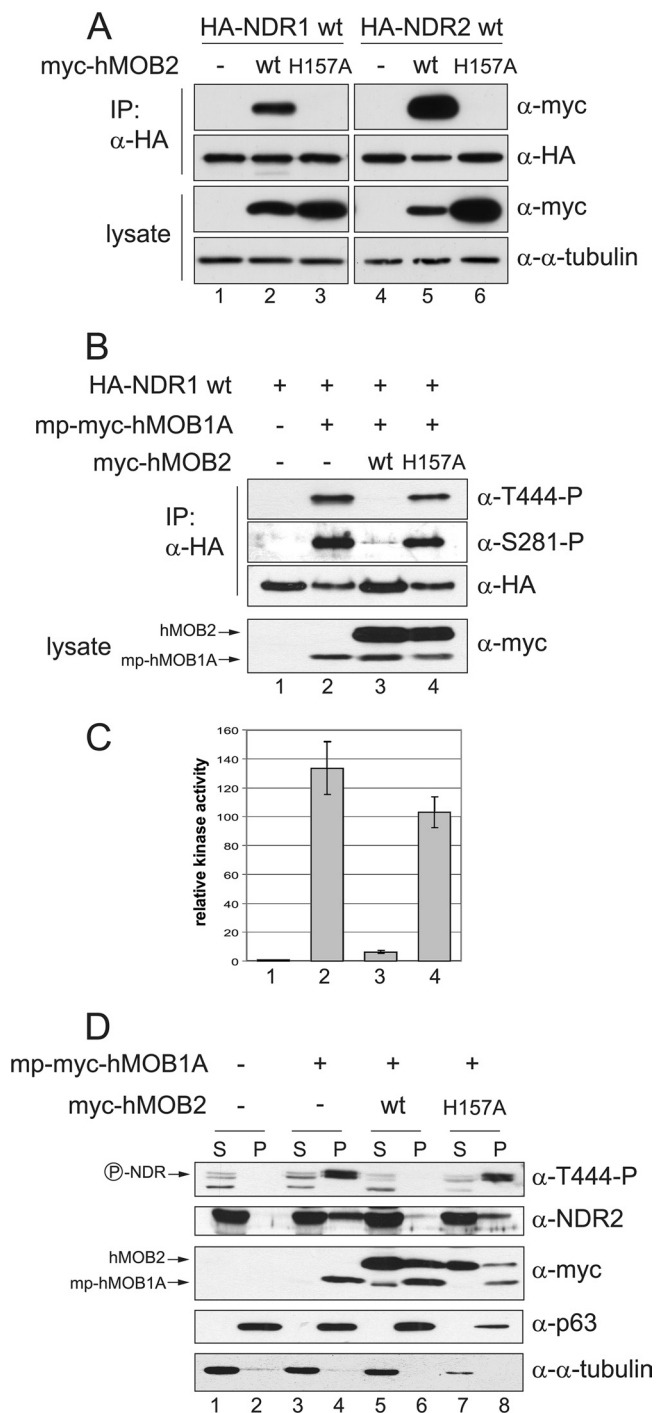


FIG. 5. hMOB2 interferes with the activation of human NDR kinases by membrane-targeted hMOB1A in an NDR binding-dependent manner. (A) COS-7 cell lysates expressing HA-tagged NDR1(wt) (lanes 1 to 3), HA-NDR2(wt) (lanes 4 to 6), myc-tagged hMOB2(wt), or myc-hMOB(His157Ala) were lysed in low-stringency lysis buffer and then subjected to IP using anti-HA 12CA5 antibody. Complexes were analyzed by immunoblotting with anti-HA (middle) and anti-myc (top) antibodies. Input lysates were analyzed by immunoblotting using anti-myc and anti- $\alpha$ -tubulin antibodies (bottom). (B) Lysates of COS-7 cells containing the indicated combinations of HA-tagged NDR1(wt), membrane-targeted hMOB1A (mp-myc-hMOB1A), and myc-tagged hMOB2(wt) and hMOB2(H157A) were analyzed by immunoprecipitation using anti-HA antibody. Complexes were assayed by immunoblotting and probed with anti-T444-P, anti-S281-P, and anti-HA anti-

either membrane recruitment of endogenous NDRs by mp-myc-hMOB1A (Fig. 5D, lane 8) or the activation of endogenous NDR at the membrane (Fig. 5D, top, lane 8). We conclude that hMOB2 competes with hMOB1A for NDR binding and can interfere with the activation of human NDR kinases in a binding-dependent manner.

**Endogenous hMOB2 physically interacts with human NDR, but not with LATS1.** In overexpression settings, hMOB2 readily coimmunoprecipitates with human NDR1/2 kinases (Fig. 1). In order to address the interaction of endogenous proteins, we raised a rabbit polyclonal antibody against hMOB2 (Fig. 6A and B). The affinity-purified anti-hMOB2 antibody detected a band at approximately 27 kDa, the predicted molecular size of the hMOB2 protein, which was reduced in cells expressing shRNA against hMOB2 (Fig. 6A, top). Furthermore, the anti-hMOB2 detected only recombinant glutathione *S*-transferase (GST)-hMOB2, but none of the other hMOBs (Fig. 6B, top). Endogenous hMOB2 coprecipitated with NDR2 when an anti-NDR2 antibody was used for immunoprecipitation, but not with control antibody (Fig. 6C, top). Conversely, when an anti-hMOB2 antibody was used to immunoprecipitate endogenous hMOB2, endogenous NDR2 coprecipitated in HEK293 cells (Fig. 6D, top). Similar results were observed using HeLa cell lysates (data not shown). Moreover, endogenous hMOB2 could not be coimmunoprecipitated using an anti-LATS1 antibody (Fig. 6E, top, lane 3). Therefore, our data show for the first time that endogenous hMOB2 is a specific binder of NDR1/2 kinases.

**hMOB2 is found preferentially in unphosphorylated NDR complexes, while hMOB1A/B is associated with active NDR kinases.** Given that we observed a putative negative role for hMOB2 in the course of NDR activation and that endogenous hMOB2-NDR complexes are readily detectable (Fig. 4, 5, and 6), we examined endogenous total NDR-hMOB complexes and active NDR-hMOB complexes by immunoprecipitation experiments using anti-NDR2 and anti-T444-P antibodies (Fig. 7). The anti-T444-P antibody recognizes only phosphorylated hydrophobic motifs of active NDR1/2 kinases (14). HEK 293 cells were subjected to immunoprecipitation with the two different anti-NDR antibodies described above and to subsequent immunoblotting experiments. When the anti-NDR2 antibody was used, a small fraction of the immunoprecipitated NDR2 protein was phosphorylated at the hydrophobic motif (T444-P), indicating that mostly inactive NDR species were immunoprecipitated (Fig. 7, lane 2). In contrast, using the anti-T444-P antibody to immunoprecipitate active NDR species, we obtained a significant amount of phospho-T444 species despite the small amount of total NDR2 pulled down (Fig. 7,

bodies. The input lysate was analyzed by immunoblotting using anti-myc antibody. (C) In parallel, complexes were subjected to peptide kinase assays. The results from two independent experiments are shown. The error bars indicate standard deviations. (D) HEK 293 cells transfected with membrane-targeted hMOB1A (mp-myc-hMOB1A) and the indicated myc-tagged hMOB2 constructs were subjected to S100/P100 (S, cytoplasm; P, membrane) fractionation before being immunoblotted with anti-T444-P, anti-NDR2, anti-myc, anti-CLIMP63 (p63) (a marker for membranous fraction), and anti- $\alpha$ -tubulin (a marker for the cytoplasmic fraction) antibodies.

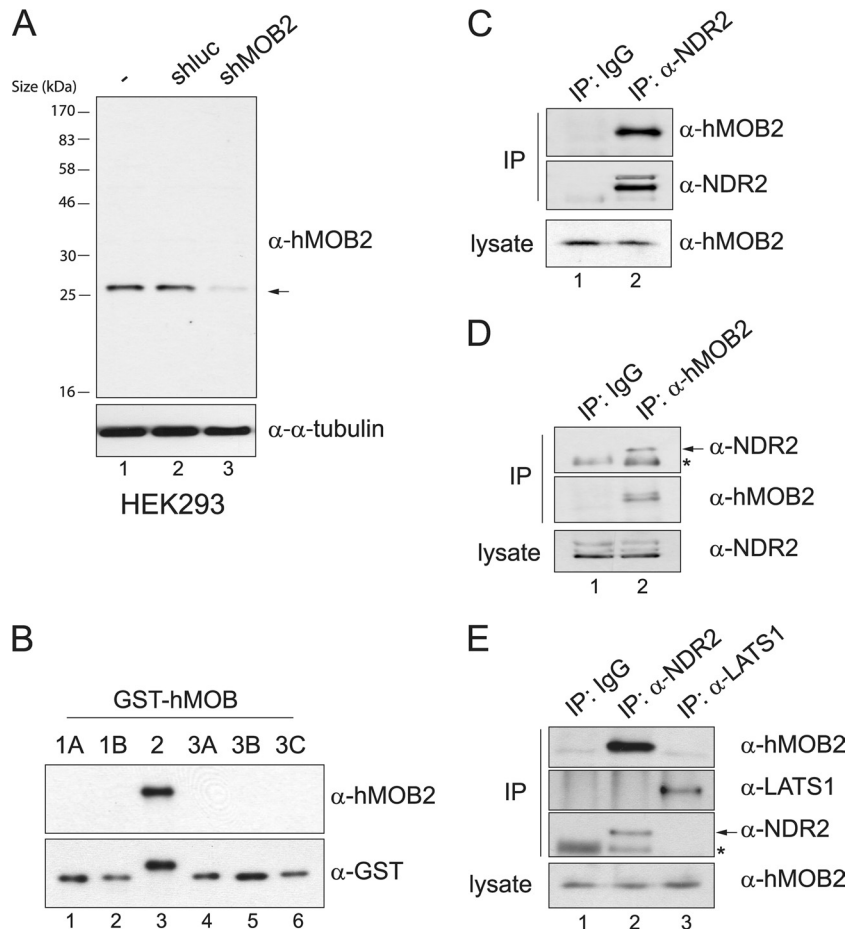


FIG. 6. Endogenous hMOB2 interacts with NDR, but not with LATS1, in tissue-cultured cells. (A) Characterization of anti-hMOB2 rabbit polyclonal antibody. HEK 293 cells transfected with short hairpin targeting either firefly luciferase (shLuc) or hMOB2 (shMOB2) were analyzed 72 h after transfection by immunoblotting using affinity-purified anti-hMOB2 antibody (top) and anti- $\alpha$ -tubulin antibody (bottom). Molecular masses are indicated. (B) Recombinant GST-tagged human MOB proteins were separated by SDS-PAGE and analyzed by immunoblotting using anti-hMOB2 (top) and anti-GST (bottom) antibodies. (C) Interaction of endogenous hMOB2 and NDR2. Whole-cell extracts of HEK 293 cells were subjected to immunoprecipitation using control rabbit IgG or anti-NDR2 antibody. Complexes were analyzed by immunoblotting using anti-hMOB2 (top) and anti-NDR2 (middle) antibodies. Input lysates were probed with anti-hMOB2 antibody. (D) Endogenous NDR2 was coimmunoprecipitated with hMOB2. Lysates of HEK 293 cells were assayed by immunoprecipitation using control rabbit IgG or anti-hMOB2 antibody. Complexes were assayed by immunoblotting using anti-NDR2 (top) or anti-hMOB2 (bottom) antibody. Antibody heavy chains are marked with an asterisk. Input lysates were analyzed with anti-NDR2 antibody. (E) Endogenous hMOB2 coimmunoprecipitates with NDR2, but not with LATS1. Lysates of HEK 293 cells were subjected to immunoprecipitation with the indicated antibodies and analyzed by immunoblotting using anti-NDR2, anti-LATS1, and anti-hMOB2 antibodies. Antibody heavy chains are marked with an asterisk.

lane 3). Interestingly, endogenous hMOB2 was enriched using anti-NDR2 antibody (Fig. 7, lane 2), whereas when anti-T444-P antibody was used to pull down active NDR species, hMOB2 was not detectable (Fig. 7, lane 3). On the other hand, hMOB1A was almost exclusively detected in phosphorylated complexes of NDR (Fig. 7, compare lanes 2 and 3). This finding is in agreement with previous reports demonstrating enhanced complex formation of hMOB1A/B and NDR kinases upon activation (36). Overall, we conclude that hMOB2 preferentially associates with unphosphorylated NDR and, in contrast, hMOB1A/B associates with phosphorylated NDR.

**Reduction of hMOB2 protein results in increased NDR1/2 kinase activity.** hMOB2 is found in complex with unphosphorylated NDR kinases (Fig. 7), and ectopically expressed hMOB2 competes with hMOB1A/B, interfering with the activation of human NDR kinases (Fig. 4 and 5). Therefore, we

addressed the role of endogenous hMOB2 by RNAi. HEK293 cells, untransfected or transfected with plasmids encoding shRNAs against firefly luciferase (Fig. 8A, lane 2) or hMOB2 (Fig. 8A, lane 3), were analyzed by immunoblotting and kinase assays on endogenous NDR proteins performed in parallel (Fig. 8A and B). hMOB2 protein levels were reduced upon transfection with shMOB2, whereas hMOB1A/B levels were not changed (Fig. 8A, lane 3). Interestingly, knockdown of hMOB2 proteins resulted in an increase of phosphorylated NDR species (Fig. 8A, top, lane 3), despite a slight reduction in total NDR protein (Fig. 8A, lane 3). The increase of phosphorylated NDR was reflected in a significant increase in kinase activity when a peptide kinase assay using immunoprecipitated NDR2 was performed (Fig. 8B, lane 3). Therefore, we conclude that endogenous hMOB2 has inhibitory properties. However, the precise mechanism by which hMOB1A/B

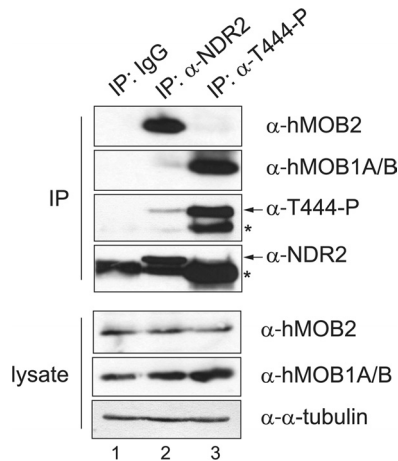


FIG. 7. Endogenous hMOB2 preferentially associates with inactive NDR kinases. Whole-cell extracts of HEK 293 cells were subjected to IP using the indicated antibodies and analyzed by immunoblotting with anti-T444-P, anti-NDR2, anti-hMOB2, and anti-hMOB1A/B. Input lysates were assayed by immunoblotting using the antibodies listed above. Antibody heavy chains are marked with an asterisk.

and hMOB2 complex formation with NDR is regulated remains unknown, since analysis of HEK293 cells treated with OA showed that hMOB2 protein levels remained unchanged (Fig. 8C) during the course of NDR activation (Fig. 8C, top) whereas

hMOB1A protein levels increased with time during the treatment (Fig. 8C). Further, we did not observe significant changes in either hMOB2 or hMOB1A/B protein levels during the course of NDR activation upon induction of apoptosis (Fig. 8D).

**hMOB2 expression affects biological functions of human NDR kinases.** Recent studies suggest that binding of hMOB1A/B to human NDR1/2 kinases is necessary for apoptosis signaling (36) and efficient centrosome duplication (13) in human cells. Our findings show that hMOB2 is preferentially located in inactive complexes with NDR (Fig. 7) and competes with hMOB1A/B for NDR binding, thereby interfering with activation of NDR (Fig. 5 and 6). Therefore, we tested whether hMOB2 binding to NDR kinases affects NDR function in apoptosis and centrosome duplication. To examine the effect of hMOB2 on apoptotic signaling, we generated U2-OS cell lines expressing myc-hMOB2(wt) or myc-hMOB2(H157A) in a tetracycline-inducible manner (Fig. 9). Cells were treated with or without tetracycline for 24 h before anti-Fas antibody in combination with cycloheximide was added. Cells were harvested at the time points indicated and analyzed by immunoblotting (Fig. 9). Unexpectedly, the hMOB2(H157A) variant displayed reduced protein stability, since no residual protein could be detected after the addition of a combination of anti-Fas antibody and CHX or CHX alone (data not shown). Overexpression of hMOB2(wt) resulted in reduced phosphorylation of the hydrophobic motif of NDR1 (T444) after 4 and 6 h of treatment compared with control cells (Fig. 9, top, compare

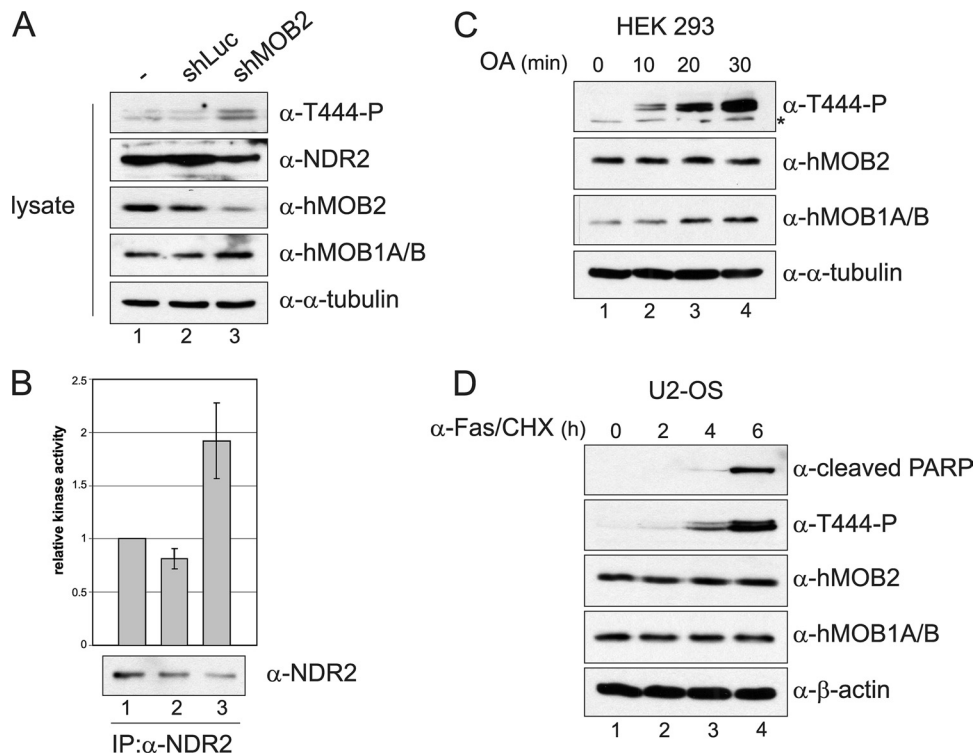


FIG. 8. Reduction of hMOB2 protein results in increased NDR1/2 activity. (A) HEK 293 cells were transfected with plasmids encoding shLuc or shMOB2 and were processed 72 h later for immunoblotting with the indicated antibodies. (B) In parallel, samples were subjected to IP using rabbit IgG or anti-NDR2 antibody before peptide kinase assays were performed. Data from at least two independent experiments with two replicates per experiment are shown. The error bars represent standard deviations. (C) HEK 293 cells were treated with 1  $\mu$ M OA for the indicated times before being processed for immunoblotting with the indicated antibodies. A background band is marked by an asterisk. (D) Apoptosis was induced in U2-OS cells by adding Fas antibody in combination with CHX for the indicated time and analyzed as for panel C.

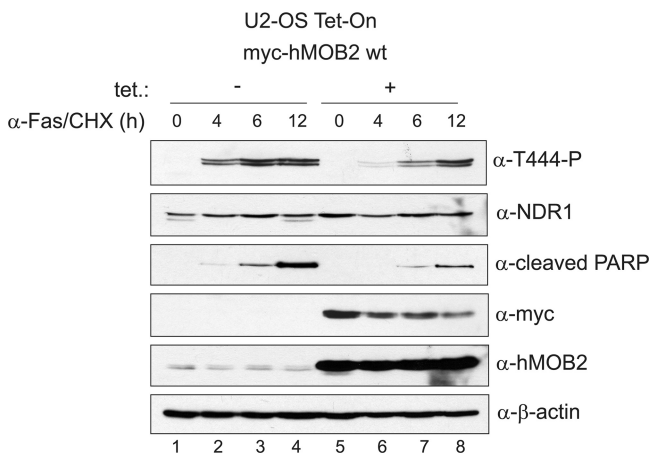


FIG. 9. Overexpression of hMOB2(wt) impairs death receptor-induced activation of NDR kinases and interferes with apoptosis signaling. U2-OS cells expressing myc-hMOB2(wt) in a tetracycline-inducible manner were incubated without (lanes 1 to 4) or with (lanes 5 to 8) tetracycline for 24 h before apoptosis was induced by the addition of Fas antibody in combination with CHX. Cells were harvested after 0, 4, 6, and 12 h and processed for immunoblotting using the indicated antibodies.

lines 2 and 3 to 6 and 7). Concurrently, we investigated whether this decrease in NDR activation was matched by a reduction in apoptotic markers. Indeed, the signal for cleaved PARP was reduced in cells overexpressing hMOB2(wt) compared with control cells (Fig. 9, compare lanes 3 and 4 to 7 and 8). These results indicate that hMOB2(wt) can interfere with the physiological activation of NDR kinases and consequently also interfere with NDR kinase apoptotic function.

We then sought to determine whether hMOB2 can also

affect NDR functions in centrosome duplication. As previously reported (1), centrosomes overduplicate in U2-OS cells upon S-phase arrest. Therefore, U2-OS cells transiently expressing empty vector, myc-tagged hMOB2(wt), or hMOB2(H157A) were arrested in S phase for 72 h and then analyzed by immunoblotting and immunofluorescence (Fig. 10A and B). As expected centrosome overduplication was observed in control cells (Fig. 10C) but was reduced by overexpression of hMOB2(wt) (Fig. 10C, lane 3). Overexpression of the NDR binding-deficient mutant hMOB2(H157A) had no effect (Fig. 10C, lane 4), despite expression and localization patterns similar to those of hMOB2(wt) (Fig. 10A and B). Overall, these results suggest that wild-type hMOB2 also negatively affects centrosome overduplication during S phase in an NDR binding-dependent manner. Therefore, two biological functions of human NDR kinases can be negatively regulated by increased hMOB2 expression.

DISCUSSION

MOB proteins are critical regulators of kinases of the NDR family and are conserved from yeast to humans (16). In budding yeast, two distinct complexes of MOB-NDR modules exist, Mob1p-Dbf2p and Mob2p-Cbk1p. Moreover, MOB proteins are essential activating subunits of the respective NDR kinases (19, 20, 22, 38). In multicellular organisms, such as *Drosophila*, dMOB1/Mats is required for the function of both warts and trc kinase (10, 24), indicating that MOB1 proteins do not specifically bind to a single NDR kinase, as in yeast. Also, in human cells, hMOB1A/B bind to and activate all four NDR kinases (2, 4, 13, 15, 29) and are essential for the function of NDR1/2 kinases in apoptosis and centrosome duplication (13, 36).

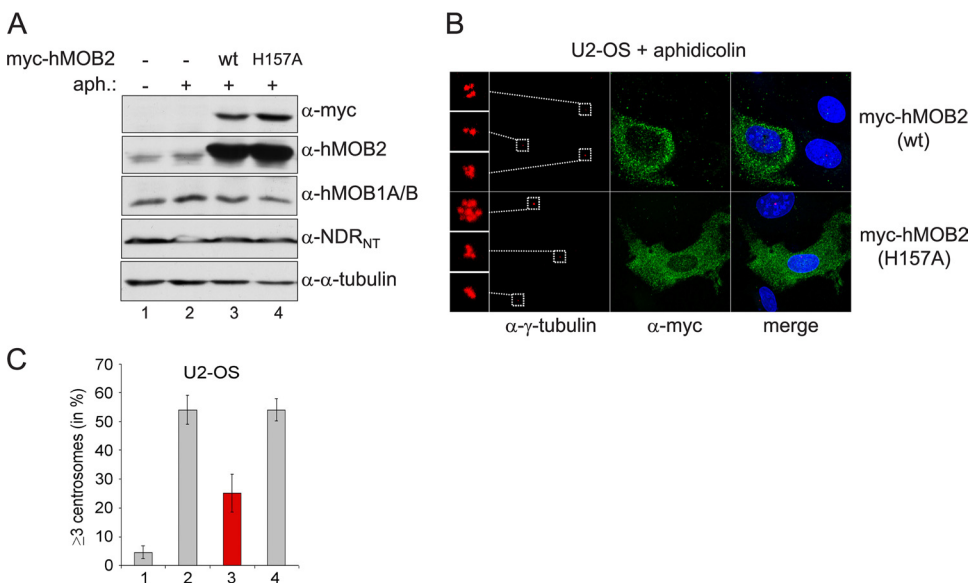


FIG. 10. Ectopic expression of hMOB2(wt) impairs centrosome overduplication. (A and B) U2-OS cells transfected with myc-tagged hMOB2(wt) or hMOB2(H157A) were treated with aphidicolin (2 μg/ml) for 72 h before being processed for immunoblotting (A) or immunofluorescence assay (B) with the indicated antibodies. The insets show enlargements of centrosomes in red. Myc-hMOB2 variants are in green. DNA is stained blue. (C) Histograms showing percentages of cells with excess centrosomes (≥3, more than three per mononucleated cell). Shown are cumulative data from at least three independent experiments with at least two replicates of 100 cells counted per experiment. The error bars indicate standard deviations.

However, human cells express six MOB proteins (Table 1) and four NDR kinases. We show here that hMOB3A, -B, and -C do not physically interact with or activate any of the four NDR/LATS kinases (Fig. 1 and 2). Despite their significant homology to hMOB1 proteins compared with hMOB2 (Table 1), hMOB3 proteins display significant sequence variation in or around amino acids previously shown to be important in conditional mutants in budding yeast MOB1p (32). Such variation might explain why hMOB3 proteins did not associate with NDR/LATS kinases. In support of this, it was shown recently that overexpression of hMOB3 proteins did not significantly affect centrosome duplication, a known function of NDR1/2 kinases (13). Therefore, the physiological binding partners and functions of hMOB3 proteins remain undefined.

Our data demonstrated that hMOB2 is a specific interaction partner of human NDR1/2 and not LATS1/2 (Fig. 1 and 2). Accordingly, we focused our investigation on hMOB2 and NDR1/2. Our findings demonstrate that hMOB2 binds to the N-terminal regulatory domain of NDR1/2 kinases (Fig. 3), the same region reported earlier for hMOB1A/B (2). Interestingly, mutational analysis of the N-terminal region of NDR1/2 revealed that the mode of binding of hMOB2 differs significantly from that of hMOB1A/B, because mutations in the NDR1/2 protein that interfere with hMOB1 binding (2) do not affect hMOB2 association (Fig. 3 and Table 2). hMOB2 binds NDR1/2, most likely through multiple contact points, since the interaction could not be ablated by single or combined point mutations (Fig. 3 and Table 2). Therefore, structural analysis of NDR1/2 kinases in complex with hMOB1 and hMOB2 proteins will be required in the future to examine differences in the two modes of interaction and also the mechanistic differences in activation/inhibition of these two complexes.

Additionally, we described for the first time competitive binding of hMOB2 and hMOB1 proteins to the N terminus of human NDR1/2 kinases (Fig. 4). Moreover, hMOB2 impaired okadaic acid-induced activation of endogenous NDR species (Fig. 4B), indicating distinct functions for different human MOB proteins in the regulation of NDR1/2 kinases, since hMOB1A was shown to potentiate NDR activity in a similar experiment (2). In addition, these data are strengthened by the concurrent use of a phosphospecific antibody to the hydrophobic motif phosphorylation (anti-T444-P) and by our biological experiments. However, in the literature, conflicting reports on the effects of hMOB2 overexpression on NDR activity describe overexpressed hMOB2 activating NDR1/2 kinases upon OA stimulation (5, 7). This could be due to the assays used to measure NDR kinase activity. In both studies, the nonspecific kinase substrates myelin basic protein and histone H1 were used. Therefore, the presence of an associated kinase may have contributed to the increase in phosphorylation of these substrates, whereas in our assays, an established NDR kinase substrate peptide was used (11, 13, 33, 34).

hMOB2 interferes with the activation of ectopic and endogenous NDR1/2 kinases by membrane-targeted hMOB1A in an NDR binding-dependent manner (Fig. 5), since an hMOB2 variant incapable of binding to NDR1/2 did not affect activation of NDR (Fig. 5). The expression of hMOB2(wt) retained NDR in the cytoplasm, and also, a fraction of mp-hMOB1A was observed in the cytoplasmic fraction (Fig. 5D). Therefore, it is possible that hMOB2 inhibits activation of NDR by mp-

hMOB1A by retention of the NDR-MOB1 complex, or even by retaining mp-hMOB1A itself in the cytoplasm. However, the analysis of this observation requires further investigation. Moreover, we analyzed endogenous complexes of NDR1/2 and hMOB1A/B or hMOB2 (Fig. 6 and 7). In full agreement with previous work (36), we showed that phosphorylated endogenous NDR species associate with hMOB1A/B. Interestingly, unphosphorylated NDR proteins coimmunoprecipitated with hMOB2, in contrast to active NDR species, which were found to be associated mostly with hMOB1A/B (Fig. 7). This finding uncovers a novel and distinct role of hMOB2 in the regulation of NDR1/2 kinases.

Strikingly, by RNAi depletion of hMOB2 in HEK293 cells, we found evidence that the endogenous role of hMOB2 is to inhibit NDR kinases, since knockdown of hMOB2 increased phosphorylation and kinase activity of endogenous NDR species (Fig. 8A and B). We did not observe an effect on hMOB1A/B protein, but we detected a decrease in total NDR protein. Therefore, it is tempting to speculate that hMOB2 might also play a role in NDR protein stability. Nevertheless, we describe for the first time an endogenous inhibitory function of a human MOB protein. We tried to address the mechanism through which hMOB1A/B and hMOB2 regulate NDR activation and inhibition by analyzing the abundance of hMOB1A/B and hMOB2 during the activation of NDR kinases (Fig. 8C and D and 10A). Whereas the hMOB2 protein level did not change during both treatments, hMOB1A/B protein increased during okadaic acid stimulation (Fig. 8), despite activation of NDR in both treatments (Fig. 8). Therefore, the endogenous mechanism through which hMOB1A/B and hMOB2 regulate activation/inhibition of NDR kinases remains unknown, since the total protein level might not represent the composition of NDR-MOB complexes during the course of activation. Future research in this direction is warranted.

We subsequently addressed the putative inhibitory function of hMOB2 in the context of two biological functions of NDR1/2 kinases, the proapoptotic role of NDR and the contribution of NDR to centrosome duplication (13, 36). Importantly, both functions depend on the interaction of hMOB1A/B proteins and NDR1/2 kinases.

First, inducible expression of hMOB2 interfered with the activation of NDR1 in U2-OS cells after anti-Fas treatment and in turn delayed apoptotic progression, as assessed by cleaved PARP (Fig. 9). Since cleaved PARP is a marker for apoptotic cells, this indicates that hMOB2 expression delayed the onset of apoptosis and most likely reduced the total apoptotic cell population in our settings. Furthermore, ectopic hMOB2 impaired centrosome overduplication in an NDR binding-dependent manner (Fig. 10). Significantly, the expression of kinase-dead NDR1 had a comparable effect on centrosome overduplication in a similar assay (13). This is indicative of an inhibitory effect of hMOB2 on NDR1 activity, which in turn was necessary for centrosome duplication in our experimental settings.

Interestingly, the role of the MOB2 protein in flies, dMOB2, appears to also differ from that of dMOB1/Mats, because mutations in the dMOB2 gene do not significantly enhance a phenotype of *trc* mutants or overexpression of a dominant-negative *trc* kinase (10). More precisely, overexpression of a truncated form of dMOB2 (amino acids 148 to 354) leads to a



phenotype similar to the *trc* mutant in fly wings (10), suggesting a dominant-negative role of dMOB2 in NDR kinase regulation in flies. Intriguingly, the truncated variant of dMOB2 shares high similarity with the full-length human MOB2 protein (data not shown). Therefore, it is tempting to speculate that dMOB2 has competitive properties similar to those of hMOB2 shown in our study. Determining whether dMOB2 negatively regulates *trc* kinase by competing with dMOB1/Mats is a question for future studies.

Our data show for the first time that hMOB2 has inhibitory effects on NDR1/2 functions. hMOB2 is found in unphosphorylated NDR complexes, and when overexpressed, hMOB2 can compete with hMOB1A/B, possibly physically displacing endogenous hMOB1A/B from NDR. hMOB2-NDR1/2 complexes that accumulate also appear to be inactive/quiescent. As a result, the activation of NDR1/2 by hMOB1A/B and possibly also by upstream kinases, such as MST1, could be impaired. Future challenges will be to address whether hMOB2 hinders NDR activation by mechanisms other than competition and steric restriction of the access of hMOB1 to the N terminus of NDR1/2, which in turn will have to be addressed by highly defined quantitative biochemical and biological assays. Moreover, the role of dMOB2 in flies has yet to be clarified. In light of our findings, the investigation by *Drosophila* geneticists of a negative function of dMOB2 on tricornered, warts, or even hippo kinase, will be of considerable interest.

In conclusion, our data indicate a novel role for hMOB2 in the regulation of NDR1/2 kinases. In contrast to hMOB1, hMOB2 is present in unphosphorylated NDR complexes. RNAi-mediated reduction of hMOB2 resulted in increased NDR activity. Overexpression negatively affects biological functions of NDR kinases, such as apoptotic progression and centrosome duplication. Altogether, our data indicate that hMOB2 plays an inhibitory role in the regulation of human NDR1/2 kinases.

#### ACKNOWLEDGMENTS

We thank D. Restuccia and P. King for editing the manuscript.

This work was supported by the Boehringer Ingelheim Fonds and Krebsliga beider Basel 19-2008 (to D.S.) and the Swiss Cancer League OCS 01942-08-2006 (to A.H.). The Friedrich Miescher Institute is part of the Novartis Research Foundation.

#### REFERENCES

- Balczon, R., L. Bao, W. E. Zimmer, K. Brown, R. P. Zinkowski, and B. R. Brinkley. 1995. Dissociation of centrosome replication events from cycles of DNA synthesis and mitotic division in hydroxyurea-arrested Chinese hamster ovary cells. *J. Cell Biol.* **130**:105–115.
- Bichsel, S. J., R. Tamaskovic, M. R. Stegert, and B. A. Hemmings. 2004. Mechanism of activation of NDR (nuclear Dbf2-related) protein kinase by the hMOB1 protein. *J. Biol. Chem.* **279**:35228–35235.
- Bosl, W. J., and R. Li. 2005. Mitotic-exit control as an evolved complex system. *Cell* **121**:325–333.
- Bothos, J., R. L. Tuttle, M. Ottey, F. C. Luca, and T. D. Halazonetis. 2005. Human LATS1 is a mitotic exit network kinase. *Cancer Res.* **65**:6568–6575.
- Chiba, S., M. Ikeda, K. Katsunuma, K. Ohashi, and K. Mizuno. 2009. MST2- and Furry-mediated activation of NDR1 kinase is critical for precise alignment of mitotic chromosomes. *Curr. Biol.* **19**:675–681.
- Colman-Lerner, A., T. E. Chin, and R. Brent. 2001. Yeast Cbk1 and Mob2 activate daughter-specific genetic programs to induce asymmetric cell fates. *Cell* **107**:739–750.
- Devroe, E., H. Erdjument-Bromage, P. Tempst, and P. A. Silver. 2004. Human Mob proteins regulate the NDR1 and NDR2 serine-threonine kinases. *J. Biol. Chem.* **279**:24444–24451.
- Gruneberg, U., and E. A. Nigg. 2003. Regulation of cell division: stop the SIN! *Trends Cell Biol.* **13**:159–162.
- Harvey, K., and N. Tapon. 2007. The Salvador-Warts-Hippo pathway—an emerging tumour-suppressor network. *Nat. Rev. Cancer* **7**:182–191.
- He, Y., K. Emoto, X. Fang, N. Ren, X. Tian, Y. N. Jan, and P. N. Adler. 2005. *Drosophila* Mob family proteins interact with the related tricornered (*Trc*) and warts (*Wts*) kinases. *Mol. Biol. Cell* **16**:4139–4152.
- Hergovich, A., S. J. Bichsel, and B. A. Hemmings. 2005. Human NDR kinases are rapidly activated by MOB proteins through recruitment to the plasma membrane and phosphorylation. *Mol. Cell. Biol.* **25**:8259–8272.
- Hergovich, A., and B. A. Hemmings. 2009. Mammalian NDR/LATS protein kinases in hippo tumor suppressor signaling. *Biofactors* **35**:338–345.
- Hergovich, A., R. S. Kohler, D. Schmitz, A. Vichalkovski, H. Cornils, and B. A. Hemmings. 2009. The MST1 and hMOB1 tumor suppressors control human centrosome duplication by regulating NDR kinase phosphorylation. *Curr. Biol.* **19**:1692–1702.
- Hergovich, A., S. Lamla, E. A. Nigg, and B. A. Hemmings. 2007. Centrosome-associated NDR kinase regulates centrosome duplication. *Mol. Cell* **25**:625–634.
- Hergovich, A., D. Schmitz, and B. A. Hemmings. 2006. The human tumour suppressor LATS1 is activated by human MOB1 at the membrane. *Biochem. Biophys. Res. Commun.* **345**:50–58.
- Hergovich, A., M. R. Stegert, D. Schmitz, and B. A. Hemmings. 2006. NDR kinases regulate essential cell processes from yeast to humans. *Nat. Rev. Mol. Cell Biol.* **7**:253–264.
- Ho, L. L., X. Wei, T. Shimizu, and Z. C. Lai. 2010. Mob as tumor suppressor is activated at the cell membrane to control tissue growth and organ size in *Drosophila*. *Dev. Biol.* **337**:274–283.
- Hou, M. C., D. A. Guertin, and D. McCollum. 2004. Initiation of cytokinesis is controlled through multiple modes of regulation of the Sid2p-Mob1p kinase complex. *Mol. Cell. Biol.* **24**:3262–3276.
- Hou, M. C., J. Salek, and D. McCollum. 2000. Mob1p interacts with the Sid2p kinase and is required for cytokinesis in fission yeast. *Curr. Biol.* **10**:619–622.
- Hou, M. C., D. J. Wiley, F. Verde, and D. McCollum. 2003. Mob2p interacts with the protein kinase Orb6p to promote coordination of cell polarity with cell cycle progression. *J. Cell Sci.* **116**:125–135.
- Koike-Kumagai, M., K. I. Yasunaga, R. Morikawa, T. Kanamori, and K. Emoto. 2009. The target of rapamycin complex 2 controls dendritic tiling of *Drosophila* sensory neurons through the Tricornered kinase signalling pathway. *EMBO J.* **28**:3879–3892.
- Komarnitsky, S. I., Y. C. Chiang, F. C. Luca, J. Chen, J. H. Toyn, M. Winey, L. H. Johnston, and C. L. Denis. 1998. DBF2 protein kinase binds to and acts through the cell cycle-regulated MOB1 protein. *Mol. Cell. Biol.* **18**:2100–2107.
- Krapp, A., M. P. Gulli, and V. Simanis. 2004. SIN and the art of splitting the fission yeast cell. *Curr. Biol.* **14**:R722–R730.
- Lai, Z. C., X. Wei, T. Shimizu, E. Ramos, M. Rohrbaugh, N. Nikolaidis, L. L. Ho, and Y. Li. 2005. Control of cell proliferation and apoptosis by mob as tumor suppressor, mats. *Cell* **120**:675–685.
- Luca, F. C., and M. Winey. 1998. MOB1, an essential yeast gene required for completion of mitosis and maintenance of ploidy. *Mol. Biol. Cell* **9**:29–46.
- Mah, A. S., J. Jang, and R. J. Deshaies. 2001. Protein kinase Cdc15 activates the Dbf2-Mob1 kinase complex. *Proc. Natl. Acad. Sci. U. S. A.* **98**:7325–7330.
- Parcellier, A., L. A. Tintignac, E. Zhuravleva, P. Cron, S. Schenk, L. Bzolic, and B. A. Hemmings. 2009. Carboxy-Terminal Modulator Protein (CTMP) is a mitochondrial protein that sensitizes cells to apoptosis. *Cell Signal.* **21**:639–650.
- Pearce, L. R., D. Komander, and D. R. Alessi. 2010. The nuts and bolts of AGC protein kinases. *Nat. Rev. Mol. Cell Biol.* **11**:9–22.
- Praskova, M., F. Xia, and J. Avruch. 2008. MOBKL1A/MOBKL1B phosphorylation by MST1 and MST2 inhibits cell proliferation. *Curr. Biol.* **18**:311–321.
- Reddy, B. V., and K. D. Irvine. 2008. The Fat and Warts signaling pathways: new insights into their regulation, mechanism and conservation. *Development* **135**:2827–2838.
- Saucedo, L. J., and B. A. Edgar. 2007. Filling out the Hippo pathway. *Nat. Rev. Mol. Cell Biol.* **8**:613–621.
- Stavridi, E. S., K. G. Harris, Y. Huyen, J. Bothos, P. M. Verwoerd, S. E. Stayrook, N. P. Pavletich, P. D. Jeffrey, and F. C. Luca. 2003. Crystal structure of a human Mob1 protein: toward understanding Mob-regulated cell cycle pathways. *Structure* **11**:1163–1170.
- Stegert, M. R., A. Hergovich, R. Tamaskovic, S. J. Bichsel, and B. A. Hemmings. 2005. Regulation of NDR protein kinase by hydrophobic motif phosphorylation mediated by the mammalian Ste20-like kinase MST3. *Mol. Cell. Biol.* **25**:11019–11029.
- Stegert, M. R., R. Tamaskovic, S. J. Bichsel, A. Hergovich, and B. A. Hemmings. 2004. Regulation of NDR2 protein kinase by multi-site phosphorylation and the S100B calcium-binding protein. *J. Biol. Chem.* **279**:23806–23812.
- Tamaskovic, R., S. J. Bichsel, H. Rogniaux, M. R. Stegert, and B. A. Hem-

- mings.** 2003. Mechanism of Ca<sup>2+</sup>-mediated regulation of NDR protein kinase through autophosphorylation and phosphorylation by an upstream kinase. *J. Biol. Chem.* **278**:6710–6718.
36. **Vichalkovski, A., E. Gresko, H. Cornils, A. Hergovich, D. Schmitz, and B. A. Hemmings.** 2008. NDR kinase is activated by RASSF1A/MST1 in response to Fas receptor stimulation and promotes apoptosis. *Curr. Biol.* **18**:1889–1895.
37. **Wei, X., T. Shimizu, and Z. C. Lai.** 2007. Mob as tumor suppressor is activated by Hippo kinase for growth inhibition in *Drosophila*. *EMBO J.* **26**:1772–1781.
38. **Weiss, E. L., C. Kurischko, C. Zhang, K. Shokat, D. G. Drubin, and F. C. Luca.** 2002. The *Saccharomyces cerevisiae* Mob2p-Cbk1p kinase complex promotes polarized growth and acts with the mitotic exit network to facilitate daughter cell-specific localization of Ace2p transcription factor. *J. Cell Biol.* **158**:885–900.
39. **Yabuta, N., N. Okada, A. Ito, T. Hosomi, S. Nishihara, Y. Sasayama, A. Fujimori, D. Okuzaki, H. Zhao, M. Ikawa, M. Okabe, and H. Nojima.** 2007. Lats2 is an essential mitotic regulator required for the coordination of cell division. *J. Biol. Chem.* **282**:19259–19271.
40. **Zhao, B., Q. Y. Lei, and K. L. Guan.** 2008. The Hippo-YAP pathway: new connections between regulation of organ size and cancer. *Curr. Opin. Cell Biol.* **20**:638–646.

## **A.2. Ablation of the kinase NDR1 predisposes mice to the development of T cell lymphoma**

Cornils H, Stegert MR, Hergovich A, Hynx D, **Schmitz D**, Dirnhofer S, Hemmings BA  
Published in *Science Signaling* 15 June 2010; Volume 3 Issue 126 ra47

“Defective apoptosis contributes to the development of various human malignancies. The kinases nuclear Dbf2-related 1 (NDR1) and NDR2 mediate apoptosis downstream of the tumor suppressor proteins RASSF1A (Ras association domain family member 1A) and MST1 (mammalian Ste20-like kinase 1). To further analyze the role of NDR1 in apoptosis, we generated NDR1-deficient mice. Although NDR1 is activated by both intrinsic and extrinsic proapoptotic stimuli, which indicates a role for NDR1 in regulating apoptosis, NDR1-deficient T cells underwent apoptosis in a manner similar to that of wild-type cells in response to different proapoptotic stimuli. Analysis of the abundances of NDR1 and NDR2 proteins revealed that loss of NDR1 was functionally compensated for by an increase in the abundance of NDR2 protein. Despite this compensation, NDR1(-/-) and NDR1(+/-) mice were more prone to the development of T cell lymphomas than were wild-type mice. Tumor development in mice and humans was accompanied by a decrease in the overall amounts of NDR proteins in T cell lymphoma samples. Thus, reduction in the abundance of NDR1 triggered a decrease in the total amount of both isoforms. Together, our data suggest that a reduction in the abundances of the NDR proteins results in defective responses to proapoptotic stimuli, thereby facilitating the development of tumors.”

*This report shows that NDR2 protein levels are up-regulated in several tissues of Ndr1 knock-out mice. Conversely, found that NDR1 protein levels are conversely up-regulated in Ndr2 knock-out mice (see Chapter I). To investigate whether the observed up-regulation is a result of increased transcription, I designed and validated quantitative real time PCR primers for Ndr1 and Ndr2. We find that neither Ndr1 nor Ndr2 transcripts are increased, indicating that the up-regulation is mediated by a post-transcriptional mechanism.*

### **A.3. NDR kinase is activated by RASSF1A/MST1 in response to Fas receptor stimulation and promotes apoptosis**

*Vichalkovski A, Gresko E, Cornils H, Hergovich A, **Schmitz D**, Hemmings BA.*  
Published in *Current Biology*; 2008 Dec 9;18(23):1889-95

“Human NDR1 and 2 (NDR1/2) are serine-threonine protein kinases in a subgroup of the AGC kinase family. The mechanisms of physiological NDR1/2 activation and their function remain largely unknown. Here we report that Fas and TNF-alpha receptor stimulation activates human NDR1/2 by promoting phosphorylation at the hydrophobic motif (Thr444/442). Moreover, NDR1/2 are essential for Fas receptor-induced apoptosis as shown by the fact that NDR knockdown significantly reduced cell death whereas overexpression of the NDR1 kinase further potentiated apoptosis. Activation of NDR1/2 by death receptor stimulation is mediated by the tumor suppressor RASSF1A. Furthermore, RASSF1A-induced apoptosis largely depends on the presence of NDR1/2. Fas receptor stimulation promoted direct phosphorylation and activation of NDR1/2 by the mammalian STE20-like kinase 1 (MST1), a downstream effector of RASSF1A. Concurrently, the NDR1/2 coactivator MOB1 induced MST1-NDR-MOB1 complex formation, which is crucial for MST1-induced NDR1/2 phosphorylation upon induction of apoptosis. Our findings identify NDR1/2 as novel proapoptotic kinases and key members of the RASSF1A/MST1 signaling cascade.”

*The 31G14 monoclonal mouse antibody is extensively used in this report to detect NDR1 and NDR2. I produced and purified recombinant MBP-NDR2 protein which was used to immunize Balb/C mice. Subsequently, I screened numerous hybridoma supernatants and isolated and characterize the 31G14 clone which detects endogenous levels of human NDR1 and NDR2 in Westernblotting.*

#### **A.4. The MST1 and hMOB1 tumor suppressors control human centrosome duplication by regulating NDR kinase phosphorylation**

*Hergovich A, Kohler RS, **Schmitz D**, Vichalkovski A, Cornils H, Hemmings BA*  
Published in *Current Biology*; 2009 Nov 3;19(20):1692-702

“BACKGROUND: Human MST/hSAV/LATS/hMOB tumor suppressor cascades are regulators of cell death and proliferation; however, little is known about other functions of MST/hMOB signaling. Mob1p, one of two MOB proteins in yeast, appears to play a role in spindle pole body duplication (the equivalent of mammalian centrosome duplication). We therefore investigated the role of human MOB proteins in centrosome duplication. We also addressed the regulation of human centrosome duplication by mammalian serine/threonine Ste20-like (MST) kinases, considering that MOB proteins can function together with Ste20-like kinases in eukaryotes. RESULTS: By studying the six human MOB proteins and five MST kinases, we found that MST1/hMOB1 signaling controls centrosome duplication. Overexpression of hMOB1 caused centrosome overduplication, whereas RNAi depletion of hMOB1 or MST1 impaired centriole duplication. Significantly, we delineated an hMOB1/MST1/NDR1 signaling pathway regulating centrosome duplication. More specifically, analysis of shRNA-resistant hMOB1 and NDR1 mutants revealed that a functional NDR/hMOB1 complex is critical for MST1 to phosphorylate NDR on the hydrophobic motif that in turn is required for human centrosome duplication. Furthermore, shRNA-resistant MST1 variants revealed that MST1 kinase activity is crucial for centrosome duplication whereas MST1 binding to the hSAV and RASSF1A tumor suppressor proteins is dispensable. Finally, by studying the PLK4/HsSAS-6/CP110 centriole assembly machinery, we also observed that normal daughter centriole formation depends on intact MST1/hMOB1/NDR signaling, although HsSAS-6 centriolar localization is not affected. CONCLUSIONS: Our observations propose a novel pathway in control of human centriole duplication after recruitment of HsSAS-6 to centrioles.”

*I cloned the MOB3 isoforms 3A, 3B and 3C which were first used in this report from cDNA libraries. Moreover, I contributed to the editing of the manuscript.*

## **A.5. The human tumour suppressor LATS1 is activated by human MOB1 at the membrane**

*Hergovich A, Schmitz D, Hemmings BA*

Published in Biochemical and Biophysical Research communications;

2006 Jun 23;345(1):50-8

“Downregulation of the LATS1 tumour suppressor protein kinase contributes to tumour formation in mammals and flies. Strikingly, the tumour suppressor activity depends on the interaction with Dmob (Drosophila Mps1-One binder) in *Drosophila melanogaster*. Recently, human LATS1 was reported to interact with human MOB1 (hMOB1), but the activation of LATS1 was not addressed. Here, we identified a highly conserved hMOB1-binding motif within LATS1's primary structure. While co-expression of LATS1 with hMOB1 did not elevate LATS1 kinase activity in mammalian cells, membrane-targeting of hMOB1 resulted in a significant increase of LATS1 activity. This stimulation was dependent on intact activation segment and hydrophobic motif phosphorylation sites, and was further found to occur a few minutes after membrane association. Therefore, we suggest a potential *in vivo* mechanism of LATS1 activation through rapid recruitment to the plasma membrane by hMOB1 followed by multi-site phosphorylation, thereby providing insight into the molecular regulation of the LATS tumour suppressor.”

*I performed sequence validation of all LATS mutants described in this report.*

## **A.6. NDR kinases regulate essential cell processes from yeast to humans**

*Hergovich A, Stegert MR, Schmitz D, Hemmings, Brian A*

Published in Nature Reviews Molecular Cell Biology 2006 Apr;7(4):253-64.

“Members of the NDR (nuclear Dbf2-related) protein-kinase family are essential components of pathways that control important cellular processes, such as morphological changes, mitotic exit, cytokinesis, cell proliferation and apoptosis. Recent progress has shed light on the mechanisms that underlie the regulation and function of the NDR family members. Combined data from yeast, worms, flies, mice and human cells now highlight the conserved and important roles of the different NDR kinases in distinct cellular processes.”

*I generated Figure 1 of this review which has been widely used and cited to illustrate the common characteristics of NDR kinases. Moreover, I contributed to the paragraph that describes the structural characteristics of NDR kinases and to general editing of the review.*

# Curriculum Vitae

## Debora Schmitz-Rohmer

Date of birth: 10 February 1979  
Address: 27 rue du Rhone  
68300 Saint Louis, France  
(+41 61 697 85 65  
Debora.Schmitz@fmi.ch

### EDUCATION

#### PhD Degree

*Title:* "Mammalian NDR Kinases in Cancer and Development"  
*Dissertationsleiter:* Dr. Brian A. Hemmings

**September 2004 to present**  
**Friedrich Miescher Institute,**  
Basel, Switzerland

#### Master of Science in Biotechnology

Ecole Supérieure de Biotechnologie de Strasbourg (ESBS)

**Oktober 2003**  
Strasbourg, France

#### Bachelor of Science in Biology

Westfälische Wilhelms – Universität

**September 2000**  
Münster, Germany

### INTERNSHIPS

#### Lead discovery unit for single-chain antibodies at Micromet

(biopharmaceutical company developing antibody-based therapeutics for cancer and other severe human diseases)

**January to July 2004**  
Munich, Germany

#### The Burnham Institute

MASTER'S THESIS

- Identification of a homing peptide for altered collagen (phage display technique)
- Targeting of magnetic nano particles to cancer cells

**January to August 2003**  
La Jolla, CA, USA

#### Deutsches Krebsforschungszentrum (DKFZ)

**July and August 2001**  
Heidelberg, Germany

#### Department of Biochemistry and Cell Biology

State University of New York at Stony Brook

**July 1999**  
NY, USA

### SCHOLARSHIPS / GRANTS

Boehringer Ingelheim PhD scholarship

September 2005 – August 2007

Krebsliga beider Basel

March 2009 – June 2010



## LANGUAGE Skills

German (mother tongue)  
English – fluent  
French – fluent

## PUBLICATIONS

- 1) Kohler, R.S., **Schmitz, D.**, Cornils, H., Hemmings, B.A., and Hergovich, A. Differential NDR/LATS Interactions with the Human MOB Family Reveal a Negative Role for hMOB2 in the Regulation of Human NDR Kinases. *Mol Cell Biol.* 2010 Sep;30(18):4507-20
- 2) Cornils, H., Stegert, M.R., Hergovich, A., Hynx, D., **Schmitz, D.**, Dirnhofer, S., and Hemmings, B.A. Ablation of the kinase NDR1 predisposes mice to the development of T cell lymphoma. *Sci Signal* 3, 2010 Jun 15;3(126):ra47.
- 3) Hergovich, A., Kohler, R., **Schmitz, D.**, Vichalkovski, A., Cornils, H., Hemmings, B.A. The MST1 and hMOB1 tumor suppressor proteins act in concert to control centrosome duplication in human cells. *Curr Biol.* 2009 Nov 3;19(20):1692-702
- 4) Vichalkovski, A., Gresko, E., Cornils, H., Hergovich, A., **Schmitz, D.**, Hemmings, B.A. NDR kinase is activated by RASSF1A/MST1 in response to Fas receptor stimulation and promotes apoptosis. *Curr Biol.* 2008 Dec 9;18(23):1889-95
- 5) Hoffmann SC, Schellack C, Textor S, Konold S, **Schmitz D**, Cerwenka A, Pflanz S, Watzl C. Identification of CLEC12B, an inhibitory receptor on myeloid cells. *J Biol Chem.* 2007 Aug 3;282(31):22370-5
- 6) Hergovich, A., **Schmitz, D.**, and Hemmings, B.A. (2006). The human tumour suppressor LATS1 is activated by human MOB1 at the membrane. *Biochem Biophys Res Commun* 2006 Jun 23;345(1):50-8.
- 7) Hergovich, A., Stegert, M.R., **Schmitz, D.**, Hemmings, B.A. NDR kinases regulate essential cell processes from yeast to humans. *Nat Rev Mol Cell Biol.* 2006 Apr;7(4):253-64. Review.

## Acknowledgements

First and foremost, I am deeply thankful for the continuous support and patience of my husband and my parents which have allowed me to complete this work.

I am very thankful to Dr. Brian A. Hemmings for giving me the opportunity and the freedom to pursue the research described in this thesis and for challenging me to stand up and defend my reasoning.

Dr. Alexander Hergovich has provided me with scientific mentoring, practical help and advice at numerous occasions and I would like to express my sincere gratitude to him. I am deeply thankful to my junior-year Biology teacher Dr. Jeannie S. Drew whose enthusiastic teaching style motivated me to study Biology. I am very grateful to Professor Rolf Zeller for his scientific advice and for facilitating and supporting our collaboration on the phenotype analysis of *Ndr*-null embryos. Simone Probst from his group has provided me with invaluable technical help, scientific advice and support and has become a good friend during our collaboration. Past and present colleagues in the Hemmings' Group have been supportive and a pleasure to work with. I am particularly thankful to Dr. Zhongzhou Yang who insisted on the heart phenotype of *Ndr*-null embryos and to Dr. Hauke Cornils for his constructive criticism on the thesis manuscript. Several FMI facilities have been of great help for my studies, namely the Transgenic, Genomics, Imaging and Histology Facilities.

Finally, I would like to thank my co-referee Professor Ruth Chiquet, my Faculty Representative Professor Michael Hall and my thesis chairman Professor Patrick Matthias for their willingness to serve on my thesis committee.